

DOCTORAL THESIS

Numerical modelling of flow, transport and reactions in hyporheic zones



Flinders
UNIVERSITY

Author:

Tariq LAATTOE

Bachelor of Science (Hons.)

A thesis submitted in fulfilment of the requirements

for the degree of Doctor of Philosophy

in the

School of the Environment

Flinders University

March 2016

Declaration

I certify that this thesis does not incorporate without acknowledgement any material previously submitted for a degree or diploma in any other university; and that to the best of my knowledge and belief it does not contain any material previously published or written by another person except where due reference is made in the text.

Signed:

Date:

Declaration of Co-authorship

This thesis comprises a series of journal publications either published or in preparation for publication in leading scientific journals. Chapters 2 and 3 were published during my candidature, while chapters 4 and 5 are currently in submission.

I am the lead author on all publications and was responsible for leading and conducting the research contained in them. My supervisors and co-authors for the publications, Dr. Vincent Post and Prof. Adrian Werner provided input and advice throughout my candidature. Their contributions to this body of work are acknowledged.

“The most exciting phrase to hear in science, the one that heralds new discoveries, is not ‘Eureka!(I found it!) but ‘Thats funny..’”

Isaac Asimov

FLINDERS UNIVERSITY

Abstract

Faculty of Science and Engineering

School of the Environment

Doctor of Philosophy

Numerical modelling of flow, transport and reactions in hyporheic zones

by Tariq LAATTOE

Hyporheic exchange is perhaps the quintessential ground and surface water interaction. It involves a continuous cycle of exchange between surface waters in streams or rivers and the pore water in their bed or bank sediments. It is now recognized as one of the most important zones in a riverine ecosystem that controls the dynamics of surface water quality. Prior to the work of Thibodeaux and Boyle [1987] the process was considered to be governed by diffusion, but their tracer experiment in a flume replicating a stream with a waveform structure on the streambed, identified advective currents in the bed sediments. Detail of the pressure distribution created by water flowing over the streambed in that experiment was soon used to develop a two dimensional numerical model, leading to the first hyporheic zone bedform model. Current research in the hyporheic zone covers significantly larger spatial and temporal scales. However, the bedform (≤ 1.0 m) scale remains a popular area for investigating hyporheic zone (HZ) process dynamics.

One of the most popular bedform scale numerical models features a boundary condition used to approximate an infinite repetition of space. Known as a spatially periodic boundary (SPB), it is a feature common to numerous computational fluid dynamics software packages but lacking in the industry standard groundwater modelling software MODFLOW. Indeed, MODFLOW, its related solute transport code MT3DMS, and reactive transport variant PHT3D, are all generally underutilized in the area of bedform

scale HZ research. Use of the single bedform model has expanded to include solute, thermal and reactive transport variants in featured in multiple studies where spatial periodicity with respect to transport is also enforced. This body of work attempts to further examine HZ processes at the bedform scale adopting the combined spatially periodic flow and transport boundary condition and concurrently promote the use of MODFLOW, MT3DMS and PHT3D in future HZ studies through development of the spatially periodic boundary condition. Specifically this work achieves the following: 1) develops, implements and assess the function of a spatially periodic boundary condition in MODFLOW; 2) Examines the effects of the periodic assumption with conservative solute transport variants of the single-bedform model; 3) develops, implements and assess the function of a spatially periodic boundary condition in MT3DMS; and 4) examines the effect of the periodic assumption on reactive transport simulations common to the single bedform model using PHT3D.

The first part of this study presents a method to implement the SPB in MODFLOW through development of the appropriate block-centered finite difference expressions. A source code modification is then made to MODFLOW's general head boundary package. The modifications are verified through a comparison of modelled results with an analytical solution of a sinusoidal head distribution over a flat streambed over a horizontally infinite domain. A second verification is also presented using a series of multi-bedform models with increasing bedform numbers to determine if the central bedform in each multi-bedform model converges on the single bedform solution. The second part of this study uses the spatially periodic flow boundary to develop a multi-bedform model with a steady-state spatially-periodic flow field. Solute distributions at an approximate steady state are then obtained for the flow field using MT3DMS and used to demonstrate a physically realistic transport solution with a spatially periodic flow field. The results indicate that lack of symmetry between the boundaries is a function of the vertical concentration gradient and two dimensionless parameters, which characterize the hyporheic and underflow regimes, and the solute exchange between them. A thermal scenario with sinusoidal temperature variation at the surface is also examined and demonstrates that

the reversal of the thermal gradient across the streambed surface promotes a spatially periodic solution. The study concludes that the solute variant of the spatially periodic boundary condition should be applied only to single-bedform models with minimal vertical diffusive and dispersive solute transfer.

The third part of this study develops the solute variant of the spatially periodic boundary for MT3DMS and PHT3D. The appropriate block-centered finite-difference approach to implementing the boundary is presented along with the necessary source code modifications to MT3DMS's sink source mixing package. The performance of the boundary is explored through comparison of a multi-bedform hyporheic zone model with a single bedform model. The boundary condition demonstrates appropriate performance for situations where dispersive effects and lateral seepage flux are minimal.

The fourth part of this study examines the effects of the solute SPB in PHT3D on a reactive transport variant of the single bedform model. Comparisons are made with a similar multi-bedform model. The reactive transport comprises a modified Monod kinetics model of dissolved organic carbon degradation, nitrification and denitrification. The solutions produced by the single bedform model are compared to the downstream trends observed in the multi-bedform model. A Damköhler number for each reactant species is used as a metric for reactivity comparison between bedforms. The results demonstrate that the solute SPB can produce single bedform solutions indicative of a nitrate sink while the corresponding multi-bedform model solution is that of a nitrate source. Observations also indicate that mixing, currently neglected in many HZ studies, has implications for studies linking reaction rates specifically to HZ residence time. . . .

Acknowledgements

I am greatly indebted to both my supervisors for their support provided throughout my candidature. I could not have asked for a better duo to aid me on this journey. To my principal supervisor, Vincent, I apologise if I wasn't your ideal first PhD student but as a parent I can tell you that it is definitely better to get the tough one first. Thank you for the myriad of skills I now have that you were instrumental in developing. They are life changing. To my co-supervisor Adrian, thank you for introducing me to groundwater to begin with and making me feel stupid when I needed to. Most people don't get it, but for me, its the fastest way to learn. Thank you also for all the financial support you obtained for me through the NCGRT and for giving me the nod with the Goyder project. Were it not for those acts, I am sure I would not be finishing today.

To my parents, for getting me to the starting line. Were it not for your courage to immigrate to a new country and leave your families behind, I would never have had the opportunity to even attempt a PhD. A special thank you also to all my colleagues at Flinders. Even though I wasn't around that much, it was nice to know I could count on you guys to turn my computer on after a power failure.

Finally I would like to thank Rachel, my beautiful wife for providing the spark which led to my second attempt at an undergraduate degree. Who would have thought this is where it would end up? Thank you to my daughters Charlotte and Esmé for reminding me every day what's really important in life.

...

Contents

Declaration	i
Declaration of Co-authorship	ii
Abstract	iv
Acknowledgements	vii
Contents	viii
List of Figures	x
List of Tables	xiii
1 Introduction	1
1.1 Background	1
1.2 Thesis Structure	2
2 Spatial periodic boundary condition for MODFLOW	4
2.1 Abstract	4
2.2 Introduction	5
2.3 Methods	7
2.4 Implementation	10
2.5 Verification	12
2.6 Discussion and conclusions	15
3 Spatial periodicity in bedform-scale solute and thermal transport models of the hyporheic zone	18
3.1 Abstract	18
3.2 Introduction	19
3.3 Methods	22
3.3.1 Flow models	23
3.3.2 Solute transport models	26
3.3.3 Thermal transport models	28

3.4	Results and Discussion	29
3.4.1	No-flow bottom boundary scenarios	29
3.4.2	Gaining and Losing scenarios	34
3.4.3	Thermal transport scenarios	38
3.5	Conclusions	40
4	A spatially periodic boundary for MT3DMS and PHT3D	42
4.1	Abstract	42
4.2	Introduction	43
4.3	Method	46
4.4	Implementation	48
4.5	Application	50
4.6	Conclusions	57
5	Effects of spatial periodic boundaries on simulations of nutrient dynamics in bedform scale hyporheic zone models	58
5.1	Abstract	58
5.2	Introduction	59
5.3	Methods	62
5.4	Results	67
5.5	Discussion	75
5.6	Conclusions	77
6	Conclusions	79
6.1	Contribution of this work to the field	79
6.2	Future work	81
A	The spatial periodic flow boundary source code	83
B	The spatial periodic solute boundary source code	96
Bibliography		119

List of Figures

2.1	A 2D vertical slice through a series of identical ripple/dune structures along a streambed. Stream flow creates eddies in the troughs, resulting in a variable head distribution along the surface-subsurface interface, which drives small-scale hyporheic exchange. Below the hyporheic exchange flows, the stream gradient drives a predominantly horizontal flow regime termed underflow. Instead of modelling multiple bedforms, a spatial periodic boundary pair can be used along the lateral boundaries of a single bedform model.	6
2.2	The modelled bedform with SPB cells on the lateral boundaries. Fictitious cells located in adjacent unmodelled bedforms provide the nodes required to apply the Δh term and maintain identical head gradients across the lateral boundaries. U and D indicate the upstream and downstream lateral boundary column indices, respectively, and Z indicates the layer number. The Δh term is now applied between a node in the model and its corresponding fictitious node, e.g. U, Z and $D + 1, Z$	8
2.3	(a) Sinusoidal head distribution used for the top boundaries of both the analytical and numerical models. (b) The analytical solution of a model using the sinusoidal head distribution as a specified condition on the top boundary. (c), (d) MODFLOW's solutions to the shaded areas of (a) and (b) when using a SPB condition on the lateral boundaries.	13
2.4	(a) The specified head profile assigned to the top boundary of the multi bedform model with a gradient of 0.01 metres maintained across the entire domain. (b) The solved head distribution for the 15 bedform model where departure from spatial repetition is clearly evident at the lateral boundaries. (c) MODFLOW solution to a single bedform model solved using the SPB. (d) MODFLOW solution for the 8 th bedform in the multi-bedform model. (e) The logarithm of absolute head difference between the two solutions for a single bedform.	16
3.1	The Darcy domain of a typical bedform model with spatially periodic lateral boundaries for both flow and concentration.	20
3.2	Top boundary head distributions used in single-bedform models and solutions to the different R scenarios. Heads are normalised as $h^* = (h - h_{min})/(h_{max} - h_{min})$ where h is the nodal head value and h_{min} and h_{max} are respectively the minimum and maximum head for each simulation. Dashed lines delineate the hydraulic divide between hyporheic flow cells and underflow.	25
3.3	Steady-state solutions to solute transport simulations with no flow bottom boundaries.	31

3.4	Horizontally integrated vertical mass fluxes for simulations with a no-flow bottom boundary. Positive values are indicative of mass migration deeper into the bedform. Advection dominates the transport of solutes in the hyporheic flow cells. In all cases dispersion is the primary transport mechanism for solute crossing the flow divide and penetrating the underflow. Spatial periodicity in this figure is represented by identical plots which overlie each another.	32
3.5	The changes in advective solute flux across lateral bedform boundaries in the underflow for all R and λ combinations. A periodic solution would produce horizontal lines.	33
3.6	Steady state solutions to $R = 2$ solute transport simulations with gain and loss from bottom boundary.	36
3.7	Horizontally integrated vertical flux in gaining and losing scenarios. Positive values are indicative of mass migration deeper into the bedform. Advection associated with ambient upward flow in gaining scenarios counteracts the dispersion driven by the concentration gradient. Dispersion is less significant as a transport mechanism for mass in losing scenarios. Spatial periodicity in this figure is represented by identical plots which overlie each another	37
3.8	Graphs showing the horizontally advected flux (J_{adh}) in the underflow as a function of bedform number for gaining and losing scenarios. A periodic solution would produce horizontal lines.	38
3.9	Average temperatures of the first 11 bedforms for the five day thermal transport simulation. The combination of $R = 2$ and $\lambda = 0.1$ is expected to show the greatest departure from periodicity based on previous solute transport experiment results.	39
4.1	A 2D vertical slice through a series of identical ripple/dune structures along a streambed. Instead of modelling multiple bedforms a spatial periodic boundary pair can be used along the lateral boundaries of a single bedform model	44
4.2	The Darcy domain of a typical bedform model with spatially periodic lateral boundaries for both flow and concentration. Descriptions of parameters are located in Table 4.1	45
4.3	SPB flux and solute concentration relationships with modelled boundary cells	47
4.4	Top boundary head distribution (left) and MODFLOW's steady state solution for the single bedform with SPB flow (right) used for all transport simulations. * Heads are normalized using feature scaling	51
4.5	The steady state uniform flow field of the 11 bedform model (*Heads are normalized using feature scaling).	51
4.6	The concentration distribution of the multi bedform model at time $t = 36$ hours.	53
4.7	Comparisons of solute distributions between bedforms number 2, 6, 11 in the multi bedform model and the singular bedform model using the solute SPB. The rows correspond to simulation times 1 hour (top), 5 hours (middle), 25 hours (bottom).	55
4.8	Total solute mass in each bedform from $t = 1$ hour to $t = 36$ hours.	56

4.9	Centre of mass comparison between: solute SPB and bedform 2 (left); solute SPB and bedform 6 (middle); solute SPB and bedform 11 (right). Points are labelled with time in hours. X axis is length into the individual bedform from the left. Y axis is height from closed boundary at the base of the bedform.	56
5.1	The modelled domain of a typical HZ bedform model with SPB lateral boundaries. Descriptions and values of parameters are located in Table 5.1	60
5.2	Head distributions and flow fields specific to each R value used in the simulations (top row). Heads are normalized $h^* = (h - h_{min})/(h_{max} - h_{min})$, where h^* is the normalized head value, h [L] is the nodal head value, h_{max} and h_{min} are, respectively, the maximum and minimum head values in each simulation direct-age distributions observed in the single bedform models with $\lambda = 0.001$ at time $t = 120$ hours (bottom row) . . .	68
5.3	Concentrations of reactants in a multi-bedform model at $t = 120$ hours for $R = 20$ and $\lambda = 0.01$	69
5.4	Concentrations of reactants in a multi-bedform model at $t = 120$ hours for $R = 2$ and $\lambda = 0.1$	70
5.5	Da_O_2 differences with changing λ values for simulations where $R = 2$. The pattern of difference between the models remains despite the change in λ	72
5.6	Subset of results demonstrating the differences to Da values in bedforms MB2, MB6, MB11 and the SPB when changing R	73
5.7	Scenario 2 simulation $R = 2$, $\lambda = 0.1$. In flowing concentrations are decreased for DOC, nitrate and ammonium. Significantly greater nitrate reactivity (denitrification) in the SPB model.	75
5.8	Scenario 3 simulation $R = 2$, $\lambda = 0.1$. DOC is limited to an extent such that nitrate is no longer completely consumed in the HZ.	75

List of Tables

2.1	MODFLOW model parameters used in the verification examples	15
3.1	Recent single bedform publications	21
3.2	Parameters used in numerical experiments	22
4.1	Parameters used in numerical experiments	48
5.1	Model geometry and input parameters used in numerical experiments *Van Cappellen and Wang [1996]	63
5.2	Reactions implemented in the reaction network	64
5.3	Inflow concentrations (M) of reactant species for 3 scenarios	66

For Rachel . . .

Chapter 1

Introduction

1.1 Background

The hyporheic zone (HZ) is one of the key elements that governs stream biochemistry and ecohydrology [Krause et al., 2009; Fleckenstein et al., 2010]. The first publication to articulate the term [Orghidan, 1959] focused on its ecological aspects and from there numerous discipline specific definitions and delineations of the HZ were made [White, 1993]. For the purposes of this thesis, it is defined as the portion of the sediments directly beneath and adjacent to a stream or river that is permeated with the surface water [Harvey et al., 1996]. The mixing of surface and ground water within the HZ contributes to its high biogeochemical activity catalysed by microbial processes [Brunke and Gosner, 1997; Boulton et al., 1998]. Slower moving water in the HZ greatly increases the time available for reaction and metabolism of nutrients in the stream [Grimm and Fisher, 1984; Dahm et al., 1998] modifying both the in stream [McClain et al., 2003; Gandy et al., 2007; Harvey et al., 2013] and groundwater chemistry [Conant et al., 2004]. The reduced rate of flow in the HZ is also responsible for a significant component of the tailing behaviour observed in solute breakthrough curves from instream tracer tests [Bencala et al., 1984]. Novel approaches for estimating in stream hyporheic flux and residence time have since been developed based on artificial tracers [Wörman et al., 2002; Gooseff et al., 2002] and natural tracers such as radon [Cook et al., 2006].

1.2 Thesis Structure

The thesis is structured as four separate papers, two of which have been published and two have been submitted. Chapter 2 [Laattoe et al., 2013] outlines the definitions of the spatial periodic boundary condition for flow and the differences between for its implementation in node-centred versus block-centred grids. A formulation of the SPB, appropriate for MODFLOW's block-centred finite-difference spatial discretization is presented. The implementation of the boundary condition in MODFLOW is analogous to the general head boundary (GHB) package and the necessary modifications to the source code are discussed.. Verification of the boundary condition is via a comparison with the analytical solution of Elliott and Brooks [1997a], which replaces a spatially-periodic, laterally-infinite domain with a single bedform model. A second verification is also provided using a multi-bedform with fixed head lateral boundaries and an increasing number of bedforms. The spatially periodic flow solution of the single bedform is compared with the central bedform of each multi-bedform model and a trend to converge with the periodic solution is demonstrated.

The SPB boundary condition for flow is then used in Chapter 3 [Laattoe et al., 2014] to develop spatially-periodic flow fields in a suite of multi-bedform models. The aim of this study is to quantify the potential error when implementing a solute variant of the SPB. Each multi-bedform model features a different combination of physical parameters combined to form dimensionless numbers that govern net mass flux in and out of a bedform model according to Qian et al. [2008]. Results of conservative solute transport simulations with MT3DMS are presented and analysed according to the dimensionless ratios. Comparisons are made using advective and dispersive component fluxes, which are horizontally integrated and normalized. The study also examines gaining and losing scenarios. A thermal transport scenario with a sinusoidal variation in temperature representing diurnal fluctuation in the surface water is also included. The study finds that increased mixing and enhanced lateral flux between bedforms are the least suitable for SPB simulation. Gaining scenarios are demonstrated to converge to a SPB solute

distribution through reduction in the mass transfer between HZ and underflow. The diurnal change in temperature cyclically reverses the thermal gradient at the surface minimizing the lateral flux in the underflow and therefore also approaches a periodic solution.

A multi-species solute transport variant of the SPB is then developed (Chapter 4). The sink source mixing package of MT3DMS is used to assign the concentration of the appropriate cell on the opposite lateral boundary to those cells receiving an advective flux into the model via the SPB. The formulation of the boundary for MT3DMS is presented and the source code modifications are discussed. The boundary condition is applied in a single-bedform model and the solution compared to that of a multi-bedform model. A suite of reactive transport PHT3D models are then developed (Chapter 5) in a similar manner to the approach taken in Chapter 3. A direct comparison between single and multi-bedform approaches is made. A Damköhler number combining residence time and reaction rate is used as a metric for the reactivity of the species in the reactive transport simulations. The results indicate that differences in reactivity with the SPB are significantly affected by the assumption of spatial periodicity. And the simulations show that it is even possible to obtain a solution that characterizes a single bedform as a nitrate sink while the multi-bedform model predicts that the HZ acts as a nitrate source. Further to this shrinking oxic zones and trend reversals in downstream reactivity were observed in the multi-bedform model. These findings have repercussions for current HZ studies that link reaction rates strictly to residence times based on flow paths. Importantly this thesis shows that the assumption of spatial-periodicity, which has gained widespread acceptance and popularity in the research field, should be applied with utmost caution. It may be appropriate to reduce the spatial extent of the problem to a single bedform in certain cases, but the validity of this assumption must always be demonstrated and justified.

Chapter 2

Spatial periodic boundary condition for MODFLOW

2.1 Abstract

Small scale hyporheic zone (HZ) models often use a spatial periodic boundary (SPB) pair to simulate an infinite repetition of bedforms. SPB's are common features of commercially available multi-physics modelling packages. MODFLOW's lack of this boundary type has precluded it from being effectively utilized in this area of HZ research. We present a method to implement the SPB in MODFLOW by development of the appropriate block-centred finite-difference expressions. The implementation is analogous to MODFLOW's general head boundary package. The difference is that the terms on the right hand side of the solution equations must be updated with each iteration. Consequently, models that implement the SPB converge best with solvers that perform both inner and outer iterations. The correct functioning of the SPB condition in MODFLOW is verified by two examples. This boundary condition allows users to build HZ bedform models in MODFLOW, facilitating further research using related codes such as MT3DMS and PHT3D.

2.2 Introduction

The hyporheic zone (HZ) is the part of the saturated zone beneath and adjacent to streams in which groundwater and surface water mix [Woessner, 2000]. Head gradients generated by stream currents flowing over the relief of stream beds cause flow through the bedform [Shum, 1992], causing exchange of water and solute on a horizontal scale of centimetres to metres between the streambed sediments and the water column above [Harvey and Wagner, 2000]. Its effects on flora and fauna [Hayashi and Rosenberry, 2002; Greig et al., 2007] and stream biogeochemistry [White, 1993; Fanelli and Lautz, 2008] have been well documented, and the number of research publications that investigate hyporheic exchange flux has increased dramatically in the last decade [Robertson and Wood, 2010; Fleckenstein et al., 2010]. In particular, numerical models to study the HZ are increasingly used [e.g. Cardenas and Wilson, 2006; Stonedahl et al., 2010; Jin et al., 2010].

Hyporheic flow paths in bedforms were first identified in flume experiments [Thibodeaux and Boyle, 1987]. A numerical investigation of this experiment by Savant et al. [1987] verified that hyporheic flow was the dominant transport mechanism of non-sorbing solutes through the bedforms. Rutherford et al. [1995] used an analytical approach to show that implementing a sinusoidal head distribution over a flat streambed produces similar hyporheic flow paths to those observed in triangular bedform models. More recent HZ investigations at the bedform scale include numerical experiments in which the surface water domain is modelled explicitly [Cardenas and Wilson, 2006; Sawyer and Cardenas, 2009; Jin et al., 2010]. Steady-state Reynolds-averaged Navier-Stokes (RANS) equations are applied to solve the surface water domain and provide a head distribution for the interface between the surface and subsurface regions. The interface head distribution is then assigned as a Dirichlet boundary condition for the groundwater flow equation along the bed surface (Figure 2.1). These models consider a single bedform structure and apply a spatial periodic boundary (SPB) condition at their lateral subsurface boundaries.

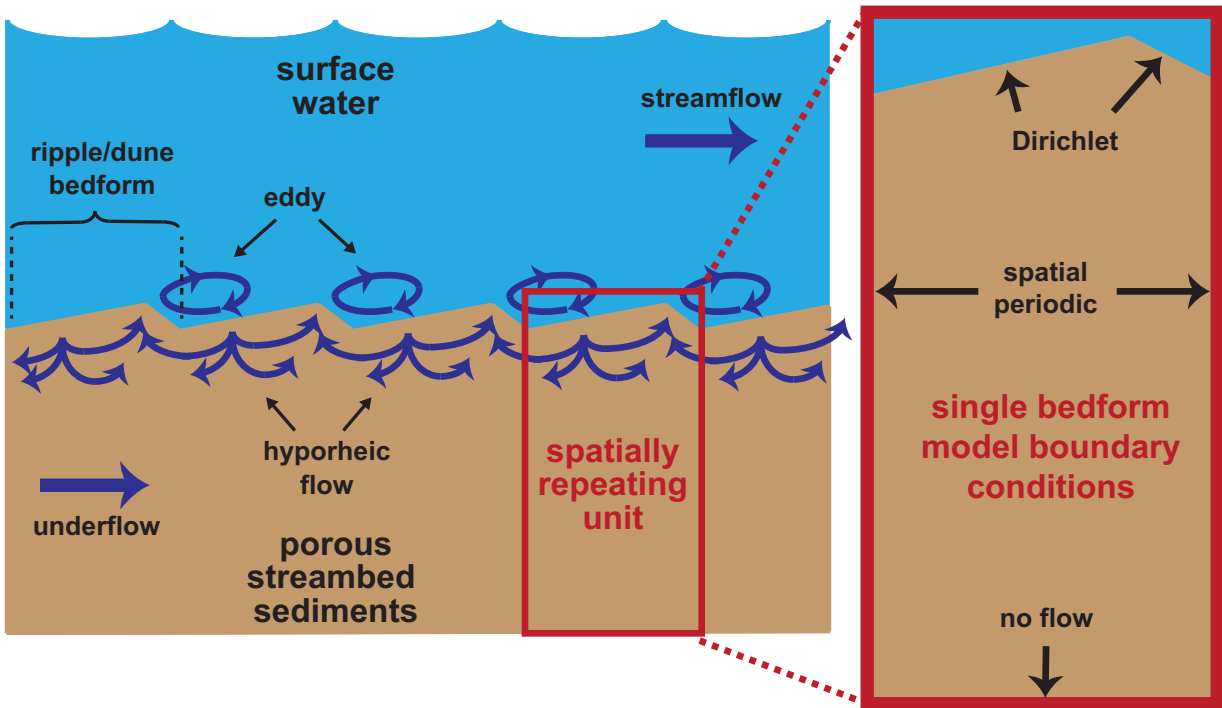


FIGURE 2.1: A 2D vertical slice through a series of identical ripple/dune structures along a streambed. Stream flow creates eddies in the troughs, resulting in a variable head distribution along the surface-subsurface interface, which drives small-scale hyporheic exchange. Below the hyporheic exchange flows, the stream gradient drives a predominantly horizontal flow regime termed underflow. Instead of modelling multiple bedforms, a spatial periodic boundary pair can be used along the lateral boundaries of a single bedform model.

This type of boundary condition allows an infinite series of identical bedforms to be represented by a single bedform [Cardenas and Wilson, 2006].

The objective of this article is to demonstrate how the SPB can be implemented in MODFLOW-2005 to enable the simulation of spatially-periodic subsurface flow underneath repeating bedforms in a stream. SPB conditions are available in multi-physics software packages such as COMSOL Multiphysics® and computational fluid dynamics packages such as ANSYS® Fluent, but are generally not supported in groundwater flow codes such as MODFLOW [Harbaugh, 2005]. The lack of a SPB condition in MODFLOW limits its applicability when investigating hyporheic flow patterns.

Development of the SPB in MODFLOW will facilitate the use of solute transport simulators such as MT3DMS [Zheng and Wang, 1999] and reactive transport simulators such as PHT3D [Prommer et al., 2003] in HZ bedform modelling research. The numerical

expressions and subsequent modifications to the source code are developed with the HZ bedform models of Elliott and Brooks [1997a] and Cardenas and Wilson [2006] as specific examples.

2.3 Methods

The geometry of a triangular bedform model typical of many HZ studies is shown in Figure 2.2. Boundary conditions for the model consist of a no-flow boundary at the base, a Dirichlet condition at the surface/subsurface interface, and spatially periodic conditions at the lateral boundaries that represent the interfaces between the adjacent bedforms. The SPB's are defined as follows [Jin et al., 2010]:

$$h(0, z) = h(L, z) + \Delta h \quad (2.1)$$

$$u(0, z) = u(L, z) \quad (2.2)$$

$$v(0, z) = v(L, z) \quad (2.3)$$

where h represents the hydraulic head [L], and u and v are the horizontal (x) and vertical (z) components of the pore water velocity [LT^{-1}], respectively. The left and right vertical faces of the SPB are denoted by $0, z$ and L, z respectively. The Δh term [L] represents a fixed difference between the heads at the left and right boundaries (which are a distance L apart), and accounts for the slope of the streambed [Cardenas and Wilson, 2006; Jin et al., 2010]. For node-centred grids, both the heads and fluxes are evaluated at the model boundaries and implementation of the SPB condition provided by Equations (3.1) to (3.3) is more straightforward than in MODFLOW, which uses a block-centred finite-difference method. With this method, the heads are calculated at the nodes in the centroids of cells, while fluxes are calculated across the cell faces. This presents some difficulty in implementing Equations (3.1) to (3.3) in MODFLOW, because the Δh term in Equation 3.1 cannot be directly evaluated between the two nodes of the boundary

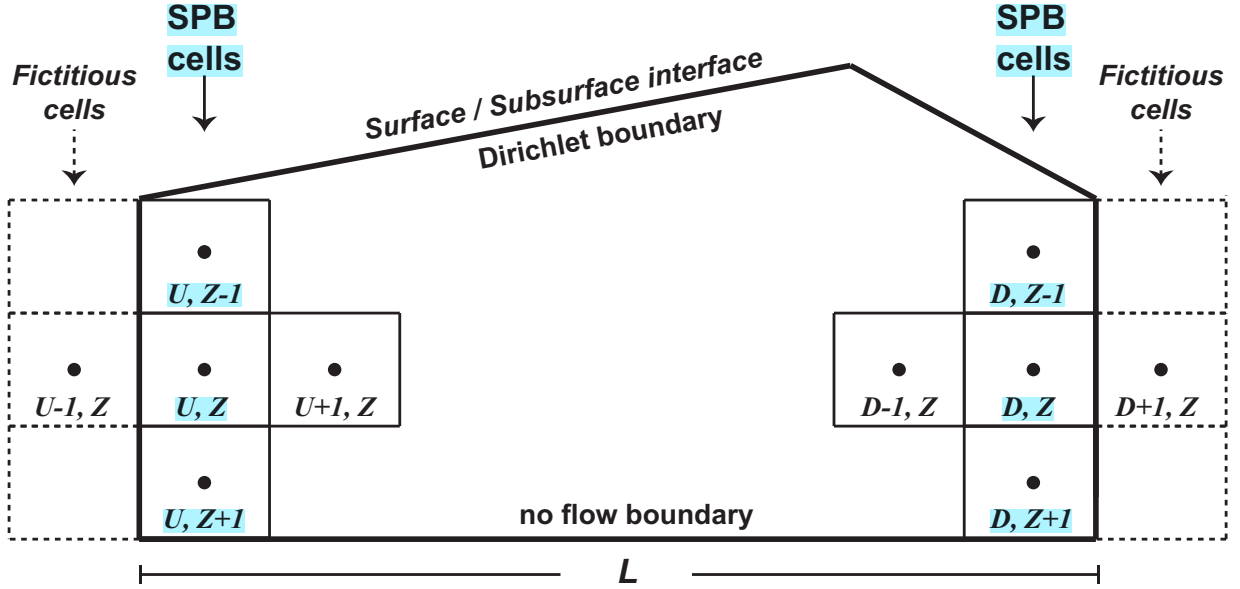


FIGURE 2.2: The modelled bedform with SPB cells on the lateral boundaries. Fictitious cells located in adjacent unmodelled bedforms provide the nodes required to apply the Δh term and maintain identical head gradients across the lateral boundaries. U and D indicate the upstream and downstream lateral boundary column indices, respectively, and Z indicates the layer number. The Δh term is now applied between a node in the model and its corresponding fictitious node, e.g. U, Z and $D + 1, Z$.

cells due to the offset by half a cell width of the nodes and cell boundaries in the finite-difference grid. Fictitious nodes attached to the SPB cells (Figure 2.2) are introduced to enable the application of Equation 3.1 in a block-centred finite-difference grid via the following expressions:

$$h_{U-1,Z} = h_{D,Z} + \Delta h \quad (2.4)$$

$$h_{D+1,Z} = h_{U,Z} - \Delta h \quad (2.5)$$

where the subscripts U and D indicate the upstream and downstream lateral boundary column indices, respectively, and Z indicates the layer number. In this manner, upstream SPB cells are related to the fictitious cells attached to the downstream SPB cells and vice versa.

To illustrate the development of the appropriate numerical formulation for the SPB in

MODFLOW, a modified form of MODFLOW's finite-difference equation can be developed by considering the flow between nodes U and $U + 1$ in Figure 2.2 according to the finite-difference form of Darcy's Law:

$$Q = \frac{KA}{d}(h_{U+1,Z} - h_{U,Z}) \quad (2.6)$$

where Q is the volumetric flow rate across the cell face [L^3T^{-1}], K is the hydraulic conductivity [LT^{-1}], A is the cross-sectional flow area [L^2], and d is the distance between two nodes [L]. Similar expressions can be written for the flow across the other cell faces. The negative sign usually incorporated into Darcy's Law can be omitted by adopting the MODFLOW convention, which considers inflows to any cell via each face as positive (Harbaugh 2005). The term KA/d is called conductance C [L^2T^{-1}] and here, for the sake of brevity, we assume constant C values between all cells (i.e., homogeneous and isotropic conditions, and uniform cell dimensions), although both the methodology and subsequent MODFLOW implementation applies to situations where C varies spatially.

To facilitate ease of explanation, the current study develops the method for steady state conditions only. In this case, conservation of mass of a constant-density fluid, non-deformable bedform requires the sum of all fluxes into and out of a cell to add up to zero. Therefore, for cell (U, Z) in the absence of external sinks or sources, it holds that:

$$C(h_{U+1,Z} - h_{U,Z}) + C(h_{U,Z-1} - h_{U,Z}) + C(h_{U-1,Z} - h_{U,Z}) + C(h_{U,Z+1} - h_{U,Z}) = 0 \quad (2.7)$$

To account for the flux from the adjacent bedform, and due to Equation 2.4, the term $C(h_{U-1,Z} - h_{U,Z})$ can be replaced with $C(h_{D,Z} + \Delta h - h_{U,Z})$, so that inserting and rearranging gives:

$$Ch_{U+1,Z} + Ch_{U,Z-1} + Ch_{U,Z+1} + (-4C)h_{U,Z} = -C(h_{D,Z} + \Delta h) \quad (2.8)$$

Similar, for a cell (D, Z) on the right SPB boundary, making use of Equation 2.5:

$$Ch_{D-1,Z} + Ch_{D,Z-1} + Ch_{D,Z+1} + (-4C)h_{D,Z} = -C(h_{U,Z} - \Delta h) \quad (2.9)$$

Equation 3.1 is satisfied by virtue of the fictitious cells and the user specified Δh term. At the same time, identical head differences between fictitious cells and their attached SPB cells exist at both boundaries, that is $|(h_{U-1,Z} - h_{U,Z})| = |(h_{D+1,Z} - h_{D,Z})|$. Provided that identical values of the conductance C are assigned to fictitious cells within the same layer, the volumetric flow rate into the modelled domain across the left boundary in Figure 2.2 equals the flow rate out of the model across the right boundary. Thus, periodicity of the total flow rate across the boundaries is satisfied, however, the constraint on the flow direction at both boundaries, specified through Equations (3.2) to (3.3), is not. This effectively results in a relaxed implementation of the SPB, which nevertheless functions appropriately as evidenced in the verification examples.

2.4 Implementation

Comparison of Equations (2.8) to (2.9) shows two differences to the finite-difference expression for a variable-head boundary cell in MODFLOW on one side (excluding any sources, sinks or head-dependent boundary conditions). The first difference is that in Equations (2.8) to (2.9), the multiplication factor for $h_{U,Z}$ and $h_{D,Z}$ is equal to $-4C$, whereas with a variable-head cell in MODFLOW this would be $-3C$. The second difference is that the right-hand sides of Equations (2.8) to (2.9) are non-zero. The required modifications to the standard finite-difference equations are easily accomplished through the modification of the appropriate terms in the HCOF and RHS arrays. Readers are referred to the MODFLOW user manual [Harbaugh, 2005] for a detailed description of the HCOF and RHS array terms. For both the upstream and downstream SPB, a value of $-C$ needs to be added to the HCOF coefficients of the cells on these boundaries. The RHS terms of the upstream boundary cells require the following addition:

$$RHS_{U,Z} = -C(h_{D,Z} + \Delta h) \quad (2.10)$$

while the downstream boundary cells require:

$$RHS_{D,Z} = -C(h_{U,Z} - \Delta h) \quad (2.11)$$

The implementation of a SPB in the MODFLOW code is in fact very similar to that of the well-known general head boundary (GHB). The difference is, however, that the RHS terms in MODFLOW normally include only those values that remain constant throughout the model run, while for the implementation of the SPB, the RHS terms must be updated with appropriate values of $h_{U,Z}$ and $h_{D,Z}$ after every outer iteration. The head values for all active model cells are continually updated and stored in the HNEW array throughout the iterative process. Altering the system of equations via iterative RHS updates rather than explicit manipulation of the coefficient matrix is preferable for codes such as MODFLOW, which rely on the coefficient matrix having a regular symmetric banded structure [Panday and Langevin, 2012]. The dynamic updating RHS terms with values from the HNEW array is not unique to the SPB implementation. For example, the drain return (DRT1) package for MODFLOW [Banta, 2000] links two cells within the grid together in a similar manner to the SPB: A drain return pair consists of one cell that holds a drain and another cell that returns a user defined percentage of the drained volume. It should be noted though that, despite the similarities between a drain return and a SPB, the DRT1 package cannot be used to provide spatial periodic function.

The SPB condition was implemented by modifying the source code of MODFLOW-2005 [Harbaugh, 2005]. SPB cells are identified through an input file, in which the conductance between modelled and fictitious cells is specified. Manual entry of conductance values for SPB cells using the method presented in this document, places the responsibility of input consistency on the user. Automated conductance calculation based on

user-specified values of K and mesh geometry is possible, and will be the subject of future development.

At the start of the model run, the entries in the HCOF array for each SPB cell are updated with the appropriate values based on the user-specified conductances of the boundary cells. The modified code determines which RHS term is applied, which is either Equation 2.10 for upstream SPB nodes, while downstream nodes receive the term given by Equation 2.11. The modified GHB package source code used in this study is provided in A.

2.5 Verification

To verify the implementation of the SPB in MODFLOW, the numerical results obtained using the modified code were compared to the results of an analytical solution of a sinusoidal head distribution over a flat bedform for a horizontally infinite, vertically semi-infinite (from 0 to $-\infty$), homogeneous and isotropic domain [Elliott and Brooks, 1997a]. The head distribution along the top boundary (Figure 2.3a) is given by:

$$h_{z=0} = h_m \sin(kx) \quad (2.12)$$

in which h_m is the amplitude of the head variation [L], x is the horizontal distance from origin [L], z is the vertical distance from the origin [L], and k [L^{-1}] is the wavenumber of variation ($k = \frac{2\pi}{\lambda}$), λ bedform wavelength [L]). The head h in the streambed is given by [Elliott and Brooks, 1997a]:

$$h = h_m \sin(kx) e^{kz} \quad (2.13)$$

The analytical solution according to Equations (2.11) to (2.12) is presented in Figure 2.3b, for a domain that extends from -1.5 m to 16.5 m in the x -direction, and 0.0 to -3.0 m in the z -direction. The semi-infinite vertical domain of the analytical solution

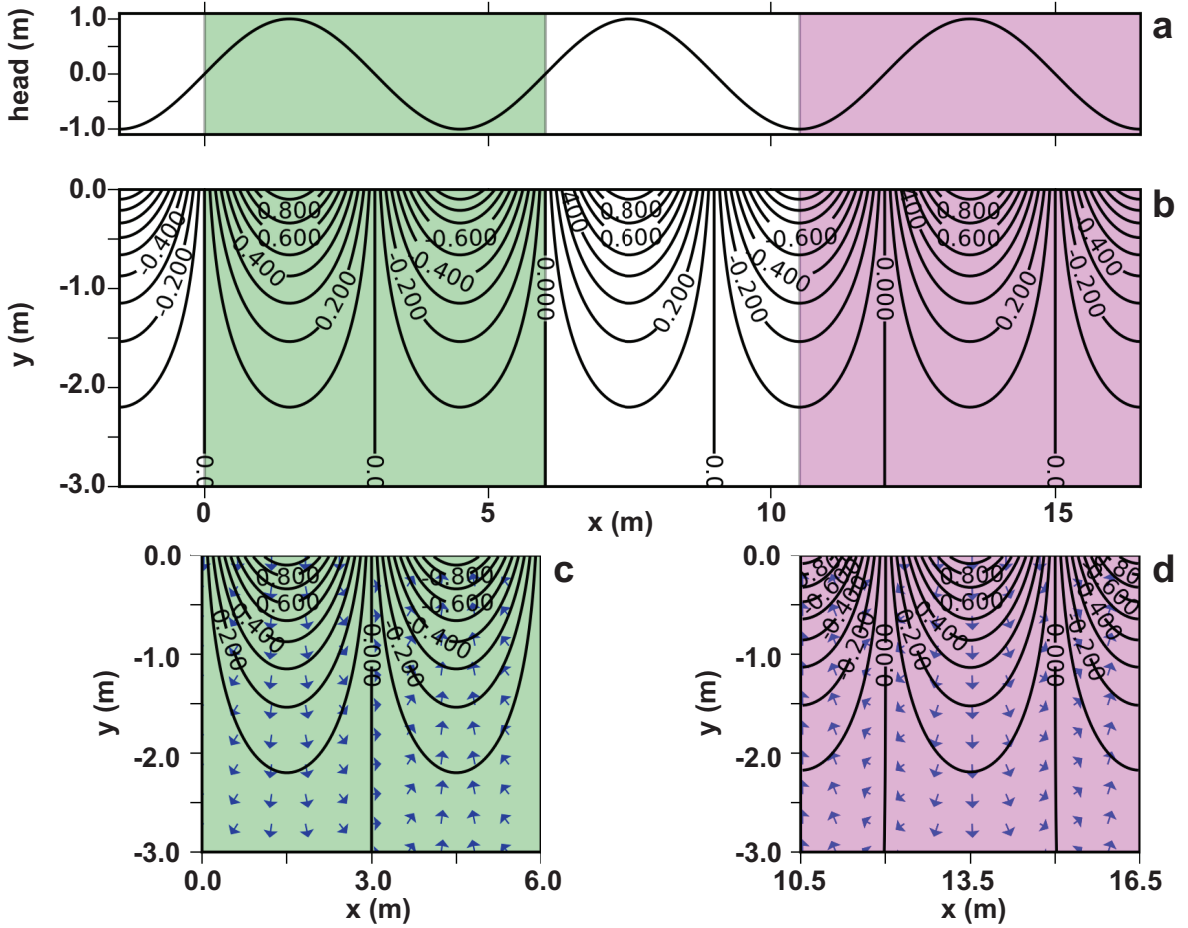


FIGURE 2.3: (a) Sinusoidal head distribution used for the top boundaries of both the analytical and numerical models. (b) The analytical solution of a model using the sinusoidal head distribution as a specified condition on the top boundary. (c), (d) MODFLOW’s solutions to the shaded areas of (a) and (b) when using a SPB condition on the lateral boundaries.

differs from the no flow condition imposed at the bottom boundary of the MODFLOW model. Following a series of trial runs, the bottom boundary was increasingly lowered to a depth of -5.70 m, after which there was no more visual improvement between the match between head contours of the numerical solution and those of the analytical. At this depth, the vertical flow velocities are less than 1% of the maximum vertical velocities found at the surface.

Parameters used in the MODFLOW models depicted in Figure 2.3c and Figure 2.3d are provided in column 2 of Table 2.1. These simulations have a Δh value of zero. The shaded regions in Figure 2.3a and Figure 2.3b indicate the domains modelled in MODFLOW using SPBs on the lateral boundaries (Figure 2.3c and Figure 2.3d).

As a second verification example, a homogeneous and isotropic bedform model, physically similar to that of [Cardenas and Wilson, 2007a] was constructed using MODFLOW, to test the application of the SPB with a non-zero Δh value. Inclusion of the Δh term creates a flow regime beneath the hyporheic exchange termed underflow, which reduces the depth penetration of the hyporheic flow cell [Cardenas and Wilson, 2007c]. Parameters for the MODFLOW bedform model are given in column 3 of Table 2.1. A hydrostatic subsurface head distribution was adopted as a starting condition for the MODFLOW simulation. The prescribed heads assigned to the top boundary nodes correspond to published interface head distributions from experiments in which the surface water domain was modelled explicitly [Cardenas and Wilson, 2007a].

The calculated head distribution and resultant flow field was compared to a multiple bedform model comprised of 15 bedforms. A similar approach was used by Savant et al. [1987] and Rutherford et al. [1995] in their numerical experiments. Both investigations utilised a 3 bedform model to minimise the effect of hydrostatic lateral boundaries on the solution of the central bedform. The purpose of the multi-bedform model in this instance was to obtain a spatially-periodic flow field to which the single bedform simulation, calculated with the SPB, could be compared. The grid of the single bedform model was repeated 15 times to create the multi-bedform model. The large number of bedforms was necessary to ensure the head distribution in the central (8th) bedform was minimally impacted by the lateral boundaries. At the two outer lateral boundaries, Dirichlet conditions were applied, with all nodes assigned the same value as the top boundary node at that boundary.

The central bedform was assigned an identical prescribed head distribution along its top boundary as in the SPB model. All other bedforms had the same upper boundary head distribution profile but the head values were adjusted to account for Δh (Figure 2.4a). In this manner, a regional gradient of 0.01 was maintained across the entire model (Figure 2.4b). A comparison of the head distribution and flow field between the SPB model (Figure 2.4c) and the 8th bedform (Figure 2.4d) shows no discernible differences.

Parameter	Sinusoidal Head Models	Bedform Models	Units
Row width Δx	1.0	1.0	m
Number of rows	1	1	
Column width Δy	0.06	0.01	m
Number of columns	100	100	
Layer width Δz	0.03	0.01	m
Number of layers	190	100	
Hydraulic conductivity K	1.0	0.01	md^{-1}
Bedform peak location	N/A	0.9	m
Peak height	N/A	1.05	m
Δh	0	0.01	m

TABLE 2.1: MODFLOW model parameters used in the verification examples

The logarithm of absolute head differences indicates that both bedform models report identical head values up to and including the 6th decimal place (Figure 2.4e).

Different MODFLOW solver packages were tested with the bedform model. The strongly implicit procedure (SIP), which only performs outer iterations, was unable to converge on a solution for the bedform model. The iteratively updated RHS terms associated with SPB's in MODFLOW perform best with a solver that performs both inner and outer iterations. This is due to the increased accuracy of the partial solution obtained during inner iterations which culminates in more accurate head values assigned to the fictitious cells. The preconditioned conjugate-gradient (PCG) solver and the direct solver (DE4) were able to converge on a steady-state solution. A large number of outer iterations was required by both solvers (≥ 1000) however. The PCG was significantly faster, converging in less than 5 minutes, compared to 11 minutes for the DE4.

2.6 Discussion and conclusions

Head contours of the MODFLOW models (Figure 2.3c and 2.3d) were found to be consistent with those of the analytical solution (Figure 2.3b). This demonstrates that the SPB in MODFLOW produces a numerical solution for a singular spatially repetitive unit, which is consistent with an analytical of infinite repetitions. The multi-bed verification example was performed using a 9, 11 13 and 15 bed model with decreasing

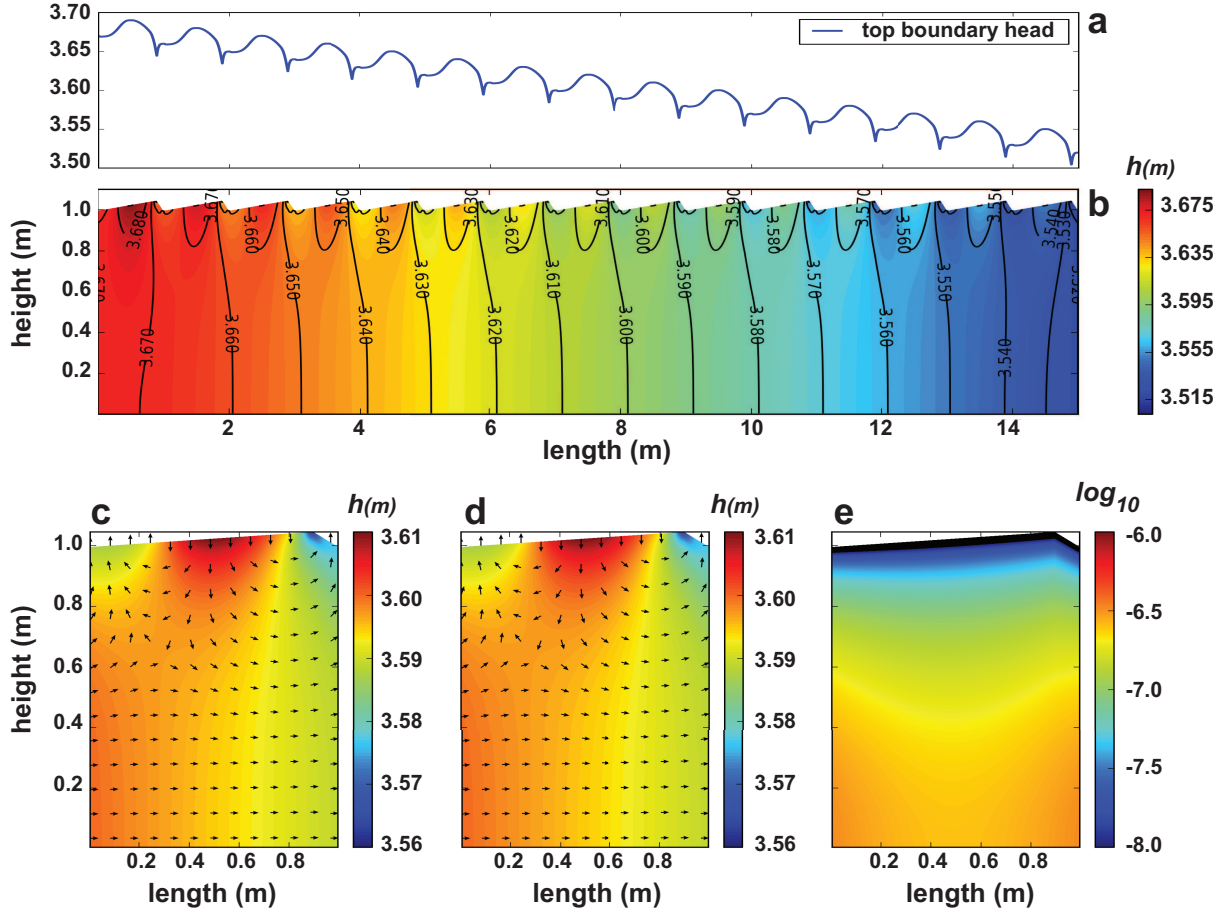


FIGURE 2.4: (a) The specified head profile assigned to the top boundary of the multi bedform model with a gradient of 0.01 metres maintained across the entire domain. (b) The solved head distribution for the 15 bedform model where departure from spatial repetition is clearly evident at the lateral boundaries. (c) MODFLOW solution to a single bedform model solved using the SPB. (d) MODFLOW solution for the 8th bedform in the multi-bedform model. (e) The logarithm of absolute head difference between the two solutions for a single bedform.

differences observed with increasing bedform numbers, suggesting that differences between the single bed and central bed of the multi-bed model are likely to decrease further with an increasing number of bedforms. The invariant head with depth specified by the Dirichlet conditions at the lateral boundaries of the multi-bed model are considered to be the cause of the increasing differences with depth observed in the lower half of Figure 2.4e. The multi-bed model converges faster and is feasible as a means for obtaining a spatially periodic flow solution. However, the number of spatial repetitions required is unknown *a priori* as it is a function of the head distribution along the top boundary. The time saved applying the SPB with a single spatial repetition far outweighs the time investment necessary to develop multiple models with increasing numbers of

spatial repetitions.

Solutions to some of the future challenges facing HZ research reside in numerical experiments capable of examining flow processes on spatial scales both too large and too small to be easily measured in the field [Krause et al., 2011]. This suggests increased use and development of theoretical type numerical models of bedform scale HZ flow processes for which the SPB is ideally suited. Recent bedform scale investigations have included solute [Jin et al., 2010] and variable density transport [Jin et al., 2010]. Review publications of the HZ [Krause et al., 2011] have further highlighted the need for reactive transport variants of these numerical models. Through the implementation of the SPB condition in MODFLOW, problems such as these can now be addressed using codes such as MT3DMS and PHT3D, provided that spatial periodicity of concentrations may be assumed.

Chapter 3

Spatial periodicity in bedform-scale solute and thermal transport models of the hyporheic zone

3.1 Abstract

Spatially periodic solute boundaries force symmetry across a model domain by ensuring that concentrations and concentration gradients are identical at the same location on opposite boundaries. They have been used in multiple publications on a hyporheic zone model of a single ripple or dune style bedform, including variable density flow and reactive transport variants. Simulations of multi-bedform models are evaluated without imposing spatially periodic transport to demonstrate that non-physical solute distributions arise from the periodic solute transport assumption. That is, the flow field within the single bedform model leads to a transport scenario that violates the forced symmetry of periodic solute boundary conditions, culminating in a physically unrealistic solute distribution. Our results show that lack of symmetry between boundaries is a function

of the vertical concentration gradient and two dimensionless parameters characterizing the hyporheic and underflow flow regimes, and the solute exchange between them. The error associated with the spatially periodic assumption is assessed based on an analysis of solute fluxes across the lateral bedform model boundaries. While the focus is on steady-state concentration distributions, the implications for transient solute transport models are also discussed. We conclude that periodic solute transport boundary conditions should be applied only to bedform models that have minimal vertical dispersive and diffusive solute transfer. This includes gaining systems and tracers such as temperature, for which a temporally-periodic flux reversal occurs across the top boundary.

3.2 Introduction

The hyporheic zone comprises the saturated subsurface sediments adjacent and beneath a stream that interact with streamflow via a bidirectional exchange of mass and momentum [Robertson and Wood, 2010; Bottacin-Busolin and Marion, 2010]. Exchanges of fluid and solutes between a stream and its hyporheic zone occur across a variety of spatial and temporal scales [Krause et al., 2011]. An important hyporheic exchange process is the flow of water through the streambed driven by the surface water pressure gradients arising from stream flow over morphological structures such as ripples or dunes [Shum, 1992; Elliott and Brooks, 1997a; Cardenas and Wilson, 2007a]. Interaction between groundwater and surface water within the hyporheic zone affects water quality in both the stream [Boulton et al., 1998; Storey et al., 2003] and the groundwater [Fleckenstein et al., 2006; Krause et al., 2009]. Quantifying hyporheic zone chemical transformation processes requires knowledge of the solute transport mechanisms associated with fluid fluxes in this region [Jin et al., 2010].

Hyporheic exchange at the ripple or dune bedform scale (≤ 1 m) was first described using dye tracers in a laboratory experiment [Thibodeaux and Boyle, 1987]. Head measurements over a bedform by Fehlman [1985] paved the way for numerical experiments investigating hyporheic exchange through streambed sediments that initially featured

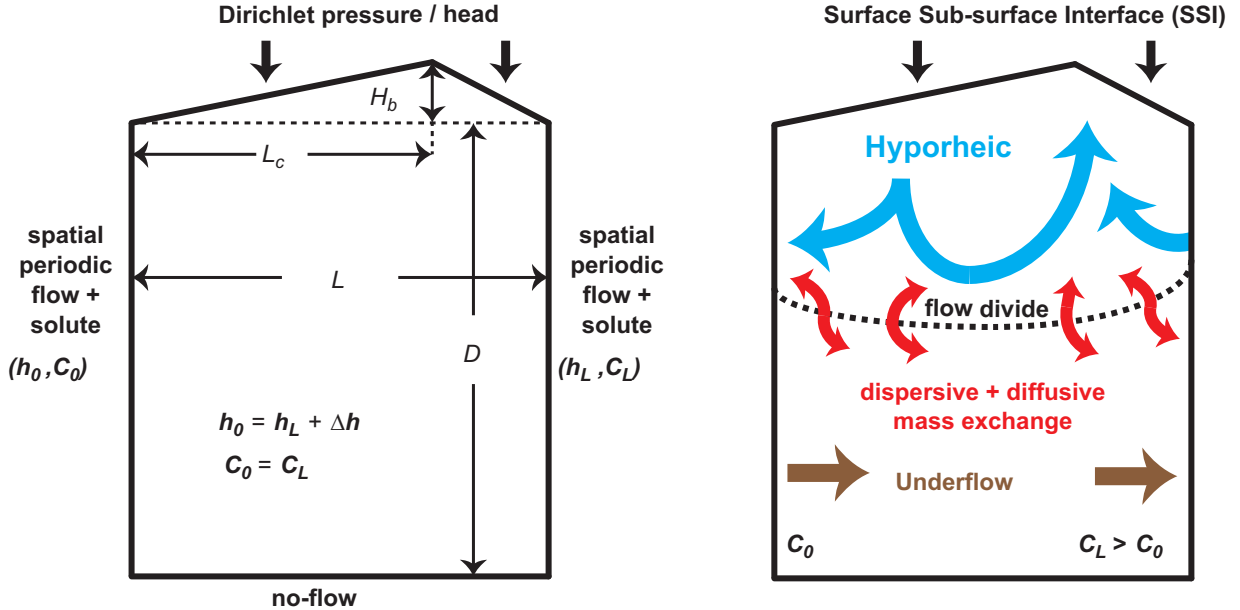


FIGURE 3.1: The Darcy domain of a typical bedform model with spatially periodic lateral boundaries for both flow and concentration.

two-dimensional, non-migrating triangular bedforms [Savant et al., 1987; Rutherford et al., 1995; Elliott and Brooks, 1997b], with measured pressure distributions applied as Dirichlet-type boundary conditions along the surface-subsurface-interface (SSI, Figure 3.1). More recent bedform numerical investigations use computational fluid dynamics (CFD) approaches, where flow in both the surface water (Navier-Stokes equations) and the subsurface sediments (Darcy's equation) is simulated [Cardenas and Wilson, 2007a; Jin et al., 2010].

The bedform model originally used by Cardenas and Wilson [2007d] is featured in numerous hyporheic flow and transport investigations, which are listed in Table 1. The physical dimensions vary slightly between studies, but in all cases the subsurface domain is bounded by a single triangular bedform (Figure 3.1), which is assumed to be one of an infinite series of physically identical bedforms with identical head distributions along the SSI. This is accomplished by using lateral boundaries that are spatially periodic with respect to both flow and head. That is, at any given elevation, the flow rate and direction are identical at opposite ends of the model domain. The flow fields that have been simulated this way are characterised, following Cardenas and Wilson [2007d], by two separate flow regimes in the subsurface (Figure 3.1): (1) A hyporheic flow cell in

Study	Transport	K (ms^{-1})	α_L (m)	α_t (m)	θ
Bardini et al. [2012]	reactive	$1.0e^{-4} - 5.0e^{-3}$	10^{-3}	10^{-4}	0.4
Cardenas et al. [2008]	reactive	$1.0e^{-4} - 1.2e^{-3}$	10^{-2}	10^{-3}	0.3
Jin et al. [2011]	variable density	$2.5e^{-4} - 4.4e^{-3}$	NP	NP	0.46
Jin et al. [2010]	solute	$1.0e^{-3}$	$10^{-3} - 10^{-1}$	$10^{-4} - 10^{-2}$	0.3
Sawyer and Cardenas [2009]	solute	$1.8e^{-4}$	10^{-3}	10^{-4}	0.3
Cardenas and Gooseff [2008a]	solute	$2.0e^{-3}$	$10^{-3} - 10^{-1}$	$10^{-4} - 10^{-2}$	NP
Cardenas and Wilson [2007a]	solute	$1.2e^{-3}$	NP	NP	0.325
Sawyer and Cardenas [2012]	thermal	$5.1e^{-5} - 1.8e^{-4}$	NA	NA	0.3
Cardenas and Wilson [2007b]	thermal	$1.0e^{-3} - 5.0e^{-2}$	NA	NA	0.3
Cardenas and Wilson [2007e]	thermal	$1.0e^{-3} - 5.0e^{-2}$	10^{-2}	10^{-3}	0.3
Cardenas and Gooseff [2008b]	None	$2.0e^{-3}$	NA	NA	NP
Cardenas and Wilson [2007c]	None	$1.0e^{-3}$	NA	NA	NP
Cardenas and Wilson [2007d]	None	$1.0e^{-3}$	NA	NA	NP

TABLE 3.1: Recent single bedform publications

the upper part of the subsurface develops due to the head distribution applied at the SSI, and (2) Underflow, which occurs beneath the hyporheic flow cells in the direction of stream flow due to the water level gradient in the stream. An imposed head difference Δh [L] between lateral flow boundaries of the bedform (Figure 3.1) accounts for the latter. It should be noted that certain situations exist where the underflow is effectively stationary (e.g. surface standing waves over a zero gradient streambed, Qian et al. [2008]) or where its direction may be vertical (e.g. gaining and losing systems, Cardenas and Wilson [2006]).

Solute transport bedform model experiments in previous studies (Table 1) have assumed that, analogous to the flow conditions, the concentration and concentration gradients at the lateral boundaries are spatially periodic. This assumption is reasonable for situations where underflow is non-existent or completely vertical. For scenarios with lateral underflow however, due to the diffusive and dispersive mass transfer that occurs between the hyporheic flow cell and the underflow in the presence of concentration gradients, true spatial periodicity for solute concentrations can never occur. Depending on the direction of the concentration gradient between the hyporheic flow cell and the underflow, water in the underflow will either gain or lose solutes from or to the hyporheic flow cell. Thus the underflow will exit the bedform with a different concentration than when it entered the bedform through the upstream boundary.

Parameter	Symbol	Value	Units
Bedform depth	D	2.0	m
Bedform length	L	1.0	m
Length to bedform crest	L_c	0.9	m
Bedform height	H_b	0.05	m
Grid spacing x direction	Δx	0.01	m
grid spacing z direction	Δz	0.01	m
Fixed head difference between SPB	Δh	$10^{-2}, 10^{-3}, 10^{-4}$	m
Amplitude of interface head distribution	a	0.022785	m
Hydraulic conductivity	K	10^{-3}	ms^{-1}
Longitudinal dispersivity	α_L	$10^{-1}, 10^{-2}, 10^{-3}$	m
Dispersivity ratio	α_T/α_L	1/3	m
Molecular diffusion	D_m	10^{-9}	ms^{-2}
Porosity	θ	0.3	
Bulk density	ρ_b	2200	kgm^{-3}
Thermal diffusivity	D_{th}	$1.36e^{-6}$	m^2s^{-1}
Thermal distribution coefficient	K_d	$1.9e^{-4}$	m^2kg^{-1}
Bulk thermal conductivity	K_o	1.71	$\text{Wm}^{-1}\text{°C}^{-1}$
Specific heat capacity of water	c_w	4187	$\text{Jkg}^{-1}\text{°C}^{-1}$
Density of water	ρ_w	1000	kgm^{-3}
Specific heat capacity of sand	c_s	795.53	$\text{Jkg}^{-1}\text{°C}^{-1}$

TABLE 3.2: Parameters used in numerical experiments

While truly periodic conditions can thus never develop, spatial periodicity may be approached when diffusive and dispersive transfer between the two flow domains is small. Our objective is to investigate the degree to which solute concentration patterns deviate from spatial periodicity for a range of model parameters used in previous studies (Table 3.1 and Table 3.2). To this end, the steady-state behaviour of a solute beneath a bedform is examined by modelling a series of multiple adjacent bedforms and evaluate the concentrations and concentration gradients across each to infer the error imposed by spatially periodic solute boundaries (SPSB).

3.3 Methods

Previous multi-bedform numerical investigations comprise studies, examining the effects of heterogeneity [Salehin et al., 2004; Sawyer and Cardenas, 2009], suspended particle filtration [Karwan and Saiers, 2012] and in conjunction with flume experiments [Janssen et al., 2012]. Three scenarios are modelled with a solute source along the SSI: (1) a

no-flow bottom boundary, (2) a gaining system and, (3) a losing system [Cardenas and Wilson, 2007a,c; Jin et al., 2010; Sawyer and Cardenas, 2009]. The number of bedforms are varied to assess whether the model converges to a periodic solution.

Here, a fourth scenario is also examined in which the solute boundary along the SSI is replaced with a time-variant, sinusoidal thermal boundary to reflect the diurnal temperature cycle. Unlike the solute boundary, the temporal variation in the thermal forcing produces a reversal of the thermal gradient, and it is hypothesised that as a result, spatial periodicity of the temperature field may develop.

To constrain our suite of experiments to scenarios of practical interest, the method of Qian et al. [2008] is adopted, who showed via dimensional analysis of the governing equations for the bedform model that the following variables control the net mass flux across the SSI: the amplitude of the variation in head distribution along the SSI of a single bedform a [L]; the longitudinal dispersivity α_L [L]; the bedform length L [L]; and the stream slope s ($= \Delta h/L$). They combined these variables in two dimensionless parameters: a steepness ratio, $R = a/(Ls) = (a/\Delta h)$ and a length-scale parameter, $\lambda = \alpha_L/L$. Qian et al. [2008] showed that R values ranging from 1 to 1000 are of practical interest, and that values greater than 100 appear to produce similar solute distributions. They also showed that λ values for bedforms found along a gravel streambed are typically between 0.001 and 0.1.

3.3.1 Flow models

The finite-difference groundwater modelling code MODFLOW-2005 [Harbaugh, 2005], which was modified by Laattaoe et al. [2013] is used to include a spatially periodic boundary (SPB) condition to solve for groundwater flow. Periodicity of flow is achieved with the following relationships at the lateral boundaries:

$$h(0, z) = h(L, z) + \Delta h \quad (3.1)$$

$$u(0, z) = u(L, z) \quad (3.2)$$

$$v(0, z) = v(L, z) \quad (3.3)$$

Where h represents the hydraulic head [L], and u and v are the horizontal (x) and vertical (z) components of the pore water velocity [LT^{-1}], respectively. The left and right vertical faces of the SPB are denoted by $(0, z)$ and (L, z) , respectively.

Three flow scenarios are modelled, each with a different bottom boundary condition. The first group of simulations features a no-flow condition at the base. The second group of simulations considers a gaining stream scenario, which is accomplished by applying a Neumann-type boundary condition along the model bottom boundary. The prescribed fluid flux across the bottom boundary is fixed at $3.0 \times 10^{-3} \text{ ms}^{-1}$, producing a gaining scenario comparable to those used in previous investigations [Cardenas and Wilson, 2006, 2007e]. The third group of simulations considers losing stream scenarios, for which the bottom boundary flux was of equal magnitude but opposite in direction to the gaining scenarios.

Physical dimensions of the single-bedform models are consistent with previously published investigations in Table 3.1, except for the model depth (D), which, in a similar manner to Bottacin-Busolin and Marion [2010], is increased in the present study to $2L$ to minimise the effect of the bottom boundary on the solute distributions. Grid cells have 0.01 m width in the horizontal direction and heights that vary between 0.01 and 0.01025 m, to accommodate variations in the bedform height. The models feature Δh at 0.01, 0.001 and 0.0001 m so that R values for simulations are 2.27852, 22.7852 and 227.852 covering the range examined by Qian et al. [2008]. The interface head distribution from the CFD-type bedform study by Cardenas and Wilson [2007a, figure 3 therein] is adopted, to apply as a Dirichlet-type boundary along the SSI. The head distribution features a maximum found approximately midway along the rising face, and steep head gradients lead to a minimum head at the peak of the bedform (Figure 3.2).

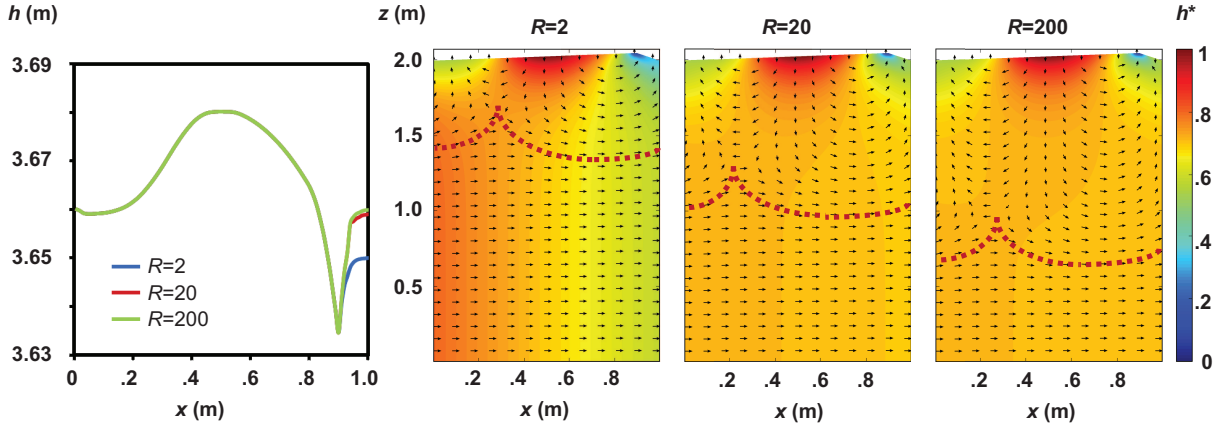


FIGURE 3.2: Top boundary head distributions used in single-bedform models and solutions to the different R scenarios. Heads are normalised as $h^* = (h - h_{min})/(h_{max} - h_{min})$ where h is the nodal head value and h_{min} and h_{max} are respectively the minimum and maximum head for each simulation. Dashed lines delineate the hydraulic divide between hyporheic flow cells and underflow.

Our multi-bedform models comprise 11 bedforms (numbered sequentially from left to right). The porous medium is considered homogeneous and isotropic, and flow is in steady-state. The flow fields in each individual bedform are derived from single-bedform models subject to the spatially periodic flow constraints at the lateral boundaries according to Equations (3.1) to (3.3). The same flow conditions as in the single-bedform models (Figure 3.2) are enforced in the multi-bedform models by specifying the heads (Dirichlet-type boundary condition) at all nodes along the model perimeter. The top, left and bottom boundary nodes of bedform 1 (i.e. the most upstream bedform) in the multi-bedform model are equal to those in the single-bedform model. Fixed heads along the top and bottom boundaries of downstream bedforms are less by Δh relative to the bedform immediately upstream. The right boundary heads of bedform 11 are assigned fixed values equivalent to the left boundary of bedform 1 less 11 times Δh . Periodicity is verified by ensuring fluid flux between the two lateral boundaries of each bedform varies by less than 10₇%. The parameters used in the flow model are presented in Table 2. Both single- and multi-bedform models are executed with calculations in double precision and head convergence criteria set at 10₁₄ m.

3.3.2 Solute transport models

Transport in the multi-bedform model is simulated with MT3DMS, which implements the following general form of the mass transport equation for solutes [Zheng and Wang, 1999]:

$$(1 + \frac{\rho_b}{\theta} K_d) \frac{\partial(\theta C)}{\partial t} = \nabla \cdot (\theta \mathbf{D} \cdot \nabla C) - \nabla \cdot (\mathbf{q} C) + q_s C_s \quad (3.4)$$

where C is concentration [ML^{-3}], t is time [T], θ is porosity, ρ_b is the bulk density [ML^{-3}], K_d is the distribution coefficient [L^3M^{-1}], \mathbf{q} is the specific discharge vector [LT^{-1}], \mathbf{D} is the hydrodynamic dispersion tensor [L^2T^{-1}] (i.e., $\mathbf{D}=\mathbf{D}_{mech}+\mathbf{D}_m$, where \mathbf{D}_{mech} is the mechanical dispersion tensor [L^2T^{-1}] and \mathbf{D}_m is the molecular diffusion coefficient [L^2T^{-1}]), q_s [LT^{-1}] is the volumetric flow rate per unit volume representing fluid sources or sinks, and C_s [ML^{-3}] is the concentration of the source.

The initial concentration in the domain is set to zero everywhere, i.e., $C(x, z, t = 0) = 0$. The solute flux into the domain through the top, left and bottom (in the gaining scenarios) boundaries is implemented by a Cauchy condition. Cauchy-type boundary conditions in MT3DMS consider only advective transport and ignore dispersive mass flux across boundaries [Zheng and Wang, 1999]. Flow entering across the top boundary is assigned a concentration of 1.0 gL⁻¹ while inflow across the lateral and bottom boundaries has a concentration of zero. In all cases outflow has the ambient groundwater concentration. Our no-flow bottom boundary simulations feature a Neumann condition for solutes along the lower boundary with a concentration gradient of zero, ensuring no mass exchange at the base of the model.

We hypothesise the departure of solute concentration patterns from spatial periodicity to be a function of the model parameters that control mass exchange between the hyporheic flow cells and underflow. The dimensional analysis of Qian et al. [2008] showed that the ratio of longitudinal to transverse dispersivity (α_T/α_L) significantly affects the transport solution. However, commensurate with previous investigations, a fixed value of 1/3

is maintained [Zheng and Bennett, 1995; Bottacin-Busolin and Marion, 2010]. Our simulations adopt the λ values 0.1, 0.01 and 0.001 used by Qian et al. [2008] which, due to our fixed bedform length of 1 m, doubles as α_L values. Effective porosity is assigned a value of 0.3 for all models. Our transport simulations are time-dependent, based on the steady-state flow fields, and transport calculations are in double precision with concentration convergence criteria set to 10^{-14} gL⁻¹. Other relevant model parameters are located in Table 3.2. An upstream weighted finite-difference solution technique is used to solve the advective component of all simulations ensuring mass conservation [Zheng and Bennett, 1995]. Our simulations are run until the concentration field reaches a steady-state, which we observe to be when the total mass gain is less than 0.1% from the previous transport step per bedform.

The number of bedforms simulated is extended by using multi-bedform models and assigning the concentrations along the right boundary of bedform 10, obtained after the solute concentrations reach steady state, to a Cauchy condition along the left boundary of bedform 1. Taking the concentrations of the tenth bedform minimizes any potential boundary effects that occur at the right boundary of bedform 11 due to the neglecting of the dispersive solute flux across the model boundary. Each repetition of this process extends the number of consecutive bedforms by 10, allowing for an extensive number of bedforms (and spatial convergence of solutes) to be assessed.

A comparison of vertical mass flux in each bedform and advective mass transfer between bedforms is performed using the analysis method of Qian et al. [2008]. The vertical mass flux at any vertical position z , integrated over one bedform length L , is separated into dispersive (J_{disp}) and advective (J_{adv}) components:

$$J_{disp}(z) = \frac{1}{L} \left(\int_0^L -D_{zz} \frac{\partial C}{\partial z} dx + \int_0^L -D_{zx} \frac{\partial C}{\partial x} dx \right) \quad (3.5)$$

and

$$J_{adv}(z) = \frac{1}{L} \int_0^L v C dx \quad (3.6)$$

Mass transfer across lateral boundaries between bedforms is analysed and values in the hyporheic flow cell are expected to be comparatively larger than in the underflow due to greater fluid fluxes and concentrations. By restricting the analysis of lateral boundary mass transfer to the underflow only, a better resolution of differences between bedforms is obtained. To this end, the dimensionless advective mass flux ($J_{adh}L/C_0Ka/\theta$) of Qian et al. [2008] is adopted for comparison of lateral boundary mass transfer between bedforms, where:

$$J_{adh}(L, z) = \int_0^H u C dz \quad (3.7)$$

and H [L] is the depth in the model where the flow divide intersects the bedform boundary.

3.3.3 Thermal transport models

Thermal transport is simulated in MT3DMS according to Ma and Zheng [2010], by replacing C in Equation 3.4 with temperature T ($^{\circ}\text{C}$), K_d [L^3M^{-1}] with a thermal distribution coefficient $c_s/c_w\rho_w$ (where c_s [$\text{ML}^2\text{T}^{-2}\Theta^{-1}$] and c_w [$\text{ML}^2\text{T}^{-2}\Theta^{-1}$] are the specific heat capacities of solid and fluid, respectively, and ρ_w [ML^{-3}] is the density of the fluid), and D_m [L^2T^{-1}] with a bulk thermal diffusivity term $\kappa_o/\theta\rho_w c_w$ (where κ_o [$\text{Wm}^{-1}\text{^{\circ}C}^{-1}$] is the bulk thermal conductivity of the porous matrix). Ma and Zheng [2010] also showed that density and viscosity effects are minor in thermal transport simulations with variations in temperature of less than 15°C across the domain, and hence changes in fluid density and viscosity induced by temperature variation are assumed negligible. The thermal transport parameters used in the study are presented in Table 3.2.

The Cauchy-type solute boundary along the top of the model is replaced with a spatially constant, time-variant thermal condition for temperature, which varies 10°C in a diurnal cycle according to:

$$T(t) = T_{ave} + T_{amp}[\sin(2\pi t/\tau)] \quad (3.8)$$

where T [°C] is the temperature of inflowing water, T_{ave} [°C] is the average temperature, T_{amp} [°C] is the amplitude of the variation, and τ [T] is the oscillation period. The following parameters are used: $T_{ave} = 20$ °C, $T_{amp} = 5$ °C and $\tau = 24$ hours. The average temperature is assigned as the initial temperature in all cells and the bottom, left and right boundaries are assigned a time-invariant thermal Cauchy condition with $T(t) = 20$ °C.

Equation 3.8 is used to alter the stream temperature every 6 minutes throughout a 5-day model run. In a similar manner to previous investigations [Cardenas and Wilson, 2007b,e], the phase-averaged temperatures are checked for each bedform to determine the time for conditions to stabilise (between days 3 and 4), after which we use a 24-hour period for analysis.

3.4 Results and Discussion

3.4.1 No-flow bottom boundary scenarios

The steady-state concentration distributions of 33 bedforms are presented in Figure 3.3, for various combinations of the dimensionless parameters R and λ . To facilitate comparison, dimensionless advective ($J_{adv}L/(C_oKa/\theta)$, cf. Equation 3.6) and dispersive ($J_{disp}L/(C_oKa/\theta)$, cf. Equation 3.5) values for the 6th, 16th and 26th bedforms are plotted (Figure 3.4) against dimensionless depth ($D^* = z/(H_b + D)$). Each graph corresponds to the simulations presented in Figure 3.3. Positive vertical flux values indicate downward migration of solute deeper into the bedform away from the SSI. Vertical

transport into the sediment in the hyporheic flow cells of each model is dominated by advection while dispersive fluxes prevail in the underflow (Figure 3.4). The transition from advective to dispersive dominated vertical transport is also an indicator for the depth of the flow divide between the hyporheic cells and underflow. These observations are consistent with the findings by Qian et al. [2008] and Jin et al. [2010]. Parameters L and a , remain constant throughout the investigation. Consequently, all changes to the dimensionless parameter R reflect changes in s the stream slope. An increase in stream slope (decrease in R) increases the horizontal flux of the underflow, which restricts the depth penetration of the hyporheic flow cell [Cardenas and Wilson, 2007d]. An order of magnitude decrease in dispersive flux is observed with an order of magnitude increase in R , which can be attributed to the weaker vertical concentration gradient, a direct consequence of the reduced horizontal flux in the underflow. All graphs reveal vertical flux differences in J_{adv} above the hydraulic divide as well as differences in J_{disp} across and below the divide. Both J_{adv} and J_{disp} flux values decrease with increasing bedform number, and peaks in J_{disp} are located deeper in the sediment as bedform number increases. This is indicative of solute concentrations fronts reaching to an ever greater depth with increasing distance downstream.

The continuously-increasing solute concentrations in the underflow of downstream bedforms act to weaken the vertical concentration gradient across the divide between the two flow regimes, which reduces the vertical solute fluxes in the hyporheic flow cells (Figure 3.4). This is because, once steady-state conditions have been attained, the mass in each bedform remains constant. As the conditions approach steady-state, less mass is lost from the hyporheic flow cell to the underflow, and the net mass flux across the SSI decreases to compensate for this. This implies that the deviation from spatial-periodicity causes a potentially significant variation along the streambed of the net solute flux across the SSI, which cannot be captured by a single bedform model using SPSB.

Figure 3.5 shows the dimensionless advective mass flux ($J_{adv}L/(C_oKa/\theta)$) between bedforms, with J_{adv} given by Equation 3.7. The plots in Figure 3.5 display a continuous increase of the horizontal advective mass flux between bedforms in the underflow, which

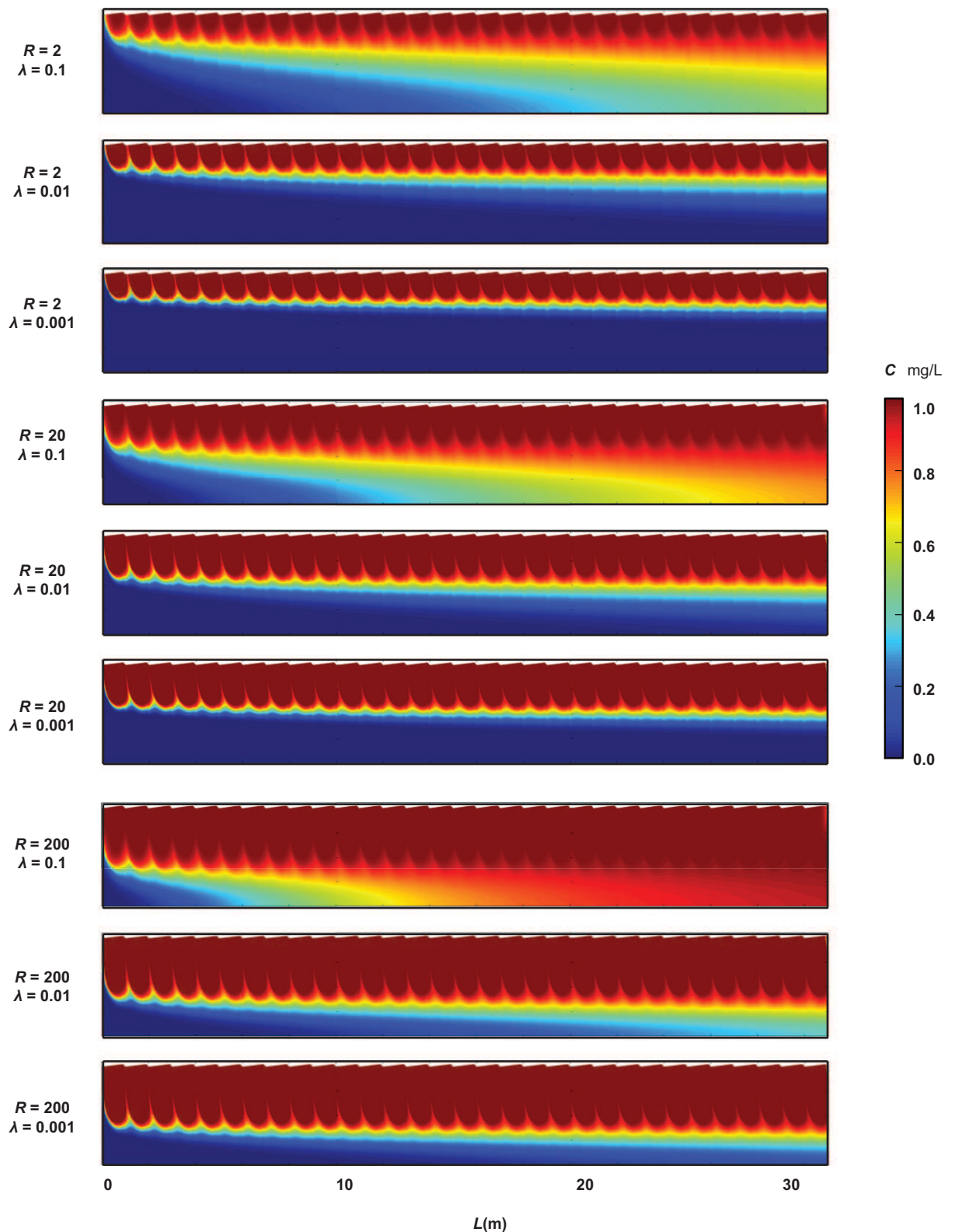


FIGURE 3.3: Steady-state solutions to solute transport simulations with no flow bottom boundaries.

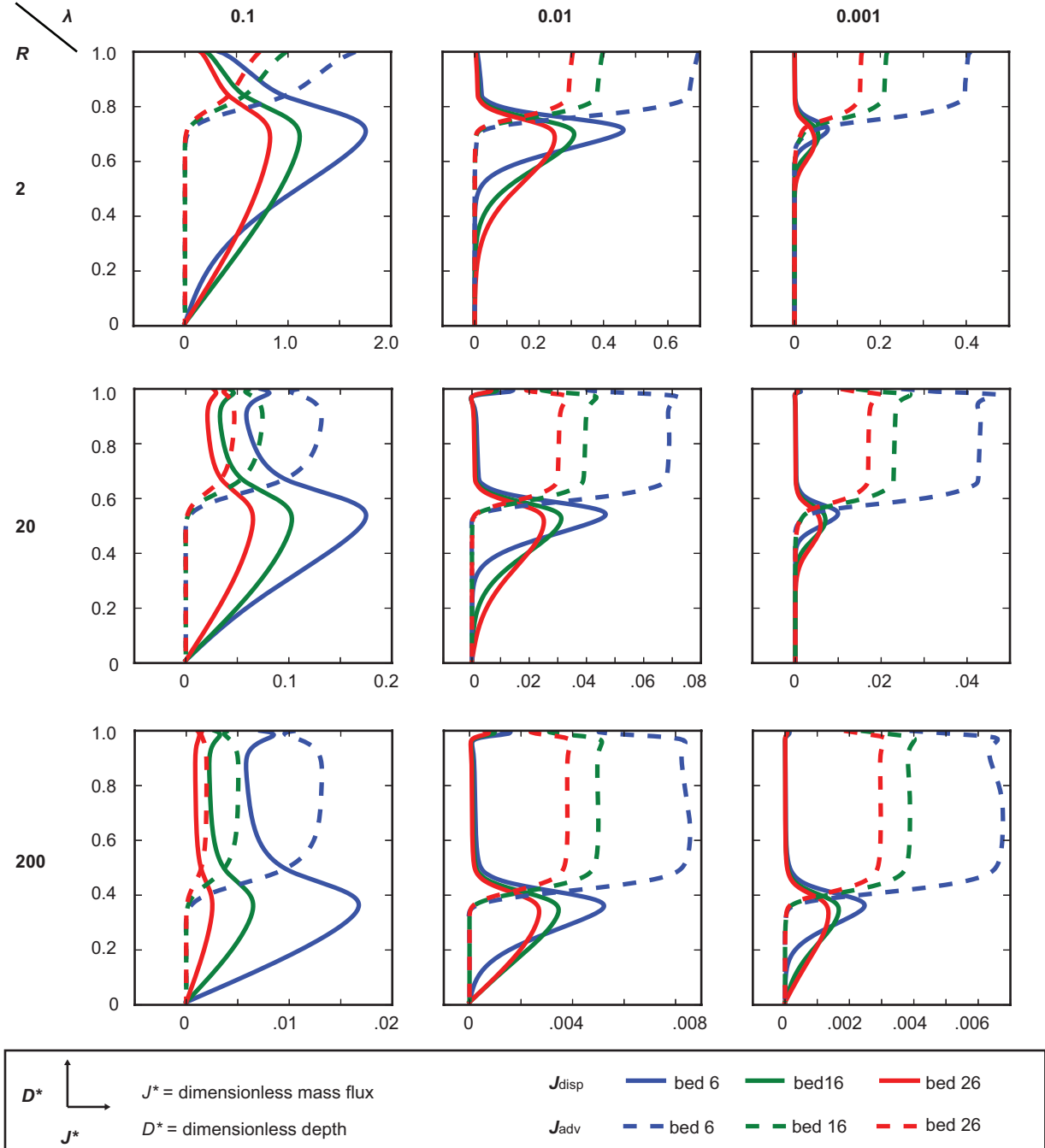


FIGURE 3.4: Horizontally integrated vertical mass fluxes for simulations with a no-flow bottom boundary. Positive values are indicative of mass migration deeper into the bedform. Advection dominates the transport of solutes in the hyporheic flow cells. In all cases dispersion is the primary transport mechanism for solute crossing the flow divide and penetrating the underflow. Spatial periodicity in this figure is represented by identical plots which overlap each other.

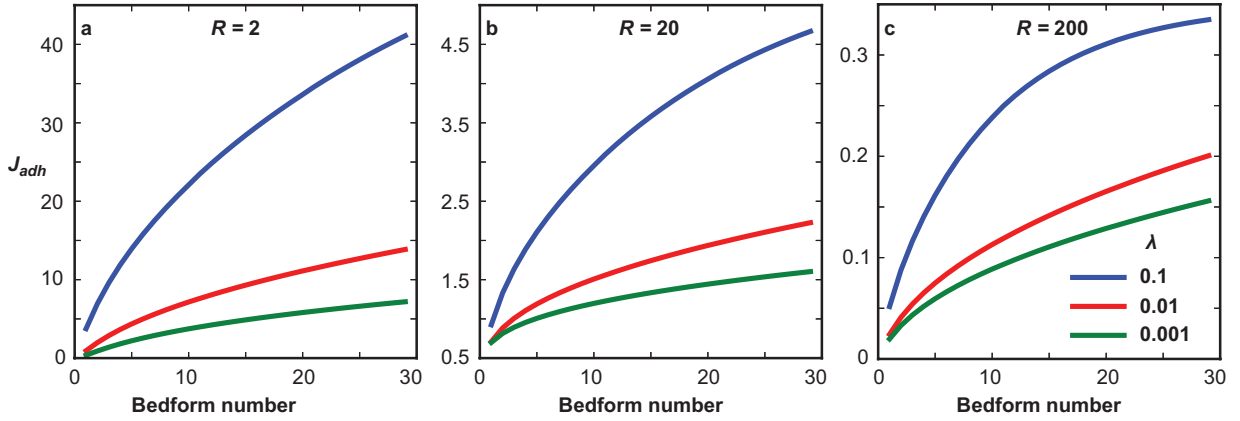


FIGURE 3.5: The changes in advective solute flux across lateral bedform boundaries in the underflow for all R and λ combinations. A periodic solution would produce horizontal lines.

is a consequence of the dispersive mass transfer from the hyporheic flow cell into the underflow. A horizontal line in this graph therefore represents spatial solute periodicity with mass transfer across the lateral boundaries identical for all bedforms. The rate of increase reduces gradually downstream, but the fact that the lines do not become horizontal indicates that spatial periodicity of the concentrations is not achieved for any of the combinations of R and λ considered. It should be noted that L remains fixed at 1.0 m for all experiments and was varied. Simulations with $\lambda = 0.1$ show significantly greater horizontal mass fluxes in the underflow but also present more pronounced curvature in Figure 3.5, specifically for $R = 200$. This is caused by the zero-concentration gradient boundary assigned to the base of the model, which acts to weaken the vertical concentration gradient (Figure 3.3).

These results confirm that, due to dispersion of solutes across the flow divide between the hyporheic flow cell and the underflow, spatially-periodic concentration distributions cannot exist, and that even for the scenario that approaches it the most ($R = 200$, $\lambda = 0.001$), the mass gain in the underflow between the upstream and downstream lateral boundaries is still in the order of 3% for each bedform. This value can be seen as the approximate lower bound of the mass balance error that would be introduced if spatial periodicity were imposed on a single bedform model in which the solute mass flux across the vertical boundaries are forced to be equal, thereby suppressing the mass

gain from one bedform to the next. The error can become as high as 20% for the highest values of R and λ .

While the focus of the present study is on steady-state solute concentration distributions, mass balance errors of comparable magnitude are expected to occur in the case of transient solute transport simulations of a single bedform in which the initial concentrations are zero and solutes are introduced through the SSI. Once solute enters the underflow, the combination of the prevailing horizontal flow and the SPSB enforces horizontal iso-concentration lines, which is a direct consequence of the fact that the concentration and the solute flux on both boundaries have to be equal. Accordingly, the mass gain in the underflow is overestimated by an amount that will increase with R and decrease with λ . As a result, the effective vertical concentration gradient will decrease, leading to an overestimation of the mass in the hyporheic flow cell as less mass is dispersed into the underflow, which in turn will affect the calculated solute transfer across the SSI.

Finally, the combination of a no-flow bottom boundary and a SPSB along the lateral boundaries in a single bedform are incompatible when non-zero solute concentrations develop at the bottom boundary during a transient simulation. This is because the periodic boundary condition prescribes that concentrations be equal at the same elevation, whereas the zero dispersive solute flux forces iso-concentration contours to be perpendicular to the bottom boundary. This induces a curvature of the concentration contour lines near the bottom boundary, which is merely an artefact of the combination of the two boundary conditions. This effect was not investigated in this study, but it further compounds the single-bedform approach for solute transport and considering all of the above, the periodic solute concentration boundary should probably be avoided altogether in single-bedform models with a no-flow bottom boundary.

3.4.2 Gaining and Losing scenarios

Gaining and losing scenarios will undoubtedly alter the flow field and with it the advectively transported solute mass. Our analysis approach examines vertical mass transfer

between the hyporheic and underflow regimes and to facilitate comparison of no-flow bottom boundary simulations with gaining and losing scenarios we chose boundary fluxes such that the flow field where the hyporheic cell and underflow interact was minimally affected. This is achieved by implementing a relatively small gain or loss flux across the bottom boundary in comparison to the lateral fluid flux of the underflow (approximately 3 orders of magnitude difference).

The deflection of the flow field in the gaining and losing simulations compared to the no-flow bottom boundary scenario is minimal, and because vector plots of the underflow visually appear identical to those of models with a no-flow boundary at the base (Figure 3.2), separate vector plots are not provided. Recent modelling by Hester et al. [2013] and experimental observations by Fox et al. [2014] showed that the solute distribution is strongly influenced by the flow field. Our results concur with these findings as relatively small differences in flow field lead to notable changes to the steady-state solute distributions (Figure 3.6). This is attributed to the impact that introducing a gain or a loss of water has on the vertical advective and dispersive fluxes compared to a no-flow bottom boundary condition (compare Figures 3.7 and 3.5). Subtle deflections of the flow field lead to enhanced vertical solute transport, causing either more (losing) or less (gaining) mass from the hyporheic flow cell to be drawn into the underflow.

In gaining scenarios, there is less mass transfer to the underflow in comparison to the simulations with a no-flow bottom boundary. Upward transport towards the SSI (indicated by negative values for horizontally integrated vertical advective flux, Figure 3.7) counteracts the downward concentration gradient driven dispersive transport and reduces the net mass gain of the underflow from the hyporheic flow cells. Visually, the gaining $R = 2$, $\lambda = 0.01$ and $R = 2$, $\lambda = 0.001$ simulations resemble a periodic solution (Figure 3.6). Moreover, solute fluxes for bedforms 16 and 26 in both simulations differ by less than 0.08% for $\lambda = 0.01$ and less than 0.003% for $\lambda = 0.001$, and are thus virtually identical (Figure 3.7).

A comparison of the horizontal advective transport in the underflow between gaining scenarios (Figure 3.8a) and no-flow bottom boundary simulations (Figure 3.5) highlights

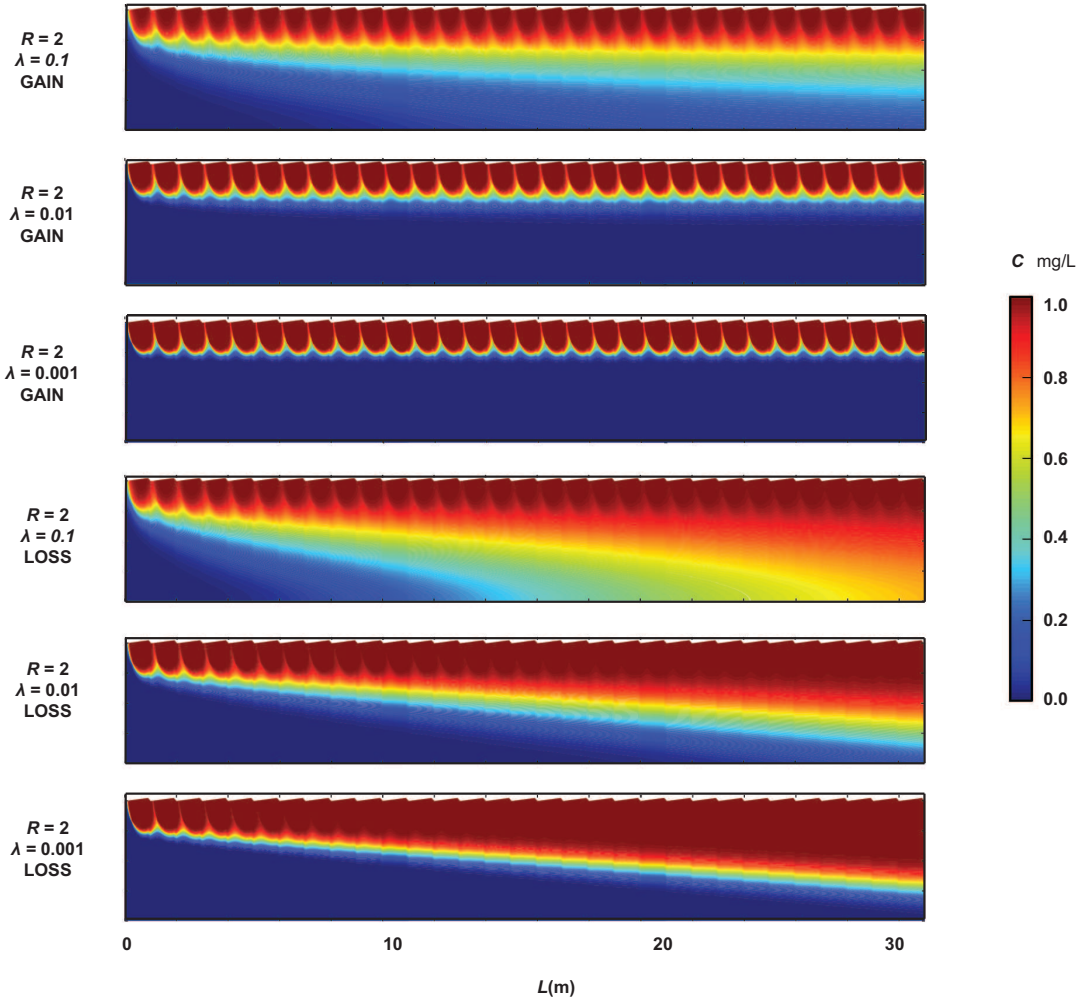


FIGURE 3.6: Steady state solutions to $R = 2$ solute transport simulations with gain and loss from bottom boundary.

the damping effect that ambient upward flow has on net mass transport across the flow divide deeper into the bedform. For gaining simulations where $\lambda = 0.01$, the advective solute flux in the underflow becomes essentially constant between bedforms past the 10th bedform. There is no observable change in the mass flux when $\lambda = 0.001$ from bedform 2 onwards. The significance of these observations is that an assumption of spatial solute periodicity is unlikely to result in a significant mass flux error for simulations with $R = 2$, $\lambda = 0.01$ and $R = 2, \lambda = 0.001$ under gaining conditions. Under these conditions a single-bedform simulation with periodic boundaries for solutes may be appropriate.

Losing scenarios are characterised by increased downward advective transport, which results in greater mass transfer from the hyporheic flow cell to the underflow (Figure

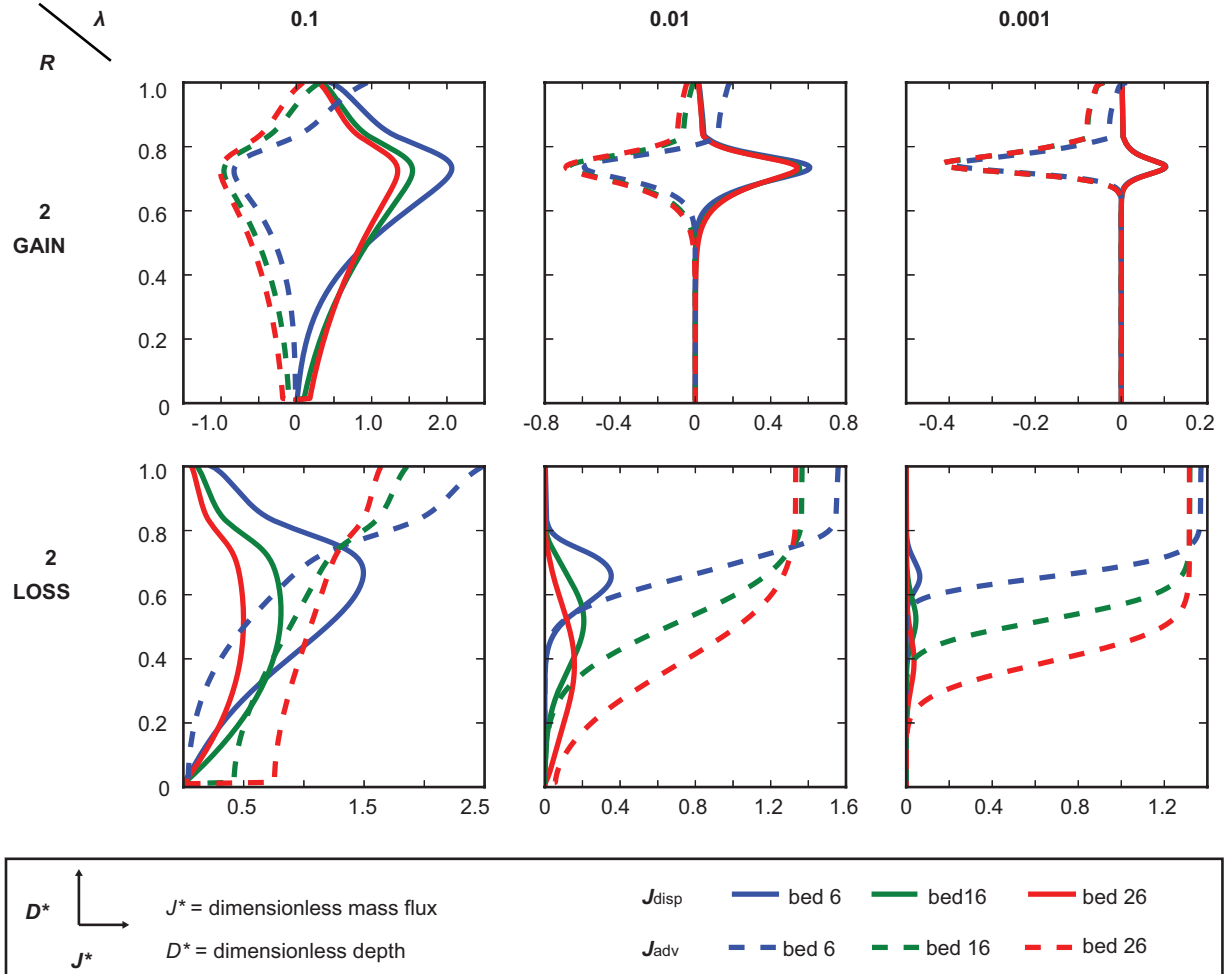


FIGURE 3.7: Horizontally integrated vertical flux in gaining and losing scenarios. Positive values are indicative of mass migration deeper into the bedform. Advection associated with ambient upward flow in gaining scenarios counteracts the dispersion driven by the concentration gradient. Dispersion is less significant as a transport mechanism for mass in losing scenarios. Spatial periodicity in this figure is represented by identical plots which overlap each another

3.7). Downward advective transport acts to overwhelm the concentration gradient across the flow divide (Figure 3.6) and dominates over vertical mass transfer by diffusion and dispersion (Figure 3.7). Moreover, the steep linear increase in mass transfer between bedforms via the underflow, for losing scenarios where $\lambda = 0.001$ and 0.01 ,, emphasises the significance of the downward advective transport component (Figure 3.8b). The curvature of the most dispersive case with $\lambda = 0.1$ is now primarily due to the loss of solute mass through the base of the model. In comparison to gaining models, as well as models with a no-flow bottom boundary, losing scenarios show the largest differences in the solute distributions between bedforms. Even for the small bottom-boundary fluxes

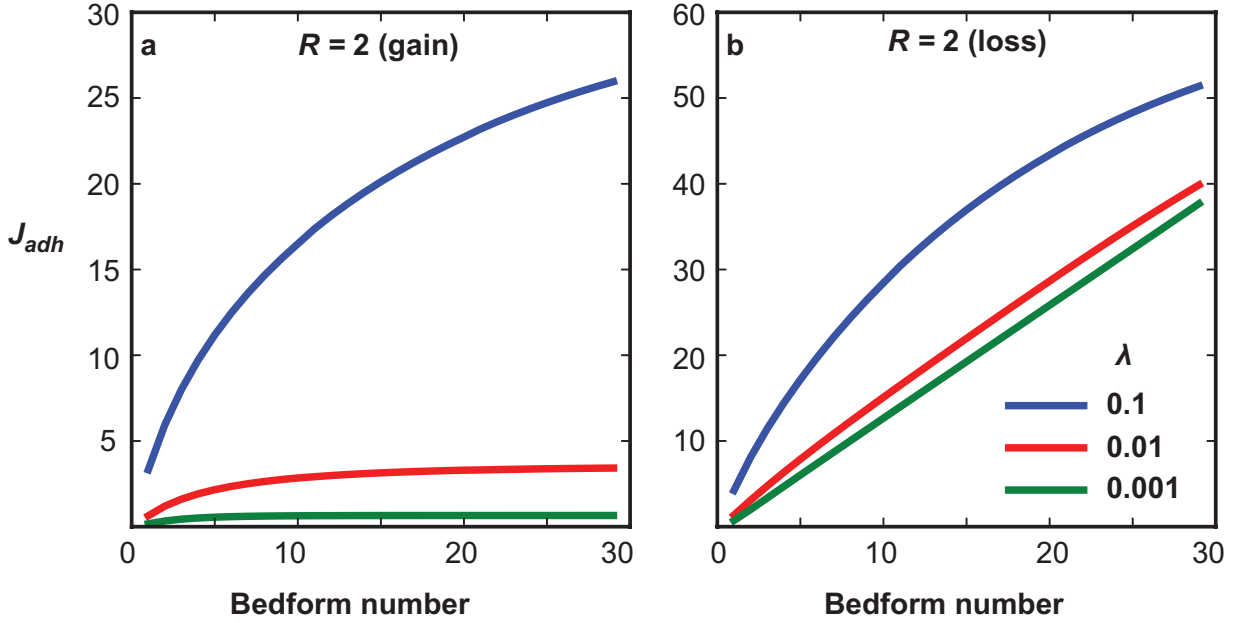


FIGURE 3.8: Graphs showing the horizontally advected flux (J_{adh}) in the underflow as a function of bedform number for gaining and losing scenarios. A periodic solution would produce horizontal lines.

considered here, losing systems are clearly the least suitable for SPSB implementation.

3.4.3 Thermal transport scenarios

Unlike the steady-state termination point of the solute transport models, thermal transport models are run for a fixed time period of 5 days. We examine transient thermal behaviour by plotting the average temperature for each bedform at every time step (Figure 3.9). For simulations where the hyporheic cell penetrates deeper into the bed sediments (i.e., $R = 20$ and $R = 200$) the effect of the bottom boundary in reducing the vertical thermal gradient is apparent in bedform 2. This is attributed to the larger diffusivity in thermal transport simulations compared to solutes, and these scenarios were not further analysed. The results for solute simulations are transferable to thermal, that is, we can expect similar outcomes with the same experimental setup implemented for solutes. The only difference is that thermal simulations are analogous to solute simulations with sorption.

In $R = 2$ simulations, very little (less than 10°C) change in temperature with time was observed below 0.7 m depth from the SSI. The first 11 bedforms in the $R = 2$,

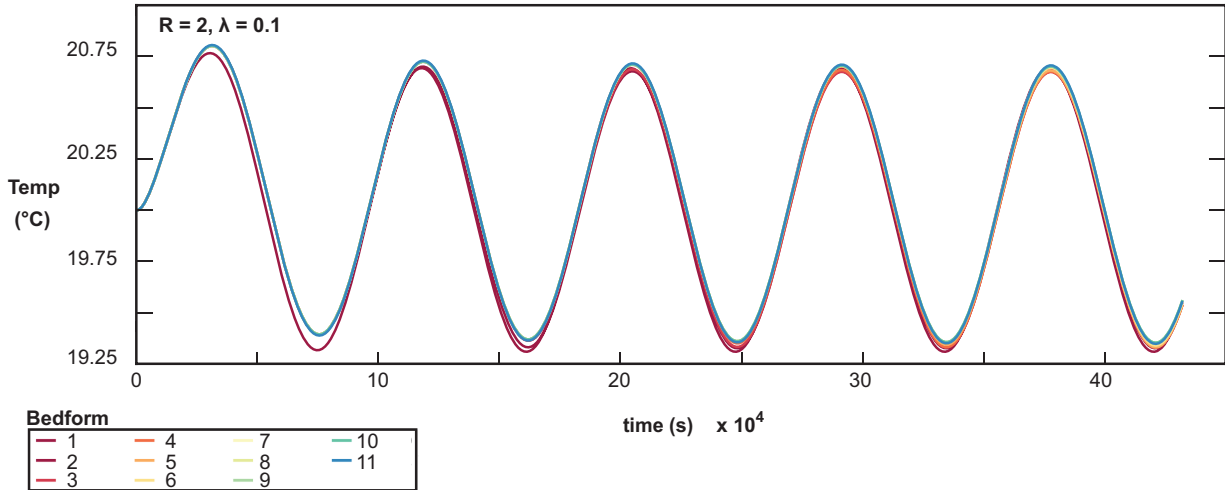


FIGURE 3.9: Average temperatures of the first 11 bedforms for the five day thermal transport simulation. The combination of $R = 2$ and $\lambda = 0.1$ is expected to show the greatest departure from periodicity based on previous solute transport experiment results.

$\lambda = 0.1$ thermal transport model reveals only slight deviation from thermal periodicity throughout the 5 day simulation, which is inferred from the near-absence of any mass gain in the underflow by successive bedforms (Figure 3.9). Detailed analysis of the transient behaviour revealed that the small deviations between the curves are attributable to cooling of less than 0.001°C per bedform caused by the propagation of the constant temperature inflow at the upstream (left) lateral boundary. Further experiments were performed at runtimes of 10 and 15 days with no significant changes to the plot for the final day.

It is worth noting that the corresponding solute transport simulations where $R = 2$, and $\lambda = 0.1$ showed the greatest deviation from a periodic solution. Based on this analysis we conclude that spatially-periodic temperature fields can exist with a temporally-periodic temperature reversal at the SSI. For the model setup here, thermal gradient reversal at the SSI appears to offset retention of thermal energy in the underflow necessary to effectuate a significant departure from periodicity.

3.5 Conclusions

This study investigates the validity of the often-made assumption of spatial periodicity for solute concentrations in hyporheic zone bedform models for a range of model configurations and parameter combinations reported in the literature. For models with a no-flow bottom boundary, we show that solute concentration patterns deviate significantly from spatial periodicity in most of the cases considered. However, where the dispersive flux between the hyporheic flow cell and the underflow is small ($R = 200$, $\lambda = 0.01$ and $\lambda = 0.001$ systems), we observe that spatial solute periodicity is approached. Our results suggest a lower bound mass balance error of 3% when assuming spatially periodic solute concentrations with the single bedform model. For losing conditions, we show that spatially-periodic solute concentration patterns are not attained in any of the simulations considered. For gaining conditions, we observe that the solute distribution becomes periodic because the upward advective flux in this case counteracts the downward dispersive flux from the hyporheic flow cell into the underflow. Our results indicate that spatially-periodic temperature patterns are possible for simulations with temporally-harmonic temperature variations along the SSI. We attribute this to the continuous, temporally periodic reversal of the temperature gradient that acts to reduce the net heat transfer from one bedform to the next in the underflow.

We demonstrate that the use of single-bedform models with a SPSB results in a greater or lesser mass into the lower regions of the bedform model. This will undoubtedly affect mass transfer across the SSI. For example, where the assumption of solute periodicity produces less solute in the underflow, vertical concentration gradients across the flow divide will be steeper, leading to more solute mass entering the streambed via the SSI to replace dispersed and diffused mass lost across the flow divide. This has significant implications for reactive transport simulations [Cardenas et al., 2008; Bardini et al., 2012] where the network of chemical reactions in the hyporheic and underflow regime may be driven by mass transfer (i.e., oxygen and dissolved organic carbon) from the stream to the bed sediments.

Other confounding factors are expected to prohibit spatial periodicity in reactive problems. We expect that the time-dependent production or decay of solutes may result in a continuous increase or decrease of solute concentrations in the underflow across bedforms. In multi-species problems, gradients between the hyporheic flow cell and the underflow may differ between species and could be in opposite directions, which may mean that periodicity could be approached for some species, but not for others. We expect further complications for variable-density simulations [Jin et al., 2011] where solute also affects the flow field, but these are not evaluated within the scope of the present study.

The assumption of spatially-periodic solute boundaries is attractive from a computational point of view because it makes that an infinite sequence of bedforms can be simulated by a single bedform. But the failure to achieve spatial-periodic concentration fields for most of the conditions considered during this study means that it can only be applied to a limited number of cases, and the outcomes of these models must be treated with caution. It is not our intent to dissuade other modellers from adopting a single bedform model with spatially periodic boundaries, but rather to identify the prevailing constraints and limitations. We strongly recommend studies consider an a-priori, quantitative assessment of the validity of the assumption, and revert to an alternative modelling approach, such as the multi-bedform simulations used in this study, when application of SPSB in a single-bedform simulation are deemed to result in significant error.

Chapter 4

A spatially periodic boundary for MT3DMS and PHT3D

4.1 Abstract

The assumption of spatial repetition is commonly made when producing bedform scale models of the hyporheic zone. Two popular solute transport codes, MT3DMS and PHT3D, do not currently provide the necessary boundary condition required to simulate spatial periodicity in hyporheic zone transport problems. In this study, we develop a spatially periodic boundary (SPB) for solutes that is compatible with a SPB that was recently developed for MODFLOW to simulate the flow component of spatially periodic problems. The appropriate block-centred finite-difference approach to implementing the boundary is presented and the necessary source code modifications are discussed. The performance of the solute SPB, operating in conjunction with the groundwater flow SPB, is explored through comparison of a multi-bedform hyporheic-zone model with a single bedform variant. The new boundary conditions perform well in situations where both dispersive effects and lateral seepage flux in the underflow regime beneath the hyporheic zone are minimal.

4.2 Introduction

The hyporheic zone (HZ) is commonly defined as the region where surface water and groundwater within sediments directly beneath and/or adjacent to streams and rivers mix [Winter, 1999; Jones and Mulholland, 2000; Woessner, 2000]. Exchange between the HZ and the surface water environment is bidirectional with respect to mass and momentum [Robertson and Wood, 2010; Bottacin-Busolin and Marion, 2010] and is often a consequence of variation in stream or river bed topography [Tonina and Buffington, 2011] that produces log-scale variability in residence times within the hyporheic flow cell [Stonedahl et al., 2010].

Despite the large range of hyporheic exchange scales, almost all published numerical experiments focus on the ripple or dune bedform scale [≤ 1.0 m Savant et al., 1987; Elliott and Brooks, 1997a; Laatooe et al., 2014]. Early investigations of bedform-scale HZ exchange using numerical experiments adopted a measured pressure distribution, obtained from flume experiments, using a Dirichlet boundary condition at the surface sub-surface interface [Savant et al., 1987; Rutherford et al., 1995; Elliott and Brooks, 1997b].

Recent numerical experiments utilize computational fluid dynamics (CFD) modelling packages to explicitly model the surface water domain in conjunction with the sub-surface [Cardenas and Wilson, 2006, 2007a; Jin et al., 2010]. A common approach to investigating bedform-scale HZ exchange with CFD packages is to assume that the streambed comprises an infinite number of identical bedforms. A single bedform structure is then simulated with spatially periodic boundary (SPB) conditions assigned to the lateral boundaries (Figure 4.1). For flow problems, the boundary condition accomplishes this by ensuring that the flow rate and direction are identical at opposing sides of the model for any given elevation. The boundary also facilitates application of a fixed head difference Δh [L], across the domain to account for gradients associated with the surface water or streambed slope. Its application induces a second flow regime in the bedform model beneath the HZ circulation termed underflow (see Figure 4.1).

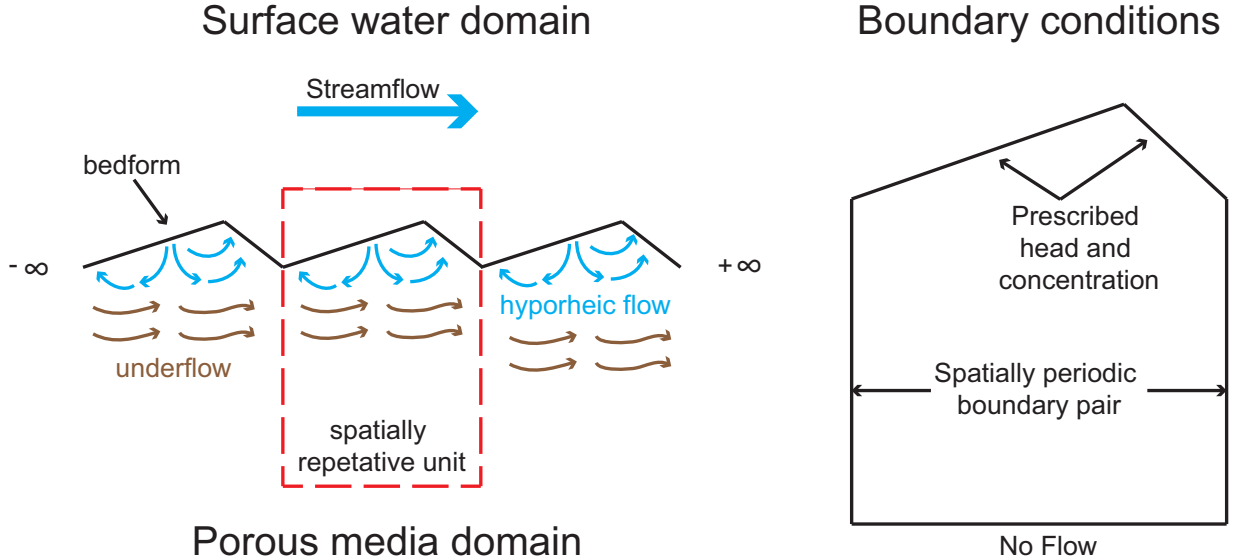


FIGURE 4.1: A 2D vertical slice through a series of identical ripple/dune structures along a streambed. Instead of modelling multiple bedforms a spatial periodic boundary pair can be used along the lateral boundaries of a single bedform model

Spatial periodicity for solutes is achieved by ensuring that the solute concentration distribution on both SPB's is an exact match [Cardenas and Wilson, 2007a; Jin et al., 2010; Bardini et al., 2012], given as:

$$C(0, z) = C(L, z) \quad (4.1)$$

Where the left and right vertical faces of the SPB are denoted by $(0, z)$ and (L, z) , respectively (see Figure 4.2), and C [ML^{-3}] is concentration of a solute species.

Laatooe et al. [2013] implemented a spatially periodic boundary condition for flow in the block-centred finite-difference groundwater modelling code MODFLOW [Harbaugh, 2005] and demonstrated its performance using a bedform-scale HZ model. In a subsequent study [Laatooe et al., 2014], they evaluated the appropriateness of the spatial periodic assumption when investigating solute behaviour in HZ bedform models implementing a SPB pair. Their study utilized the SPB developed for MODFLOW but did not consider a solute variant in a single bedform due to the limitations of the MT3DMS code.

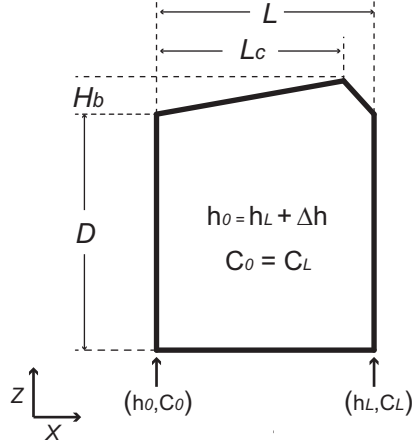


FIGURE 4.2: The Darcy domain of a typical bedform model with spatially periodic lateral boundaries for both flow and concentration. Descriptions of parameters are located in Table 4.1

Hester et al. [2013] used both MODFLOW and MT3DMS to simulate HZ bedforms and examined tracer behaviour during mixing between upwelling deeper groundwater and down-welling surface water. They utilized closed lateral boundaries on a single bedform model by assuming no head gradient between the lateral boundaries and that the flow field in the modelled bedform below the HZ circulation was either completely vertical or non-existent. This constrained the investigation to two very specific flow and transport mixing scenarios.

Both Hester et al. [2013] and Laatooe et al. [2014] could potentially have benefited from a solute transport variant of the SPB had it been available in MT3DMS [Zheng and Wang, 1999]. For Hester et al. [2013], this would have facilitated the inclusion of mixing scenarios where head gradients are present that drive underflow beneath the HZ. For Laatooe et al. [2014], it would have facilitated a direct comparison between the solute concentration patterns of a single-bedform SPB model and of a multi-bedform model with a spatially periodic flow field.

The objective of this article is to demonstrate how a multi-species solute variant of the SPB can be implemented in both MT3DMS [Zheng and Wang, 1999] and PHT3D [Prommer et al., 2003]. Development of the boundary condition for these simulators will facilitate their use in numerical investigations of conservative and reactive solute behaviour in bedform-induced HZ exchange, including nutrient cycling, which has recently

received significant interest [Zarnetske et al., 2012; Bardini et al., 2012, 2013; Boano et al., 2014].

4.3 Method

MT3DMS implements the following general form of the mass transport equation for solutes [Zheng and Wang, 1999]:

$$(1 + \frac{\rho_b}{\theta} K_d) \frac{\partial(\theta C)}{\partial t} = \nabla \cdot (\theta \mathbf{D} \cdot \nabla C) - \nabla \cdot (\mathbf{q} C) + q_s C_s \quad (4.2)$$

where C is concentration [ML^{-3}], t is time [T], θ is porosity, ρ_b is the bulk density [ML^{-3}], K_d is the distribution coefficient [L^3M^{-1}], \mathbf{q} is the specific discharge vector [LT^{-1}], \mathbf{D} is the hydrodynamic dispersion tensor [L^2T^{-1}] (i.e., $\mathbf{D}=\mathbf{D}_{mech}+\mathbf{D}_m$, where \mathbf{D}_{mech} is the mechanical dispersion tensor [L^2T^{-1}] and \mathbf{D}_m is the molecular diffusion coefficient [L^2T^{-1}]), q_s [LT^{-1}] is the volumetric flow rate per unit volume representing fluid sources or sinks, and C_s [ML^{-3}] is the concentration of the source. \mathbf{q} and q_s are obtained from MODFLOW's solution to the flow problem in this study. The implementation of a solute SPB in MT3DMS is thus predicated on a spatially periodic flow solution from MODFLOW. The implementation of the SPB in MODFLOW is detailed in Laatooe et al. [2013].

Explicitly satisfying Equation 4.1 with block-centred finite-difference spatial discretization is problematic because concentrations are assigned to nodes that are located in the centroids of the boundary cells, and not at the model extremities. Instead, we adopt an approach that ensures that the concentration used to calculate the advective mass inflow into a SPB cell at one boundary is equal to the concentration at the node associated with the outflow from the corresponding SPB cell at the opposite lateral boundary (Figure 4.3).

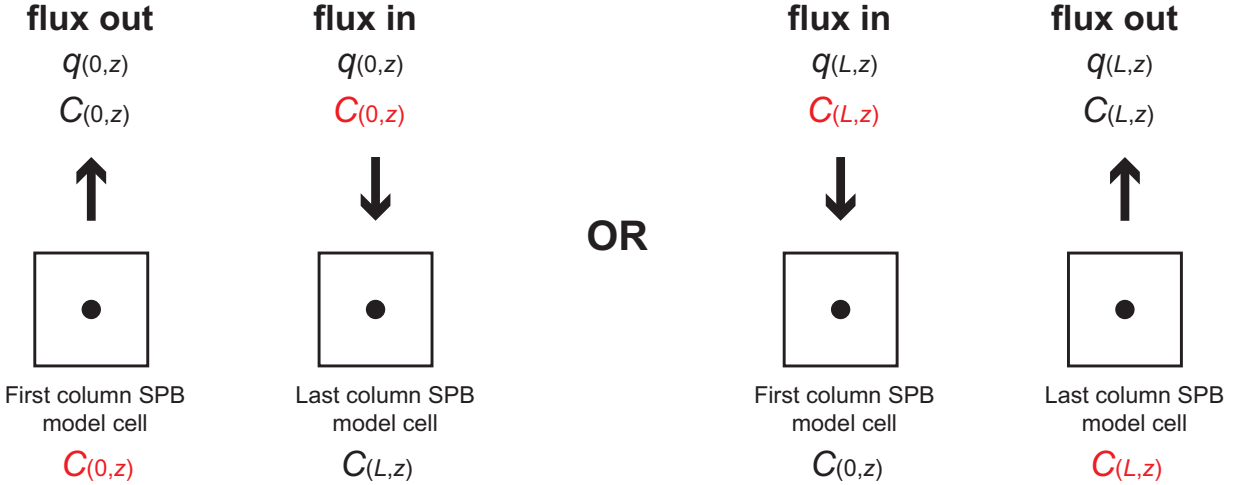


FIGURE 4.3: SPB flux and solute concentration relationships with modelled boundary cells

For cross-boundary fluxes, MT3DMS assumes that dispersive flux is insignificant in comparison to advection. This modified Cauchy condition results in a boundary definition that is of a similar format to the sink/source term in Equation 4.2, given as:

$$-q_0C = g_0(x, z, t) \quad (4.3)$$

where $g_0(x, z, t)$ is a model-derived or user-defined function representing the advective flux normal to the boundary. A spatially-periodic variant in MT3DMS then requires:

$$-q_0C(0, z) = -q_L C(L, z) \quad (4.4)$$

The SPB flow solution from MODFLOW provides MT3DMS with the value for q_0 ($= q_L$) as the flux across the faces of the cells at the lateral boundaries of the bedform [Laatooe et al., 2013].

Flow fields observed in bedform models often comprise an advectively dominated hyporheic circulation cell and an underflow, which occurs beneath the hyporheic flow cell in the direction of streamflow (see Figure 4.1). Neglecting a dispersive flux term in the boundary implementation is likely to have minimal impact if analyses of hydrodynamic

Parameter	Symbol	Value	Units
Bedform depth	D	2.0	m
Bedform length	L	1.0	m
Length to bedform crest	L_c	0.9	m
Bedform height	H_b	0.05	m
Grid spacing x direction	Δx	0.05	m
grid spacing z direction	Δz	0.05	m
Fixed head difference between SPB	Δh	10^{-2}	m
Hydraulic conductivity	K	10^{-3}	ms^{-1}
Longitudinal dispersivity	α_L	10^{-2}	m
Dispersivity ratio	α_T/α_L	1/10	m
Molecular diffusion	D_m	10^{-9}	ms^{-2}
Porosity	θ	0.3	-
SSI* concentration	C	10, 1.0, 0.1	mgL^{-1}

* Surface sub-surface interface

TABLE 4.1: Parameters used in numerical experiments

processes are constrained to the advectively dominated hyporheic flow cell. For parameter sets used in typical bedform models the concentration gradient driven flux across the lateral boundaries within the HZ is expected to be between 3 and 4 orders of magnitude less than advective

4.4 Implementation

We present details for the necessary modifications to the source code of MT3DMS when using a solute SPB. For brevity, we describe only the modifications that will produce solute periodicity between vertical lateral boundaries assigned to columns in a two-dimensional cross-sectional model. Readers are referred to the MT3DMS user manual [Zheng and Wang, 1999] and the MODFLOW user manual [Harbaugh, 2005] for more detailed descriptions of all source code and input file variables mentioned in this section.

The sink/source mixing (SSM) package for MT3DMS handles the solute fluxes for all point sinks and sources in the model. The source code for the SSM package includes separate modules that perform various functions. The formulate module is responsible for adjusting the entries in the model matrices prior to a solution attempt by the solver. Within the formulate module are two loop constructs specific to the solution method

of the advection terms. One loop is specific to Eulerian methods while the other is specific to Eulerian-Lagrangian methods [Zheng and Wang, 1999]. Our complete source code modification (available as electronic supplementary material) for SPB function in MT3DMS comprises a single block of code inserted into the formulate module of the SSM package within each of the two loop constructs that handle point sinks and sources. Both SPB source code insertions are identical and achieve the following:

1. Determine if a cell listed in the SSM input file belongs to a SPB;
2. Identify if the flow is from the cell on the right-hand to cell on the left-hand lateral boundary, or vice versa;
3. Based on 2, assign the concentration (for all species) to the SPB flux entering the cell with the concentration of the opposite boundary cell.

The standard MT3DMS approach to calculate mass fluxes from external sources based on the flow solution is to associate them with a user-defined concentration (CSS variable) in the SSM input file. CSS generally differs to the concentration of modelled boundary cells as it is only applied to any flux entering the cell from a specific source. The CSS variable is assigned model-predicted concentrations based on the SPB pairing, as per step 3 above. That is, the value of CSS is dynamically set to the appropriate value from the opposite lateral boundary of the model (obtained from MT3DMS's CNEW array), as

$$\text{CSS}(0, z, t) = \text{CNEW}(L, z, t) \quad (4.5)$$

$$\text{CSS}(L, z, t) = \text{CNEW}(0, z, t) \quad (4.6)$$

Equations 4.5 and 4.6 are invoked prior to MT3DMS's calculation of the RHS array entry of the SSM package. It should be noted that MT3DMS's modification of the RHS entry in this instance is conditional on a source flux entering the domain. The CNEW array comprises the current iterations' solution of the concentrations in all modelled

cells. For multi-species simulations CSS is replaced by CSSMS(1,2,... n). Our code modification works on all n species.

Constant head boundary cells in the top layer of the bedform model, representing the surface water pressure distribution, are also handled by the SSM package. In the SSM input file, the type of sink or source term is identified by the value assigned to the ITYPE variable, whereby GHB (and consequently SPB) cells are identified by an ITYPE value of 5. Our modification to the SSM source code affects only entries with ITYPE values of 5 that are located in the first and last columns. This is accomplished via a simple conditional statement inserted into the source code. The modified SSM package source code used in this study is provided in B.

4.5 Application

To demonstrate the application and effect of the solute SPB we compared a single bedform model with a multi-bedform variant that comprised 11 bedform repetitions (numbered sequentially from left to right). Physical dimensions and input parameters for models used in the simulations are given in Table 4.1. The porous medium was considered homogeneous and isotropic. Steady state periodic flow fields obtained from MODFLOW simulations were used with multi-species transient transport simulations in MT3DMS. The horizontal and vertical seepage flux components of each bedform in the multi-bedform model were compared with those of the single bedform model. The maximum difference observed was 8×10^{-6} m, which is small enough to be considered inconsequential for the purposes of this investigation.

The bottom boundary for all models was set as a zero-mass flux for water and solutes. The lateral boundaries of both the single and multi-bedform models were periodic with respect to flow [Laattee et al., 2013]. Only the single-bedform featured the solute SPB as described above. The top boundary for both multi-bedform and SPB models was set as Cauchy condition with constant concentration for inflow and model derived concentration for outflow.

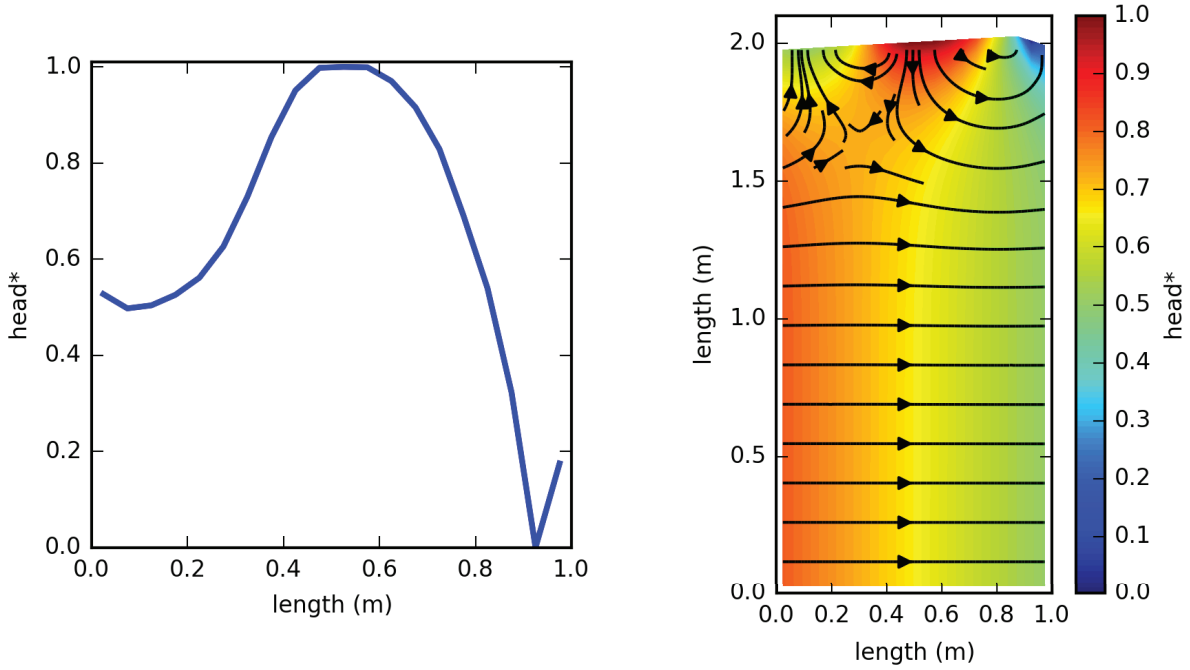


FIGURE 4.4: Top boundary head distribution (left) and MODFLOW’s steady state solution for the single bedform with SPB flow (right) used for all transport simulations.

* Heads are normalized using feature scaling

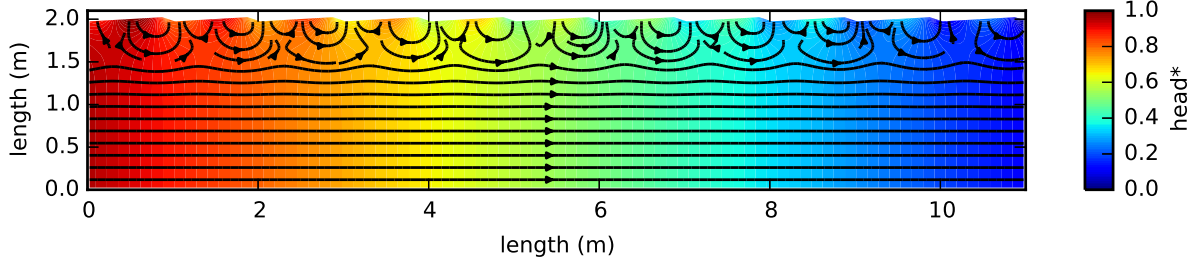


FIGURE 4.5: The steady state uniform flow field of the 11 bedform model (*Heads are normalized using feature scaling).

We adopted as the starting condition for the single bedform MODFLOW simulations (Figure 4.4), a hydrostatic subsurface head distribution that corresponds to published interface head distributions from experiments where the surface water domain was modelled explicitly [Cardenas and Wilson, 2007a]. The same head distribution was applied to all bedforms but adjusted to account for Δh in the 11-bedform model. This resulted in a uniform flow field spanning all 11 bedforms, in which each individual bedform had identical flows that matched the single bedform model (Figure 4.5).

Three species were modelled that all had different CSS values assigned as Cauchy conditions to the top boundary of each bedform. The different concentrations were used to examine dispersive solute flux across the lateral boundaries in the multi-bedform model and as a check to ensure the multi-species source code modifications functioned correctly. Initial concentrations in both the single and multi-bedform models were set to zero everywhere, i.e., $C(x, z, t = 0) = 0$. The concentration convergence criterion for the generalized conjugate gradient solver was set at 10^{-7} mgL⁻¹ for all simulations.

We initially selected the upstream-weighted finite-difference method for the advection terms to test the code modifications in the Eulerian-specific section of the SSM package. A second run of simulations was then performed where the advection terms were solved with the hybrid method of characteristics testing the code modifications in the mixed Eulerian-Lagrangian section. There was no discernible visual difference between results using either method to solve the advection term. The duration of the transport simulations was 97 hours. An approximate steady state (defined as a total system mass gain between successive transport steps less than 0.1%) was observed in the solute distribution of the multi-bedform model around 76 hours. For brevity, we focus on the results up to 36 hours simulation time of a single species solved with the upstream-weighted finite-difference advection term solution method.

The advective and dispersive component fluxes between bedforms in the multi-bedform model were examined to validate the assumption of negligible dispersive transport for the SPB. In the HZ, the advective flux between bedforms was between 3 to 4 orders of magnitude greater than the dispersive, while in the underflow regime beneath the HZ, this decreased to between 3 and 2 orders of magnitude. Three dimensionless parameters characterize net mass flux in the presented bedform model, $d = \alpha_T/\alpha_L; \lambda = \alpha_L/L; R = a/L\Delta h$, where a is the amplitude of head variation prescribed at the top boundary [Qian et al., 2008]. The practical range of interest for bedforms in streams and rivers is between 0.1 - 0.3 for d ; 0.001 - 0.1 for λ and 1 - 1000 for R , however R values ≥ 100 do not show much variation in fluxes. The model used in the demonstration has $R = 20$, $\lambda = 0.01$, and $d = 0.1$, which is at the middle of the range but with less dispersion.

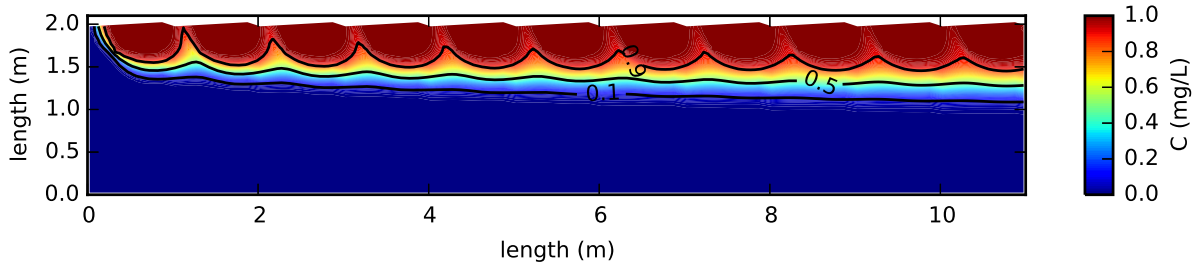


FIGURE 4.6: The concentration distribution of the multi bedform model at time $t = 36$ hours.

Previous studies indicated that increasing values of R coupled with decreasing values of λ increase the difference between a spatially periodic and multi-bedform solute distribution [Laatooe et al., 2014].

SPB's are considered attractive from a computational point of view as they are able to reduce a model featuring spatial repetition to a single repetitive unit. The total CPU time reported by MT3DMS for the SPB model was 51.5 seconds. The multi-bedform model took 4 minutes 28.2 seconds. Simulations were performed on a 64-bit Windows[®] PC with second generation Intel[®] I7 2600K @ 3.40GHz CPU, 16 GB DDR1600 RAM and an OCZ[®] Vertex 3 SSD hard drive on a 6Gb/s SATA port.

Laatooe et al. [2014] found that significant differences in the solute concentrations between individual bedforms became apparent once the solute front entered the underflow regime below the hyporheic cell (Figure 4.6). Since all bedforms in the multi-bedform behave differently, we examine the performance of the solute SPB used in the single bedform model with the second (MB2), sixth (MB6) and eleventh (MB11) bedform in the multi-bedform model. Comparisons are made at selected times as the solute front moves deeper into the bedform. Figures with flooded contour plots of solute distributions also feature concentration contour lines of 0.1, 0.5 and 0.9 mgL⁻¹ to aid in discerning differences visually. To quantify differences, we examine the total solute mass in each bedform in conjunction with the centre of mass over time.

Figure 4.7 depicts the solute distributions for bedforms MB2, MB6 and MB11 in the multi-bedform model compared with the single bedform of the solute SPB model. After

1 hour, there are small but notable differences between the SPB and multi-bedform model. There is virtually no difference between MB2, MB6 and MB11. This is also evident from the total solute mass (Figure 4.8) and the centre of mass (Figure 4.99) of each bedform.

The single-bedform concentration distribution at 1 hour appears more diffuse relative to the corresponding multi-bedform representation. This is demonstrated by the deeper penetration of the 0.1 mgL^{-1} contour and the shallower 0.9 mgL^{-1} contour. The 0.1 mgL^{-1} contour indicates that, in comparison to MB2, MB6 and MB11, there is greater solute mass at the left lateral boundary, and there is a marginal increase in total bedform solute mass. An increase in mass is expected because the SPB's ensure there is no net mass loss from the model via the lateral boundaries. Once concentrations at the top boundary reach a steady state then the mass increase in the model becomes linear and rates correspond to the net advective mass flux across the top boundary. The SPB model mass center is located deeper than, and slightly more to the right of the other bedforms. After 5 hours, there is still no discernible difference between the solute distributions in MB2, MB6 and MB11. The SPB model continues to produce a more diffusive solute front compared to each bedform in the multi-bedform model, with greater total system mass and deeper but now left-shifted mass centre.

The rate of increase in total system mass of the SPB bedform appears constant after 17 hours and is significantly greater than in the multi-bedform model. Reduction in the rate of mass gain continues well past 8 hours for MB6 and MB11 while MB2's increase in total system mass plateaus at approximately 15 hours (Figure 4.8). This is also evidenced by the centre of mass for MB2, which does not vary between 25 and 36 hours simulation time (Figure 4.9). The solute distribution at 25 hours (Figure 4.7) indicates less solute mass towards the left lateral boundary for MB2 in comparison to MB6 and MB11 with both the 0.1 and 0.5 mgL^{-1} contour closer to the top of the bedform. MB6 and MB11 remain matched after 25 hours with no identifiable visual difference in solute distribution or total mass and mass centre. However, the SPB model at this time displays significantly greater solute mass (Figure 4.8) and a mass centre that

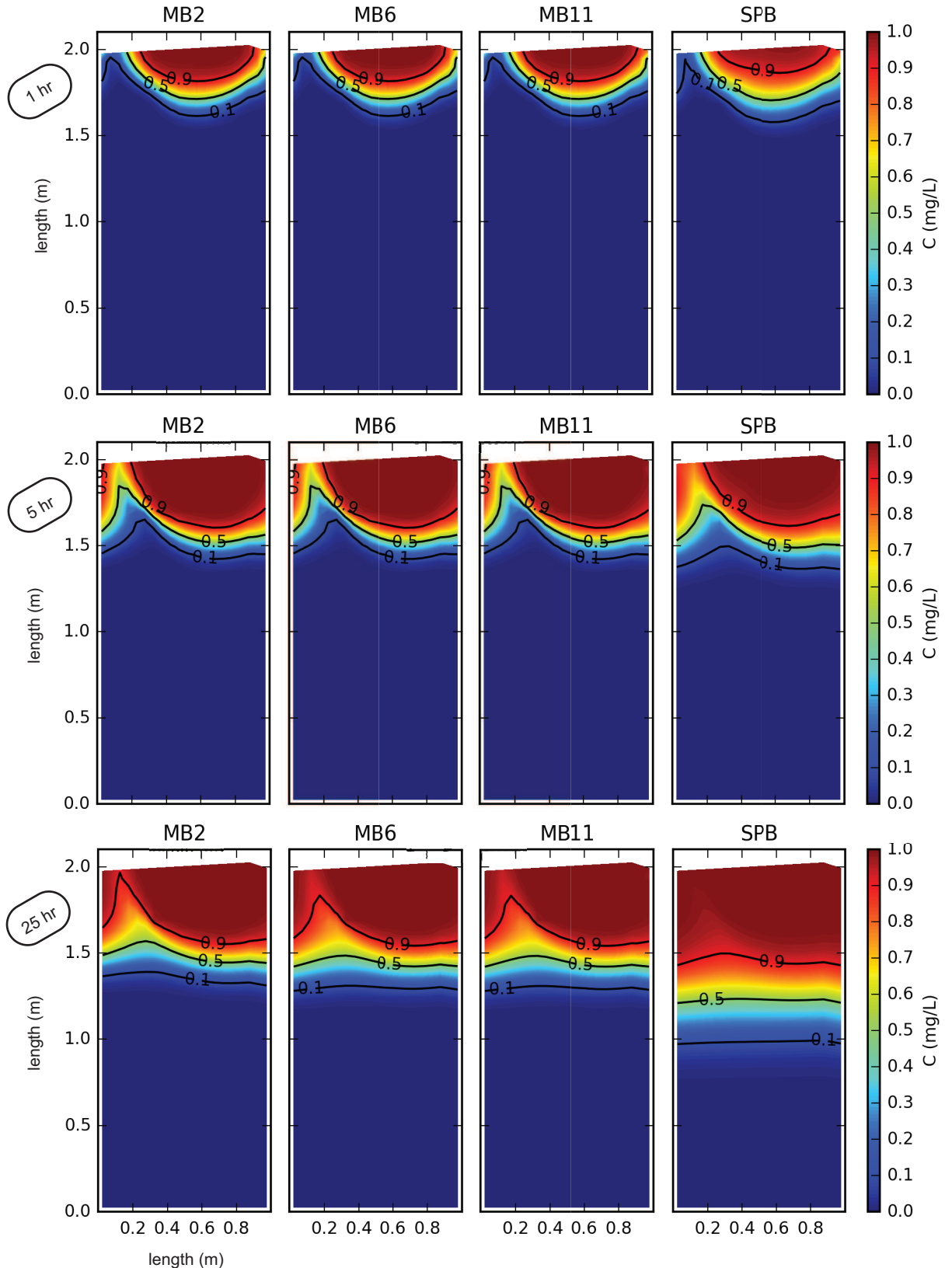


FIGURE 4.7: Comparisons of solute distributions between bedforms number 2, 6, 11 in the multi bedform model and the singular bedform model using the solute SPB. The rows correspond to simulation times 1 hour (top), 5 hours (middle), 25 hours (bottom).

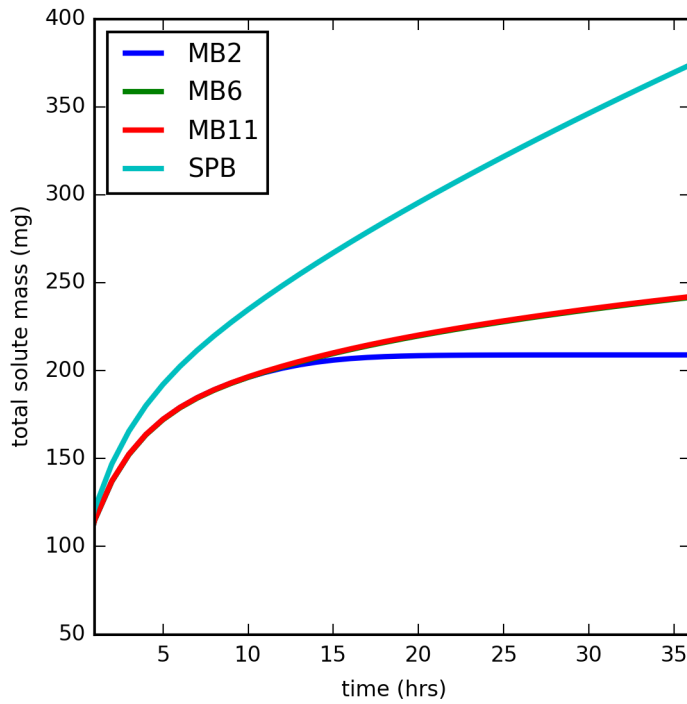


FIGURE 4.8: Total solute mass in each bedform from $t = 1$ hour to $t = 36$ hours.

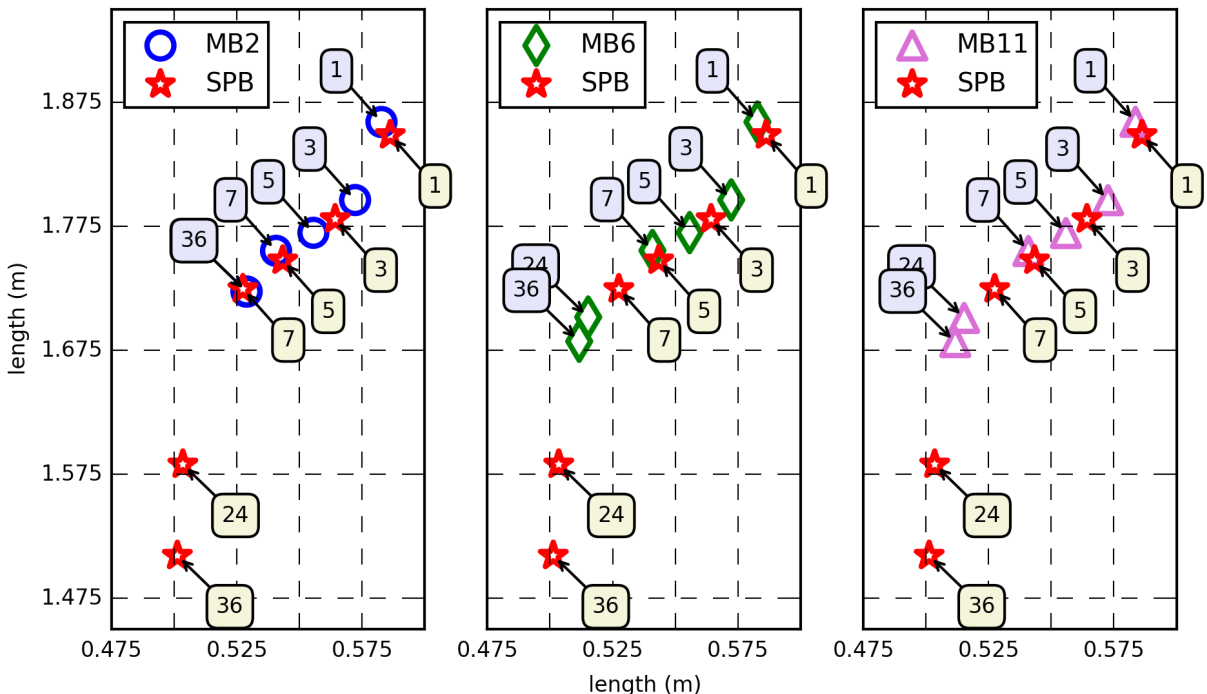


FIGURE 4.9: Centre of mass comparison between: solute SPB and bedform 2 (left); solute SPB and bedform 6 (middle); solute SPB and bedform 11 (right). Points are labelled with time in hours. X axis is length into the individual bedform from the left. Y axis is height from closed boundary at the base of the bedform.

is constantly shifting deeper and towards the left lateral boundary (Figure 4.9). As a consequence of the spatial periodicity, the rate of mass gain for the single bedform model remains significantly larger than both MB6 and MB11 with no indication of diminishing after 36 hours.

4.6 Conclusions

It was demonstrated how a SPB bedform model can be implemented in MT3DMS for advection-dominated systems. The demonstrated differences in mass transport behaviour quantify the findings of Laatooe et al. [2014]. They reasoned that application of spatially periodic boundaries to bedform models enforce a symmetrical solute distribution throughout the domain and will introduce greater solute mass into the model. However, they also noted that a reduction in dispersion and the Δh parameter is likely to converge on a periodic solution

The solute SPB is useful for computational gain with theoretical type numerical investigations that attempt to address transport processes where spatial repetition occurs [Jin et al., 2010; Bardini et al., 2012, 2013]. However, caution is warranted if the processes investigated include significant dispersive mass flux and enhanced lateral seepage flux in the underflow. The boundary condition may also find use in flow circulation experiments involving porous media, for example, in waste water processing where adsorptive clays or reactive carbons are used in closed system column reactors. These experiments often involve a media chamber analogous to a Darcy column, which is plumbed in a manner so that fluid exiting one end of the chamber is returned to the other via a pump.

Recent investigation by Briggs et al. [2014, 2015] discovered, theorized and measured the formation process of redox micro zones in bulk oxic hyporheic flow fields. Developing numerical models to further analyse this process is a likely next step. The development of the SPB for MT3DMS and PHT3D makes both simulators viable alternatives to solute capable CFD modelling packages in future HZ bedform numerical experiments.

Chapter 5

Effects of spatial periodic boundaries on simulations of nutrient dynamics in bedform scale hyporheic zone models

5.1 Abstract

Small scale numerical models of the hyporheic zone often adopt the assumption of spatial repetition. The solute variant of the spatially periodic boundary forces symmetry in concentration across the model domain and is featured in numerous studies of single ripple or dune style bedforms. The effect of this symmetrical forcing on reactive transport simulations is unclear. Comparisons of the chemical reactions in a multi-bedform model with those of a single bedform model, in PHT3D, are made where only the single adopts the periodic assumption for solute. A modified Monod kinetics model comprising oxygen, ammonium, nitrate and dissolved organic carbon is simulated over a steady-state spatially-periodic flow field. Comparisons are made using a Damköhler number for each reactant species evaluated as the product of reaction rate and residence

time. Results indicate that the SPB solution deviates from the reactivity trend in the multi-bedform model when lateral transfer of solutes between bedforms is increased. The results demonstrate that the SPB model can produce a result characterized as a nitrate sink while the multi-bedform, model with identical parameters, is characterized as a nitrate source. Observations also indicate that mixing processes can lead to a shift between oxic and anoxic environments along the same length flow path, which has implications for approaches that link reaction rates specifically to HZ residence time.

5.2 Introduction

The hyporheic zone (HZ), defined as the region where surface and groundwater mixes beneath and adjacent to streams or rivers, plays a significant role in nutrient cycling [Rutherford et al., 1995; Findlay and Ab, 1995; Boulton et al., 1998]. Hyporheic exchange fluxes occur over a range of spatial and temporal scales [Stonedahl et al., 2010]. Bedform hyporheic exchange (scale ≤ 1.0 m) results from variations in the surface water pressure gradient on the bed sediments created by streamflow over morphological structures such as ripples or dunes [Shum, 1992; Elliott and Brooks, 1997a; Cardenas and Wilson, 2007d]. Scientific understanding of hydrodynamics at this scale has become well-established with contributions from both physical experiments [Thibodeaux and Boyle, 1987; Elliott and Brooks, 1997a; Fox et al., 2014] and numerical experiments [Savant et al., 1987; Elliott and Brooks, 1997b; Cardenas and Wilson, 2007d]. Recent numerical investigations at this scale also include solute [Sawyer and Cardenas, 2009; Jin et al., 2010; Hester et al., 2013] and reactive transport [Cardenas et al., 2008; Bardini et al., 2012, 2013].

Physical experiments of bedform HZ exchange often comprise a flume featuring numerous physically identical triangular bedforms [Elliott and Brooks, 1997a; Janssen et al., 2012; Fox et al., 2014]. Consequently, a popular approach to simulating bedform HZ exchange is to assume the stream or river bed comprises an infinite repetition of identical bedform structures. This assumption facilitates development of a numerical model featuring a single bedform structure with spatially periodic boundaries (SPB's) at its

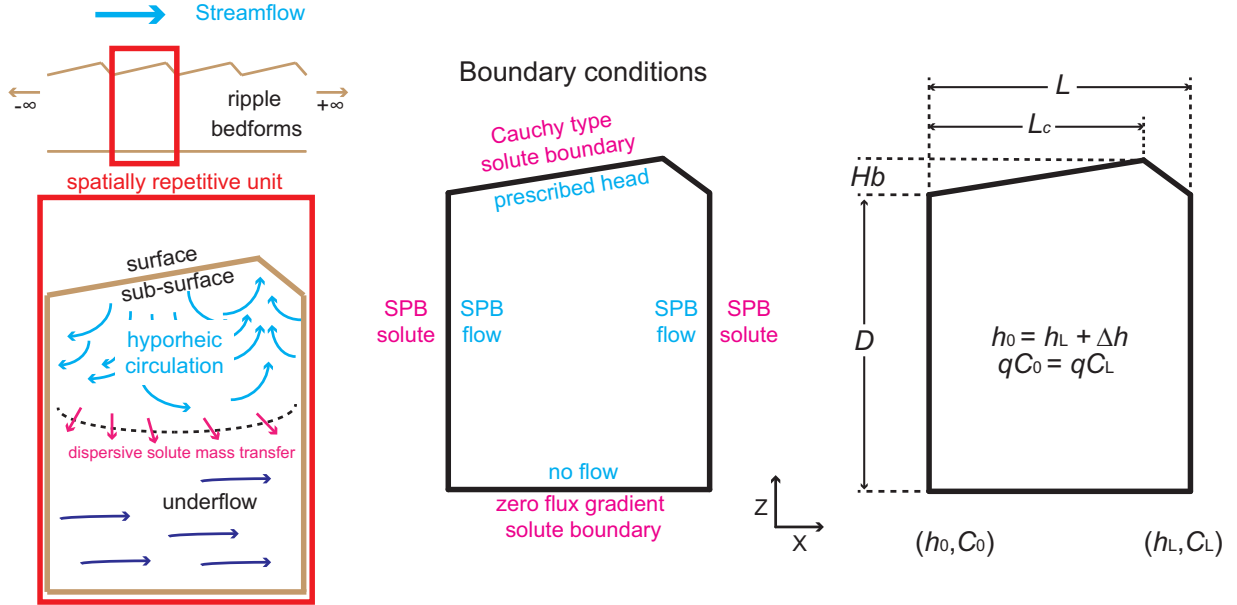


FIGURE 5.1: The modelled domain of a typical HZ bedform model with SPB lateral boundaries. Descriptions and values of parameters are located in Table 5.1

lateral margins. The boundaries behave in a manner that reflects an infinite series of laterally-adjacent identical bedforms (Figure 5.1). For any given elevation at the lateral boundaries, hydraulic head and flow are identical. Laatooe et al. [2014] list the recent studies that have adopted this approach with their numerical experiments.

Surface water effects, responsible for developing the hyporheic flow cells, are accounted for through application of a specified head or pressure distribution to the triangular shaped upper boundary of the model. The SPB for flow also allows for a head difference Δh [L] to be imposed between the lateral flow boundaries, which accounts for the effect of stream level gradient [Jin et al., 2010; Bardini et al., 2012]. If applied, it induces a second, sub-horizontal flow regime (see Figure 5.1) in the region below the hyporheic circulation termed underflow [Cardenas and Wilson, 2007d].

A SPB for solute transport is analogous to the flow equivalent in that it ensures concentrations are also spatially periodic at the lateral boundaries. Previous studies established that solute transport in the hyporheic cell is advectively dominated [Cardenas and Wilson, 2007d; Bottacin-Busolin and Marion, 2010], while mass transfer to the underflow from the HZ is dependent on dispersive and diffusive fluxes [Qian et al., 2008; Jin et al.,

2010]. Reactive transport HZ experiments often involve chemical-reaction models of nutrient transformations that are dependent on multiple reactants entering the hyporheic zone via the surface sub-surface interface (SSI).

Cardenas et al. [2008] used the single bedform model to investigate denitrification in a marine environment and found that when advective transfer of oxygen into the sediments was considered, rates were approximately halved compared to diffusive transfer. Bardini et al. [2012] also used a single bedform model to evaluate denitrification in stream sediments and discovered that concentrations of dissolved organic carbon in the surface water have a pivotal role in the behavior of a streambed as a sink or source of nitrate. In a follow up study they also examined the effects of heterogeneity on denitrification using a multi-bedform model that also implemented SPB's for flow and solute at the lateral margins [Bardini et al., 2013].

The assumption of spatial periodicity on the behavior of chemical reactions in numerical experiments has not been investigated, and to date remains unclear. Denitrification, being an anaerobic process, is considered more prevalent in the underflow [Bardini et al., 2012]. The implication here is that transfer of solutes between HZ and underflow in a SPB bedform model may exert significant control on the denitrification processes observed. Laatooe et al. [2014] used a multi-bedform model to show that the vertical transfer of solutes into the underflow causes a difference in solute concentrations between the up- and downstream parts of the model, which is a violation of the periodicity assumption. They also demonstrated in a separate study that the SPB could significantly overestimate the mass transfer between the hyporheic and underflow [Laatooe et al., tted]. This suggests that there are unexplored interactions and feedbacks between the flow in multi-bedform systems and reactive transport, which will be the focus of this paper.

The objective of this study is to examine the effects of bedform repetition on nutrient cycling. To this end, simulations of a multi-species chemical reaction network in a single bedform model with solute SPB's are compared to the results to a multi-bedform variant of the same model without the periodic solute assumption. The effect of the solute SPB

on reactive transport simulations is multifaceted due to the complexity of the reaction network and its dependence on mass flux across the SSI and mass flux between the flow regimes.

5.3 Methods

Both single and the multi-bedform flow models were developed using the finite-difference groundwater simulator MODFLOW [Harbaugh, 2005]. The two dimensional (x, z) bedform model (see Figure 5.1) is identical to those adopted in our previous studies [Laatooe et al., 2013, 2014, tted] with all relevant model parameter details listed in Table 5.1. The bedform shape is asymmetric with the position of the crest (L_c) located closer to the downstream end of the structure reflecting the constant direction of streamflow above the bedform along the x axis. The multi-bedform model is made up of 11 identical repetitions (numbered left to right) of the single bedform model grid. SPB lateral flow boundaries are implemented on both models via modifications to MODFLOW's general head boundary (GHB) package [Laatooe et al., 2013]. A fixed head difference (Δh) is applied to the SPB's that drives underflow. The porous medium is considered homogeneous and isotropic with a hydraulic conductivity of 0.01 ms^{-1} .

The SSI head distribution is adopted from published investigations where the surface water was modelled explicitly [Cardenas and Wilson, 2007d]. It features a peak approximately half way up the rising slope with steep gradients to a minimum at the crest of the bedform structure. For the multi-bedform model, the same head distribution is used for each individual bedform but offset vertically by Δh in each application. This ensures consistency with the conditions assigned to the SPB's and produces a horizontal underflow across the whole domain. No flow boundaries are used at the base of all simulations. The lower boundary is located 2.0 m below the SSI to minimize its effect on concentration gradient driven fluxes between the flow regimes [Bottacin-Busolin and Marion, 2010; Laatooe et al., 2014]. Readers are referred to a previous study for further

Parameter	Symbol	Value	Units
Bedform depth	D	2.0	m
Bedform length	L	1.0	m
Length to bedform crest	L_c	0.9	m
Bedform height	H_b	0.05	m
Grid spacing x direction	Δx	0.05	m
grid spacing z direction	Δz	0.05	m
Fixed head difference between SPB	Δh	$10^{-1}, 10^{-2}, 10^{-3}$	m
Amplitude of interface head distribution	a	0.022785	m
Hydraulic conductivity	K	10^{-3}	ms^{-1}
Longitudinal dispersivity	α_L	$10^{-1}, 10^{-2}, 10^{-3}$	m
Dispersivity ratio	α_T/α_L	1/10	m
Molecular diffusion	D_m	10^{-9}	ms^{-2}
Porosity	θ	0.3	-
*Limiting concentration O ₂	$C_{1,lim}$	3.125×10^{-5}	M
*Limiting concentration NO ₃	$C_{2,lim}$	8.065×10^{-6}	M

TABLE 5.1: Model geometry and input parameters used in numerical experiments *Van Cappellen and Wang [1996]

details on the setup of both the single and multi-bedform model, which also includes comparisons when simulating conservative solutes [Laatooe et al., tted].

For the reactive transport simulations PHT3D was used [Prommer et al., 2003], which combines MT3DMS [Zheng and Wang, 1999] and PHREEQ-C [Parkhurst and Appelo, 1999]. Coupling of the codes is via a sequential split-operator technique. The solute transport equation solved by PHT3D is

$$\frac{\partial(\theta C^k)}{\partial t} = \frac{\partial}{\partial x_i} \left(\theta D_{ij} \frac{\partial C^k}{\partial x_j} \right) - \frac{\partial}{\partial x_i} (\theta v_i C^k) + W C_s^k + \sum R^k \quad (5.1)$$

where θ is porosity of the porous medium [dimensionless], C^k is the dissolved concentration of species k [ML^{-3}], x_i , x_j is the distance along the respective Cartesian coordinate axis [L], D_{ij} is the hydrodynamic dispersion coefficient tensor [L^2T^{-1}], v_i is seepage [LT^{-1}], C_s^k is the concentration of the source or sink flux for species k [ML^{-3}], and $\sum R^k$ is the chemical reaction term of species k [$\text{ML}^{-3}\text{T}^{-1}$]. For all presented simulations, MT3DMS solves the transport step for each species using the steady state flow field from MODFLOW prior to the reaction calculation step handled by PHREEQC.

Reaction index	Reaction
$r1$	$\text{CH}_2\text{O} + \text{O}_2 \rightarrow \text{CO}_2 + \text{H}_2\text{O}$
$r2$	$5\text{CH}_2\text{O} + 4\text{NO}_3^- + 4\text{H}^+ \rightarrow 5\text{CO}_2 + 2\text{N}_2 + 7\text{H}_2\text{O}$
$r3$	$\text{NH}_4^+ + 2\text{O}_2 \rightarrow \text{NO}_3^- + 2\text{H}^+ + \text{H}_2\text{O}$

TABLE 5.2: Reactions implemented in the reaction network

The chemical reaction network was adopted from Bardini et al. [2012]. It follows the oxidation and reduction (redox) reaction kinetics described in Hunter et al. [1998]. The simulated network comprises 3 redox reactions catalyzed by sub-surface micro-organisms (Table 5.2), where the $r1$, $r2$, and $r3$ are, respectively, aerobic respiration, denitrification and nitrification. Reaction $r1$ and $r2$ account for dissolved organic carbon (DOC) degradation with oxygen (in $r1$) and nitrate (in $r2$) as the electron acceptors. Reaction $r3$ characterizes the oxidation of ammonium into nitrate with oxygen as the electron acceptor.

Degradation of DOC is assumed to follow a first-order reaction rate:

$$\Gamma_{\text{DOC}} = k_{\text{DOC}} \cdot C_{\text{DOC}} \quad (5.2)$$

where $k_{\text{DOC}} = 5.0 \times 10^{-6} \text{s}^{-1}$ [Van Cappellen and Wang, 1996] is the DOC decay constant, Γ_{DOC} (Ms^{-1}) is the DOC oxidation rate, and C_{DOC} is the DOC molar concentration. The rate of reduction for oxygen and nitrate is given by:

$$\Gamma_{\text{red},i} = \beta_i \cdot \Gamma_{\text{DOC}} \cdot f_i \quad (5.3)$$

Where $i = 1$:oxygen or 2 :nitrate, $\Gamma_{\text{red},i}$ (Ms^{-1}) is the reduction rate, and β is a stoichiometric ratio between the moles of transferred electrons per mole of oxidized DOC and moles of electrons acceptor ($\beta_1 = 1$ and $\beta_2 = 0.8$). The parameter f ensures a Monod-type behavior and is determined by:

$$f_i = \left(1 - \sum_{n=0}^{i-1} f_n \right) \cdot \alpha_i \quad (5.4)$$

with $f_0 = 0$ and:

$$\alpha_i = \frac{C_i}{C_{i,lim}} \text{ if } C_i < C_{i,lim} \quad (5.5)$$

or:

$$\alpha_i = 1 \text{ if } C_i \geq C_{i,lim} \quad (5.6)$$

where C_i and $C_{i,lim}$ are, respectively, the molar concentration and molar limiting concentration of oxygen or nitrate. The parameter α therefore characterizes the dependence of the reduction rate on the availability of electron acceptors in the form of oxygen and nitrate concentrations. If oxygen is present at concentrations greater than its limiting value, then the reduction reaction proceeds at a rate which is independent of the oxygen concentration. With concentrations below the limit, the rate of the reduction reaction is linearly proportional to the concentration.

The rate expression for nitrification Γ_{nitr} (Ms^{-1}) is:

$$\Gamma_{nitr} = k_n \cdot C_{\text{NH}_4^+} \cdot C_{O_2} \quad (5.7)$$

Where $C_{\text{NH}_4^+}$ and C_{O_2} are the molar concentrations of ammonium and oxygen, respectively and $k_n = 0.159 \text{ M}^{-1}\text{s}^{-1}$ is the second-order molar rate coefficient [Van Cappellen and Wang, 1996].

The upper model boundary was set as a Cauchy type with constant concentration for inflow and model derived concentration for outflow. Molar concentrations of each species were assigned values commensurate with those of Bardini et al. [2012]. Three different scenarios were considered in which the specified concentrations varied (Table 5.3). For the multi-bedform model the lateral boundaries were Cauchy type with zero concentration for the inflow on the left and model derived concentrations for outflow on the right.

Reactant	sceanrio 1	sceanrio 2	sceanrio 3
DOC	4.99×10^{-3}	1.63×10^{-3}	1.63×10^{-3}
O ₂	3.125×10^{-4}	3.125×10^{-4}	3.125×10^{-4}
NO ₃	1.29×10^{-4}	1.613×10^{-5}	1.613×10^{-5}
NH ₄ ⁺	2.78×10^{-4}	2.78×10^{-6}	2.78×10^{-6}

TABLE 5.3: Inflow concentrations (M) of reactant species for 3 scenarios

The single bedform model adopted the SPB boundary for PHT3D [Laatooe et al., tted]. The no-flow lower boundary was set as zero mass flux for both models. Initial concentrations were set to zero everywhere. Advective terms were solved using mass-conservative upstream-weighted finite-difference and a convergence criterion for the generalized conjugate gradient matrix solver was set at 10^{-9} [moles] in all simulations. All reactive transport simulations were transient with total simulation time set at 120 hours. This selection was based on the establishment of an approximate steady-state, defined as a change of less than 0.1% mass between time steps, for a conservative solute in the multi-bedform model.

Qian et al. [2008] showed via dimensional analysis that controls on mass flux across the SSI can be described by two dimensionless parameters, a steepness ratio R ; and a length scale parameter λ . For our investigation $R = a/\Delta h$, where a is the amplitude of head variation at the surface [L]; and λ is α_L/L , where α_L is the longitudinal dispersivity [L] and L is the downstream length of the bedform [L]. Laatooe et al. [2014] showed that the potential for error in the solute distribution with the periodic solute assumption is greatest with combinations of $R < 200$ and $\lambda > 0.001$. Here, 9 models comprising combinations of R (2, 20, 200) and λ (0.1, 0.01, 0.001) values were examined for each scenario, which corresponds to a range that is still of practical interest [Qian et al., 2008; Laatooe et al., 2014]. The fixed bedform length of 1.0 m for this investigation makes λ equivalent to α_L .

A metric from Zarnetske et al. [2012] was adopted to facilitate comparison between bedforms. They characterized HZ regions as net nitrifying or net denitrifying with a Dahmköhler number [dimensionless] defined as the species reaction rate, Γ [T^{-1}] multiplied by residence time, τ [T]. In this study, residence time was obtained through direct

age simulation in PHT3D using a zeroth-order reaction [Goode, 1996]. Reaction rates at each node were then determined based on modelled concentrations and multiplied by the residence time. The Dahmköhler number for each species thus obtained was averaged for each bedform at every time step. Evaluating the performance of the SPB, with respect to its ability in replicating infinite series was then made through examination of the downstream reactivity trend between bedforms in the multi-bedform model and comparing them to the results produced by the single bedform SPB model.

It is also worth noting that simulation times were significantly different between the single bedform SPB model and the 11 bedform variant. For simulations where $\Delta h = 0.1$, the multi-bedform models required 16 hours while the SPB simulations on the same processing platform required approximately 30 minutes.

5.4 Results

Steady state flow fields for the single bedform models are presented in Figure 5.2. Multi-bedform models feature identical flow fields repeated in each bedform. Greater R values effectuate an increased depth of penetration of the hyporheic flow cell (Figure 5.2), which is a direct response to the decrease in the lateral seepage flux of the underflow regime beneath the hyporheic flow cell [Cardenas and Wilson, 2007d]. The effect of symmetrical solute concentration forcing between lateral boundaries by the SPB in a transient simulation is more significant as R decreases (for the same value of λ). This is evidenced by the wider transition zone of simulated ages between the flow regimes (Figure 5.2), which agrees with Laatooe et al. [2014], who suggested that vertical concentration gradients, in this instance age gradients, will be decreased with smaller R value models implementing an SPB.

Solute distributions in scenario 1 for 2 ($R = 20$ and $\lambda = 0.1$, and $R = 2$ and $\lambda = 0.1$) specific multi-bedform simulations (Figure 5.3 and Figure 5.4) are presented to demonstrate the complex interactions that are not observable when using a SPB model. Figure 5.3 presents the reactant species concentration distributions in the multi-bedform

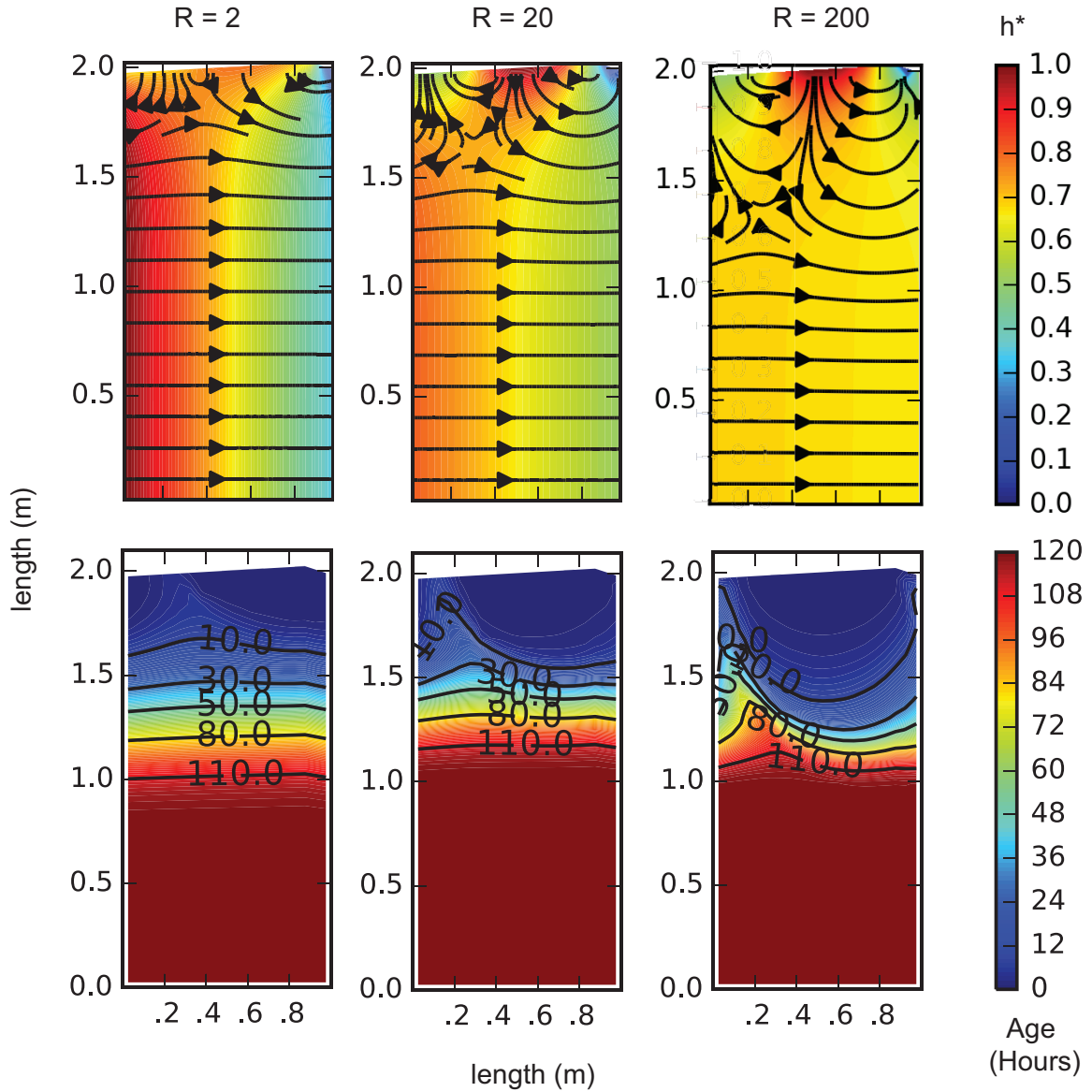


FIGURE 5.2: Head distributions and flow fields specific to each R value used in the simulations (top row). Heads are normalized $h^* = (h - h_{min})/(h_{max} - h_{min})$, where h^* is the normalized head value, h [L] is the nodal head value, h_{max} and h_{min} are, respectively, the maximum and minimum head values in each simulation direct-age distributions observed in the single bedform models with $\lambda = 0.001$ at time $t = 120$ hours (bottom row)

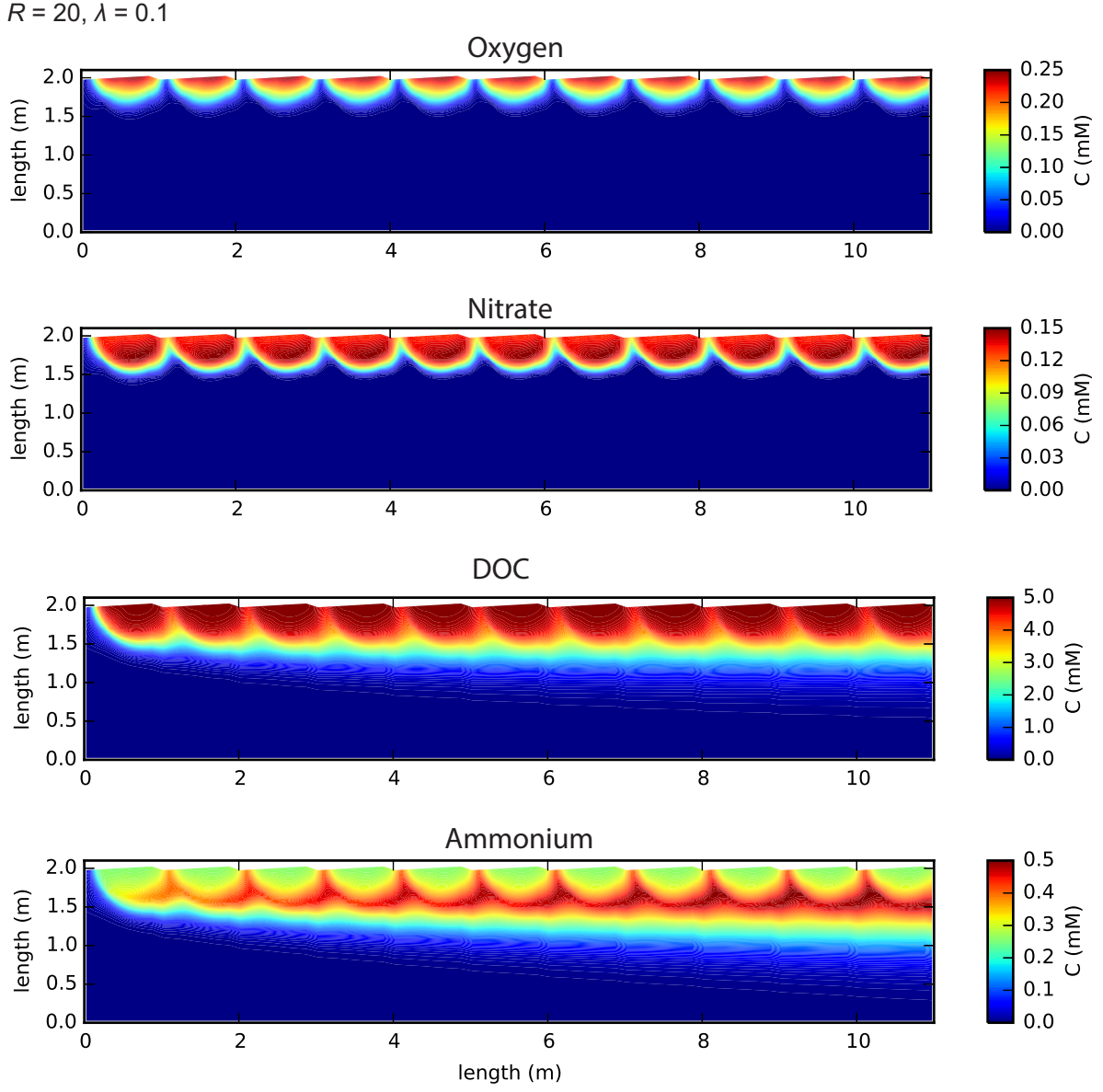


FIGURE 5.3: Concentrations of reactants in a multi-bedform model at $t = 120$ hours for $R = 20$ and $\lambda = 0.01$

model at $t = 120$ hours for simulation $R = 20$ and $\lambda = 0.01$. For this scenario the depth penetration of the HZ is approximately 0.5 m below the surface (see Figure 5.2). Oxygen does not penetrate the hyporheic cell to its full extent because it is rapidly reduced by both DOC oxidation and nitrification. This implies that some flow paths in the HZ circulation traverse both oxic (oxygen present) and anoxic (oxygen absent) environments before returning to the surface water. A flow path traversing both oxic and anoxic is capable of completely converting ammonium to nitrogen gas provided the reaction rates are faster than reactant supply [Hunter et al., 1998].

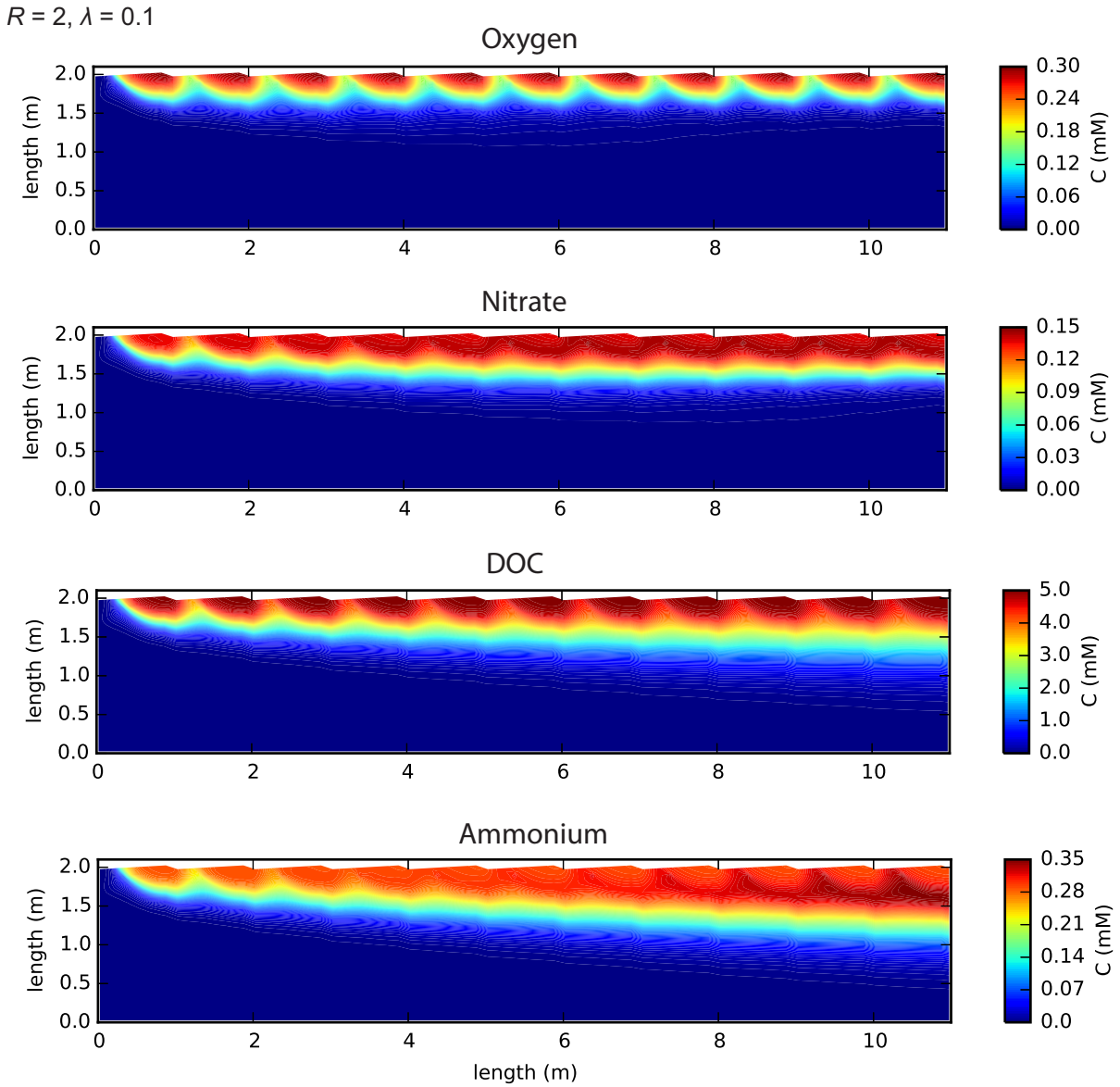


FIGURE 5.4: Concentrations of reactants in a multi-bedform model at $t = 120$ hours for $R = 2$ and $\lambda = 0.1$

Nitrate is found deeper in the hyporheic flow cell with a comparatively sharper concentration front than oxygen. Also noteworthy are the regions, within the HZ, displaying reversal in vertical concentration gradient for nitrate from increasing to decreasing with depth. (see Figure 5.3). These coincide with the extent of oxygen penetration and are the result of nitrification processes converting ammonium to nitrate within the oxic environment. Denitrification in the anoxic region of the hyporheic flow cell is proceeding at rates faster than supply of nitrate by advection and dispersion. This results in a complete conversion of all nitrate to nitrogen gas and constrains its presence in the

simulation to the hyporheic flow cell.

Both ammonium and DOC are supplied at rates faster than they are consumed and are dispersed across the flow divide between the HZ and underflow. DOC concentrations are not visually periodic and appear to have concentration distributions typical of conservative solutes in similar multi-bedform models (cf. Figure 3.3). The ammonium distribution within the hyporheic flow cells is quite complex, with each successive bedform displaying noticeably greater concentrations in the anoxic part of the circulation cell, thus violating the assumption of periodicity in the HZ. Here, ammonium is converted to nitrate in the oxic part of the HZ thereby diminishing its concentration. As oxygen becomes depleted the rate of conversion decreases and the concentration of ammonium increases. The concentrations are further increased by residual ammonium in the underflow that is laterally transferred to downstream bedforms.

For simulations where $R = 2$ the HZ circulation is significantly shallower (see Figure 5.2). When increasing the lateral seepage flux of the underflow ($R = 2$) and the dispersion ($\lambda = 0.1$), the solute front of oxygen noticeably retreats towards the SSI with increasing bedform number (Figure 5.4). A narrower oxic zone facilitates denitrification closer to the surface evidenced by the raised location of the nitrate solute front in downstream bedforms. Oxygen and nitrate both decrease in penetration depth of the solute front in successive bedforms starting at bedform number 7. These observations imply increased concentrations of DOC and ammonium in the HZ of successive downstream bedforms, which may be attributed to the increased lateral flux of these reactants between bedforms. The retreat of solute fronts back towards the SSI in downstream bedforms highlights the potential impact that mixing and solute concentrations in the underflow have on biogeochemical processes occurring within the hyporheic flow circulation.

A subset of the results comprising all R values of scenario 1 with $\lambda = 0.01$; scenario 2 $R = 20, \lambda = 0.1$; scenario 3 $R = 20, \lambda = 0.1$, are presented for analysis and discussion. Plots comparing the species specific Damköhler number revealed that altering λ values, produced very little change to the observable trend of the Damköhler number versus

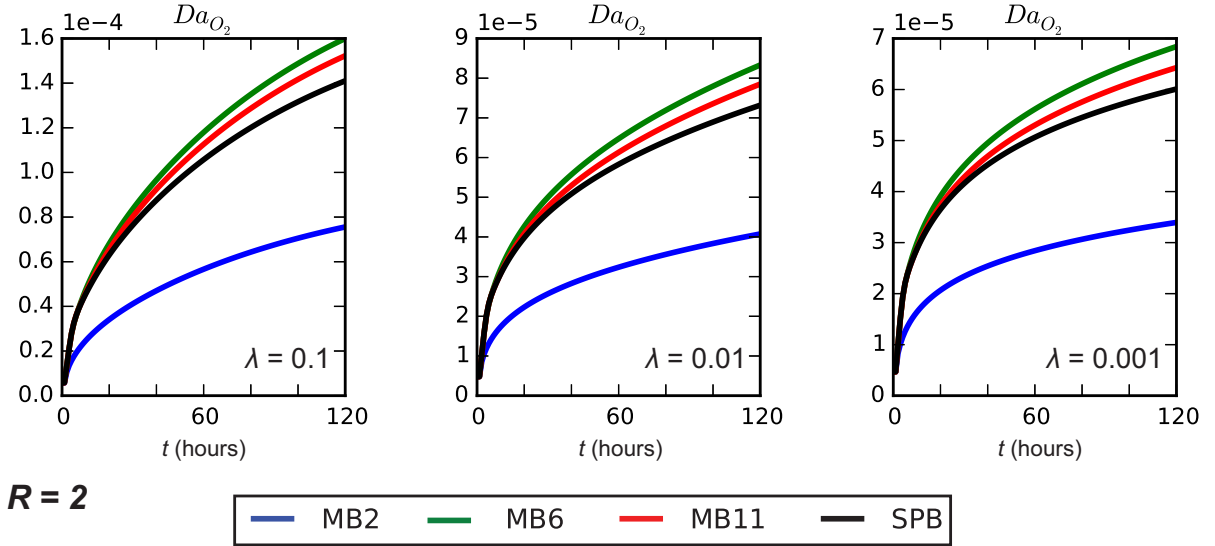


FIGURE 5.5: Da_{O_2} differences with changing λ values for simulations where $R = 2$. The pattern of difference between the models remains despite the change in λ .

time in bedforms MB2, MB6, MB11 and SPB (Figure 5.5), albeit that the magnitudes change. Increasing values of R (reduced underflow) show reduced differences between bedforms (Figure 5.6), which agrees with a previous study that identified greater R values approximate a periodic solution for conservative solutes [Laatooe et al., 2014].

For simulations where $R = 200$, lateral advective transport in the underflow is minimal. The Damkhöler values for DOC (Da_{DOC}) and nitrate (Da_{NO_3}) are well matched by all bedforms, while ammonium ($Da_{NH_4^+}$) and oxygen (Da_{O_2}) indicate the SPB is a closer match for MB6 and MB2. A noteworthy observation is the reduced reactivity in MB11 when compared to MB6, evidenced by the greater Da_{O_2} and $Da_{NH_4^+}$ values for MB6. This is also observable for Da_{NO_3} albeit to a lesser extent. The greater Da_{O_2} in MB6 signals a greater flux of DOC, ammonium or oxygen entering the oxic zone in comparison to MB11 and the SPB. A greater Da_{NO_3} implies increased fluxes of both DOC and nitrate into the anoxic region of the HZ cell and underflow.

The SPB appears to perform equally well with scenarios where $R = 20$, $\lambda = 0.01$. Here there is very little difference between the reactivity of each species in all bedforms. The stepped increase observed with Da_{DOC} between bedforms is indicative of increased DOC mass flux in the underflow, which now has greater lateral seepage velocity in

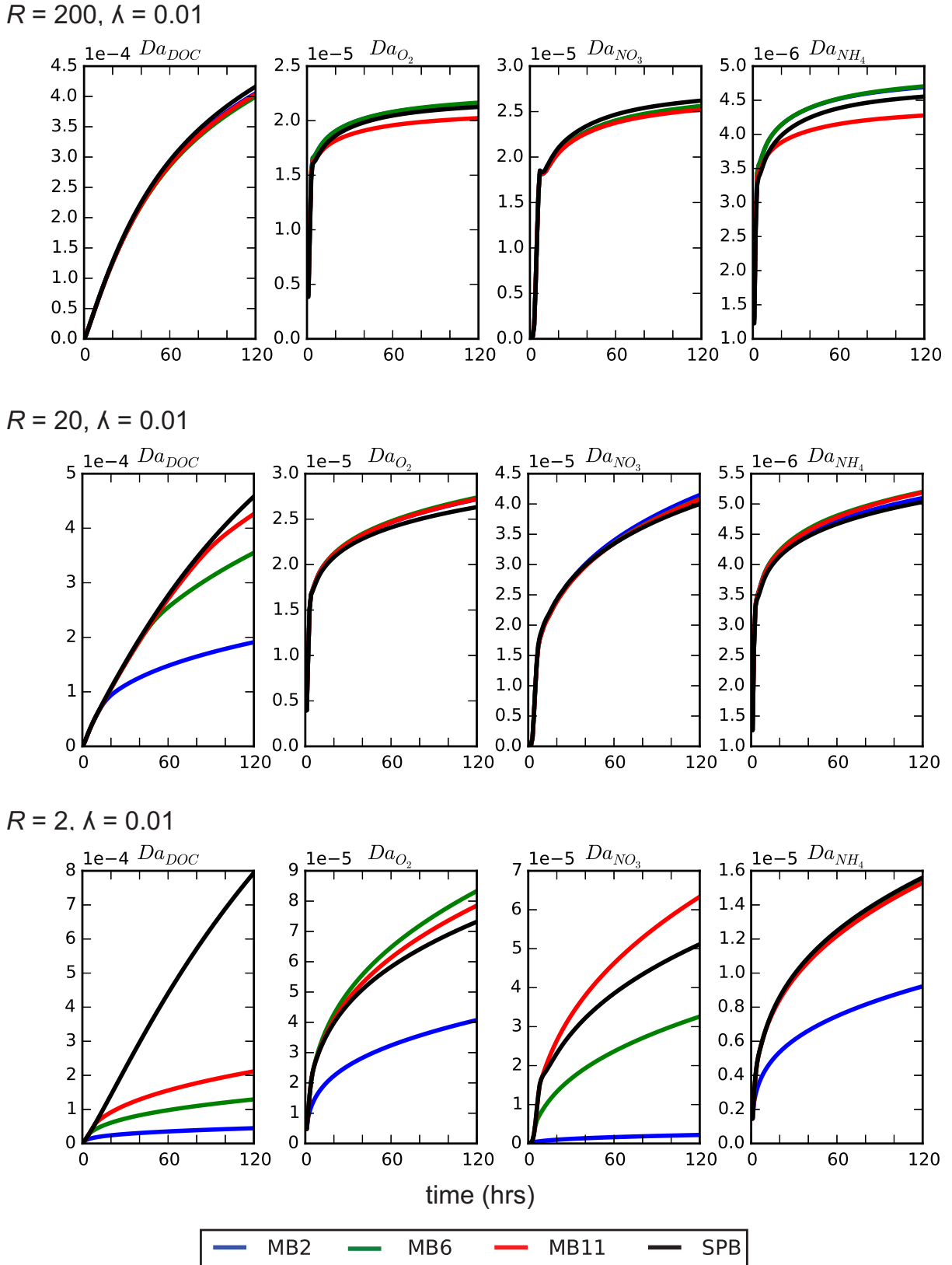


FIGURE 5.6: Subset of results demonstrating the differences to Da values in bedforms MB2, MB6, MB11 and the SPB when changing R .

comparison to models where $R = 200$. For this scenario, excess DOC in the underflow does not significantly alter the reactivity of other species because there are no other species present in the underflow to react with.

Lateral advective transfer between bedforms is greatest in simulations with $R = 2$ and has a significant effect on the differences in reactivity between all bedforms. Differences between bedforms can be attributed to the reactivity of the underflow as the HZ is very shallow (see Figure 5.2). MB2 displays large reactivity differences to its downstream counterparts, due to smaller solute mass gains from upstream bedforms. The Da_{DOC} in the model is significantly greater with the SPB although, this appears to have little effect on the reduction of oxygen and nitrate. Reactivity for all other species in the SPB model appears to trend closer to that of MB11 than MB6, which is in accordance with the assumption of infinite series.

Scenario 2 has lower concentrations of ammonium, nitrate and DOC entering the system via the SSI. This results in diminished reactivity for Da_{DOC} in all bedforms (Figure 5.7). The lower concentrations of DOC and ammonia decrease the demand for oxygen in the HZ and results in greater depth penetration of the oxic region. This facilitates conversion of ammonium to nitrate in the underflow and also limits denitrification to the underflow. Overall, the inflow concentrations for all species in scenario 2 place greater emphasis on reactions in the underflow. Most notable is the significant difference in Da_{NO_3} between the multi-bedform and the single.

A further decrease in the DOC concentration with scenario 3 leads to greater concentrations of oxygen, nitrate and ammonium dispersing to the underflow and triggers significant differences in MB2 reactivity for all species when compared to MB6, MB11 and SPB (Figure 5.8). Da_{NO_3} for the SPB model is significantly greater than in the previous scenario and there is also a corresponding increase in $Da_{NH_4^+}$.

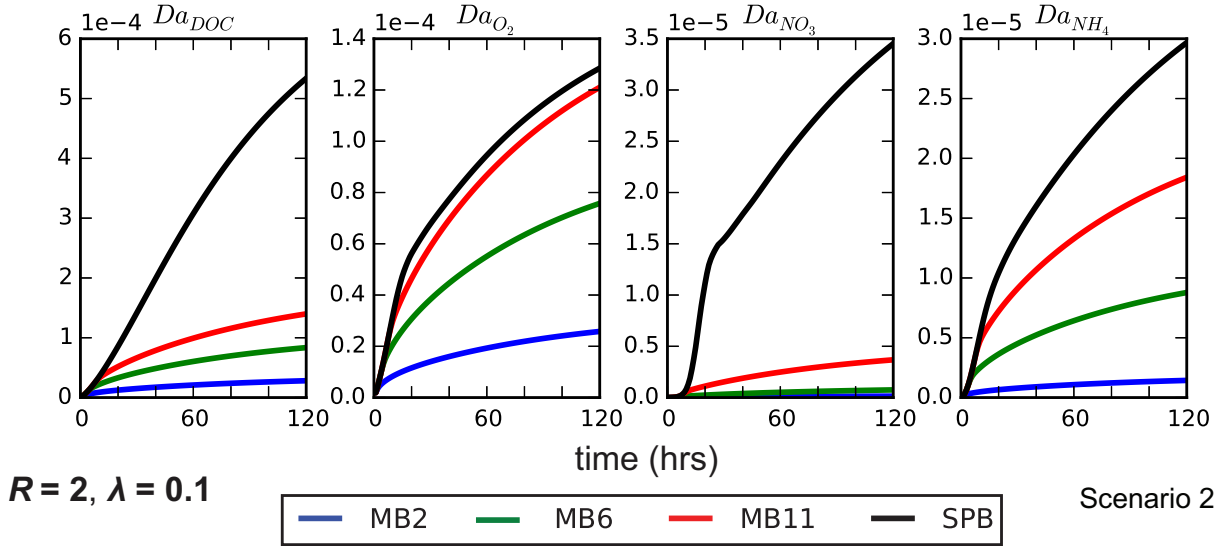


FIGURE 5.7: Scenario 2 simulation $R = 2, \lambda = 0.1$. Inflowing concentrations are decreased for DOC, nitrate and ammonium. Significantly greater nitrate reactivity (denitrification) in the SPB model.

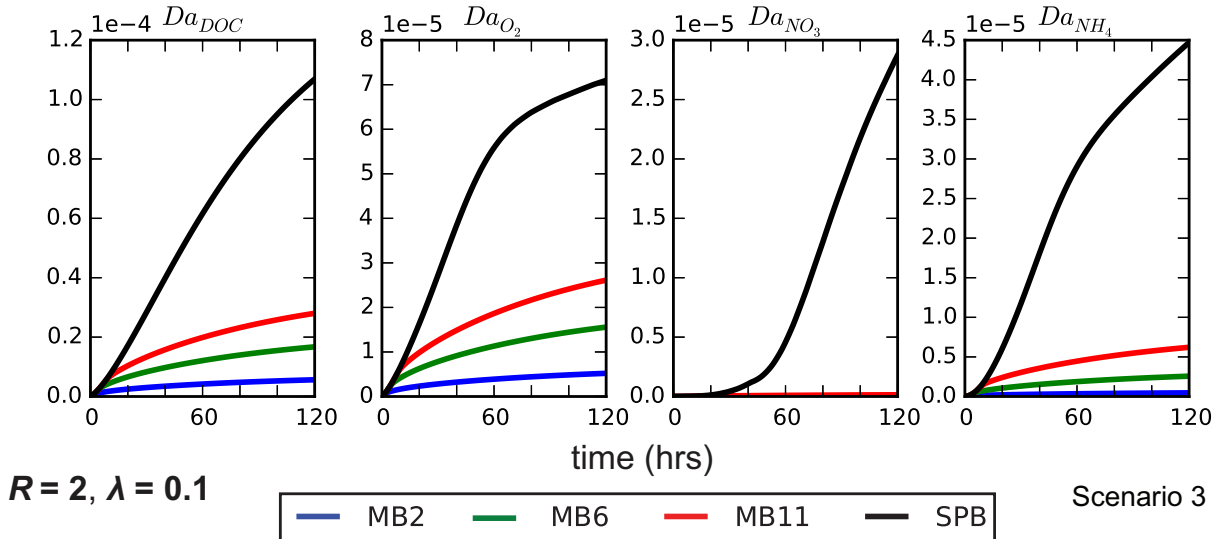


FIGURE 5.8: Scenario 3 simulation $R = 2, \lambda = 0.1$. DOC is limited to an extent such that nitrate is no longer completely consumed in the HZ.

5.5 Discussion

The scenario 1 concentration set used for inflowing reactant species results in the majority of redox processes constrained to the HZ flow cell and very little reactivity contributed from the underflow. Excess concentrations of ammonium and DOC in the underflow caused by the SPB contribute indirectly to a reduction in bedform reactivity by altering the dispersive and diffusive fluxes across the SSI. The HZ flow cell is advectively

dominated [Cardenas and Wilson, 2007d] and once established, changes to dispersive and diffusive fluxes across the SSI are dependent on the vertical concentration gradient between the HZ and underflow [Qian et al., 2008; Jin et al., 2010; Bottacin-Busolin and Marion, 2010]. The concentration gradient driven flux across the SSI is significantly smaller than advective and variations have limited effect on chemical reactivity within the HZ for this model. Consequently, the bulk reactivity produced by the single bedform model is similar to those of the multi-bedform model when the majority of the reactions are constrained to the advectivley dominated HZ flow cell. This reflects observations with conservative solutes where it was demonstrated that periodicity is approached when the transfer of solute mass to the underflow is minimized [Laattoe et al., 2014].

Past use of the HZ bedform reactive model focused on identifying controls for net nitrification or net denitrification conditions [Cardenas et al., 2008; Bardini et al., 2012, 2013]. These are determined via the ratio of Da_{NO_3} to $Da_{NH_4^+}$ where $Da_{NO_3}/Da_{NH_4^+} > 1$ characterizes a nitrate sink and $Da_{NO_3}/Da_{NH_4^+} < 1$ a nitrate source. For Scenario 2, $R = 2, \lambda = 0.01$, (Figure 5.7) the multi-bedform results are suggestive of the bedform being a nitrate source with $Da_{NH_4^+}$ always greater than Da_{NO_3} while the SPB equivalent is a nitrate sink. This is a clear indication that careful consideration is required when implementing a SPB in reactive transport simulations.

The current experiment includes reactants entering via the SSI only with no gaining or losing stream effects. Experiments with conservative solutes identified that the mass difference between bedforms was exacerbated with losing conditions [Laattoe et al., 2014]. It is reasonable to assume that this is also the case for reactive transport simulations with the SPB. For gaining stream scenarios with steep upward gradients the HZ itself may become reduced in extent [Cardenas and Wilson, 2007e; Sawyer and Cardenas, 2009]. In situations where the gaining flux is weaker, the mixing zone between the HZ and underflow will be reduced [Hester et al., 2013]. Either type of gaining scenario produces conservative solute distributions that constrain solutes to the HZ approximating periodicity and is therefore considered also suitable for SPB simulation.

Shrinking of the oxic zone in response to lateral transfer of solutes between bedforms (Figure 5.4) suggests that mixing effects should not be neglected when investigating processes occurring in the HZ. Mixing in these experiments caused significant variation to rates of reactions along a specific flow path. It is common to compare biogeochemical process time scales to HZ residence times to predict streambed net nitrate source-sink function [Marzadri et al., 2011; Zarnetske et al., 2012; Gomez et al., 2012]. A flow path in one bedform may only traverse the oxic zone, while the same flow path in another bedform traverses both oxic and anoxic zones. The implication here is that HZ residence times obtained in the field should not be directly translated into net nitrification or net denitrification. Add to this recent work identifying anoxic micro-zones within the bulk oxic HZ's [Briggs et al., 2014, 2015] and the idea of linking biogeochemical transformations strictly to residence time becomes less plausible.

In reality, the steady-state concentration distribution of an infinite series of bedforms with a conservative solute occurs when the stream solute concentration is uniform throughout the bedform (see Laatooe et al. [2014]). As a consequence, it is likely that observations of conservative solute concentration gradients in streambeds under field conditions will be milder and possibly extend to greater depths than single bedform model simulations predict. However, this is clearly not the case when investigating reactive solutes with multiple species and competing rates of reaction. Here, concentration changes associated with chemical reactions produce complex dispersive and diffusive fluxes between hyporheic, underflow and adjacent bedforms that cannot be replicated by the SPB model due to the symmetrical forcing of solute concentrations at the lateral boundaries.

5.6 Conclusions

This study demonstrated that the effect of the SPB on chemical reactions in HZ simulations is minimal when the bulk reactivity for each species is constrained to the HZ flow

cell. The SPB model reactivity was matched closest to the last bedform in the multi-bedform model, which is in accordance with the SPB assumption of infinite repetition. For the reaction network considered, the SPB approach to simulating HZ processes is very attractive from a computational point of view with multi-bedform models with 11 times more cells requiring 30 times more processing time. The reactivity trends observed in the multi bedform simulations where $R = 20$ and $R = 200$ were closely matched by the SPB.

Departure of the SPB model from trends observed in the multi-bedform model increased with greater reactivity in the underflow. Simulations with $R = 2$ produced greatest overall reactivity indicating that lateral transport between bedforms in the HZ and underflow enhances biogeochemical reactions. This corresponds to observations with conservative solutes although, the effect is less pronounced than the net difference in solute distribution because reactivity is dependent on the presence and concentration of all reactants.

The multi-bedform experiments also revealed that mixing should not be neglected when assessing HZ flow paths based on residence time as net nitrification or net denitrification. Our results showed that with a single bedform model scenarios with $R = 2$ and $\lambda = 0.1$ could be characterized incorrectly as a nitrate sink when a multi-bedform model with identical parameter set behaves as a nitrate source. Careful consideration is therefore required before utilizing the SPB in a reactive-transport bedform model, particularly when examining scenarios with enhanced lateral seepage flux. Despite the potential for increased model runtimes, the multi-bedform model is a superior choice with no potential for boundary mass flux errors and is essential for investigating the complex chemical interactions that occur through downstream mixing processes in the HZ.

Chapter 6

Conclusions

6.1 Contribution of this work to the field

Two of the studies in this thesis focused on the development and implementation of spatially periodic boundary conditions in block-centred finite difference groundwater modelling software. The other two studies assessed the effects of the boundaries on a popular hyporheic zone bedform model. Processes that were investigated include solute, thermal and reactive transport. The key contributions of the thesis to the field of hyporheic zone research are summarized below. The implementation of a spatially periodic boundary (SPB) in MODFLOW extends the capabilities of this code to the numerical modelling of single bedforms in an infinite sequence. Previous applications of MODFLOW were restricted to specific flow patterns and thus the use of this code has remained limited to date. This thesis has lifted this restriction, providing a scope for future HZ research. Moreover, the SPB in MODFLOW can be applied to other flow simulations [Durlofsky and Brady, 1987] and effective media parameter calculations such as permeability; [Durlofsky, 1991; Renard and de Marsily, 1997].

An approach for implementing a spatially-periodic boundary was also derived for the MODFLOW-based simulators MT3DMS and PHT3D for conservative and reactive solute transport. Previous work on HZ transport and chemical transformations has been

based on proprietary computational fluid dynamics software. Although couplings between such tools and geochemical codes like PHREEQC have been achieved [Cardenas et al., 2008; Bardini et al., 2012, 2013], the potential use of the native reactive transport code PHT3D provides major advantages in terms of versatility, speed and ease of access.

The modified codes formed the modelling platform for the detailed analysis of the general validity of spatial-periodicity in stream bedforms. While the computational gain of using a single bedform SPB model over a multi-bedform variant is significant (computation times were found to differ by a factor of 4.5 to 30 for the various setups considered), the single bedform model poses some significant limitations. Steady state concentration distributions of conservative solute transport, multi-bedform models featuring spatially periodic flow fields demonstrated that the single bedform SPB approach produces physically unrealistic solute distributions. It was shown that the departure from spatial periodicity becomes greater when the lateral seepage flux of the underflow is enhanced or when mixing through diffusion and dispersion increases. Losing stream scenarios exacerbate the potential mass flux error while gaining stream conditions promoted spatial periodicity. A temporally sinusoidal variation in the transport flux at the upper boundary of the multi-bedform model results in a reversal of the concentration gradients in the HZ, which also lead to improved approximations of spatial periodicity. The lower bound of the potential mass flux error when using SPB's with the single bedform model is estimated at 3%. The effects of the SPB on reactive transport are revealed to be minimal when the bulk of the reactions are constrained to the hyporheic zone and the lateral transfer between bedforms is also minimal. Significant differences arise in both the HZ and underflow when downstream seepage flux increases due to the effects of the chemical reactions on solute distributions. This also affects fluxes in and out of the top boundary and the vertical dispersion into the underflow, with follow on effects to the chemical reactions. Departure of the SPB model from trends observed in the multi-bedform model increases with greater reactivity in the underflow. The multi-bedform experiments also reveal that mixing should not be neglected when assessing HZ flow

paths based on residence time as net nitrification or net denitrification. A single bedform model scenario with enhanced flux in the underflow and mixing characterized the single bedform as a nitrate sink when the multi-bedform model with identical parameter set behaves as a nitrate source.

6.2 Future work

The models and methods developed in this study may have potential application in numerous future investigations. Cook et al. [2006] demonstrated a method to estimate HZ residence time with radon concentrations sampled instream and from the bed sediments. Their methodology is based on an assumption that the HZ is well mixed, which represents highly idealized conditions. The limitations of the methodology with respect to HZ chemical reactive variability are not well understood. Variations in the concentration of sorbed radium in the porous media attributed to redox conditions will affect radon production rates in the HZ. Groundwater with a significantly higher concentration of radon will also lead to an incorrect estimation of the HZ residence time. A multi-bedform model with closed lateral boundaries produces a shallow HZ exchange model with losing conditions at the upstream boundary and gaining conditions at the downstream boundary. This flow pattern is analogous to the superposition of two commonly examined HZ flow scales 1) the shallow bedform scale and 2) the slightly deeper pool-riffle sequence scale. There have been no studies to date which have examined HZ process with both scales simultaneously.

Mixing of reactive species in the HZ was shown to have a significant impact on reaction rates for a specific flow path. This topic requires further investigation as the common approach used with HZ chemical transformations is to link the rates strictly to HZ residence times. The multi-bedform model is a useful tool to explore these effects further under different conditions and with different chemical species. Recent work by Briggs et al. [2015] demonstrated the formation of anoxic microzones in a bulk oxic HZ using a pore network model. The effect of these anoxic regions will also significantly affect

reaction rates linked strictly to HZ residence times. A dual porosity single or multi-bedform model is capable of accounting for the effects of anoxic microzones and well suited to exploring this further.

Appendix A

The spatial periodic flow boundary source code

The modified FORTRAN source code of MODFLOW's general head boundary package is presented below. The changes made to the code which provide spatial periodic function are highlighted via comments. In addition, the author is happy to provide the compiled MODFLOW executable with SPB function and/or any assistance with implementation.

```
C ****
C Supplement to 'Spatial Periodic boundary for MODFLOW' by Laatooe
C et al., 2013 published in Ground Water.
C This file demonstrates the implementation of the Spatial Periodic
C Boundary condition in MODFLOW by showing the required changes to
C the GHB module. The changes shown are for illustrative purposes
C and do not intended to guarantee universal, generic applicability
C of the code.
C Additions/changes to original GHB code are highlighted by comment
C lines C(SPB)**** preceding the required modification for SPB
C function.
C ****
MODULE GWFGBMODULE
    INTEGER ,SAVE ,POINTER :: NBOUND ,MXBND ,NGHBVL ,IGHBCB ,IPRGHB
    INTEGER ,SAVE ,POINTER :: NPGHB ,IGHBPP ,NNPGHB
C
```

```

C(SPB)**** Declare DH as a new variable ****
C      DH is the fixed difference between the SPB boundary pair (see
C      manuscript). The input file for the GHB package in MODFLOW requires
C      the user to define head values for the external cells. This is not
C      required with SPB pairs. Instead users should insert the value for
C      DH at all locations in the GHB input file where heads are required.
C

      REAL ,    SAVE , POINTER   ::DH

C

      CHARACTER(LEN=16),SAVE,  DIMENSION(:),   POINTER      ::GHBAUX
      REAL ,           SAVE ,  DIMENSION(:, :),  POINTER     ::BNDS

TYPE GWFGHBTYP
      INTEGER ,POINTER  ::NBOUND ,MXBND ,NGHBVL ,IGHBCB ,IPRGHB
      INTEGER ,POINTER  ::NPGHB ,IGHBPB ,NNPGHB

C

C(SPB)**** Set type for DH ****
      REAL     ,POINTER   ::DH

C

      CHARACTER(LEN=16),  DIMENSION(:),   POINTER      ::GHBAUX
      REAL ,           DIMENSION(:, :),  POINTER     ::BNDS

END TYPE
TYPE(GWFGHBTYP),  SAVE::: GWFGHBDAT(10)
END MODULE GWFGHBMODULE

SUBROUTINE GWF2GHB7AR(IN,IGRID)
C ****
C      ALLOCATE ARRAY STORAGE AND READ PARAMETER DEFINITIONS FOR GHB
C      PACKAGE
C ****
C
C      SPECIFICATIONS:
C
C      -----
      USE GLOBAL ,          ONLY:IOUT ,NCOL ,NROW ,NLAY ,IFREFM
C
C(SPB)**** Add DH onto the end of the USE list below ****
      USE GWFGHBMODULE ,  ONLY:NBOUND ,MXBND ,NGHBVL ,IGHBCB ,IPRGHB ,NPGHB ,
      1                  IGHBPB ,NNPGHB ,GHBAUX ,BNDS ,DH
C
      CHARACTER*200 LINE
C
C      -----
      ALLOCATE(NBOUND ,MXBND ,NGHBVL ,IGHBCB ,IPRGHB)

```

```

      ALLOCATE(NPGHB ,IGHBPB ,NNPGHB)

C
C(SPB)**** Allocate memory for DH ****
      ALLOCATE(DH)

C
C1-----IDENTIFY PACKAGE AND INITIALIZE NBOUND.
      WRITE(IOUT,1)IN
1 FORMAT(1X,/1X,'GHB -- GENERAL-HEAD BOUNDARY PACKAGE, VERSION 7',
1     ', 5/2/2005',/,9X,'INPUT READ FROM UNIT ',I4)
      NBOUND=0
      NNPGHB=0

C
C2-----READ MAXIMUM NUMBER OF GHB'S AND UNIT OR FLAG FOR
C2-----CELL-BY-CELL FLOW TERMS.
      CALL URDCOM(IN,IOUT,LINE)
      CALL UPARLSTAL(IN,IOUT,LINE,NPGHB,MXPB)
      IF(IFREFM.EQ.0) THEN
          READ(LINE,'(2I10)') MXACTB ,IGHBCB
          LLOC=21
      ELSE
          LLOC=1
          CALL URWORD(LINE,LLOC,ISTART,ISTOP,2,MAXCTB,R,IOUT,IN)
          CALL URWORD(LINE,LLOC,ISTART,ISTOP,2,IGHBCB,R,IOUT,IN)
      END IF
      WRITE(IOUT,3) MXACTB
3 FORMAT(1X,'MAXIMUM OF ',I6,' ACTIVE GHB CELLS AT ONE TIME')
      IF(IGHBCB.LT.0) WRITE(IOUT,7)
7 FORMAT(1X,'CELL-BY-CELL FLOWS WILL BE PRINTED WHEN ICBCFL NOT 0')
      IF(IGHBCB.GT.0) WRITE(IOUT,8) IGHBCB
8 FORMAT(1X,'CELL-BY-CELL FLOWS WILL BE SAVED ON UNIT ',I4)

C
C3-----READ AUXILIARY VARIABLES AND PRINT OPTION.
      ALLOCATE (GHBAUX(20))

      NAUX=0
      IPRGHB=1

10 CALL URWORD(LINE,LLOC,ISTART,ISTOP,1,N,R,IOUT,IN)
      IF(LINE(ISTART:ISTOP).EQ.'AUXILIARY' .OR.
1           LINE(ISTART:ISTOP).EQ.'AUX') THEN
          CALL URWORD(LINE,LLOC,ISTART,ISTOP,1,N,R,IOUT,IN)
          IF(NAUX.LT.5) THEN
              NAUX=NAUX+1
              GHBAUX(NAUX)=LINE(ISTART:ISTOP)
          END IF
      END IF

```

```

        WRITE(IOUT,12) GHBAUX(NAUX)
12      FORMAT(1X,'AUXILIARY GHB VARIABLE: ',A)
      END IF
      GO TO 10
ELSE IF(LINE(ISTART:ISTOP).EQ.'NOPRINT') THEN
      WRITE(IOUT,13)
13      FORMAT(1X,'LISTS OF GENERAL-HEAD BOUNDARY CELLS WILL NOT BE',
&           ' PRINTED')
      NPRGH = 0
      GO TO 10
END IF

C3A----THERE ARE FIVE INPUT DATA VALUES PLUS ONE LOCATION FOR
C3A----CELL-BY-CELL FLOW.

NGHBVL=6+NAUX

C
C4-----ALLOCATE SPACE FOR THE BNDS ARRAY.

IGHBPB=MXACTB+1
MXBND=MXACTB+MXPB
ALLOCATE (BNDS(NGHBVL, MXBND))

C
C-----READ NAMED PARAMETERS.

WRITE(IOUT,1000) NPGHB
1000 FORMAT(1X,//1X,I5,' GHB parameters')
IF(NPGHB.GT.0) THEN
  NAUX=NGHBVL-6
  LSTSUM=IGHBPB
  DO 120 K=1,NPGHB
    LSTBEG=LSTSUM
    CALL UPARLSTRP(LSTSUM, MXBND, IN, IOUT, IP, 'GHB', 'GHB', 1,
&                 NUMINST)
    NLST=LSTSUM-LSTBEG
    IF (NUMINST.EQ.0) THEN
C5A----READ LIST OF CELLS WITHOUT INSTANCES.
    CALL ULSTRD(NLST, BNDS, LSTBEG, NGHBVL, MXBND, 1, IN, IOUT,
&             'BOUND. NO. LAYER   ROW   COL     STAGE   STRESS FACTOR',
&             GHBAUX, 20, NAUX, IFREFM, NCOL, NROW, NLAY, 5, 5, IPRGHB)
    ELSE
C5B----READ INSTANCES
    NINLST=NLST/NUMINST
    DO 110 I=1,NUMINST
      CALL UINSRP(I, IN, IOUT, IP, IPRGHB)
      CALL ULSTRD(NINLST, BNDS, LSTBEG, NGHBVL, MXBND, 1, IN, IOUT,

```

```

&      'BOUND. NO. LAYER    ROW    COL     STAGE    STRESS FACTOR',
&      GHBAUX ,20 ,NAUX ,IFREFM ,NCOL ,NROW ,NLAY ,5 ,5 ,IPRGHB)
LSTBEG=LSTBEG+NINLST

110      CONTINUE

      END IF

120      CONTINUE

      END IF

C
C6-----RETURN

      CALL SGWF2GHB7PSV(IGRID)

      RETURN

      END

      SUBROUTINE GWF2GHB7RP(IN,IGRID)

C      ****
C      READ GHB HEAD, CONDUCTANCE AND BOTTOM ELEVATION
C      ****
C
C      SPECIFICATIONS:
C
C      -----
      USE GLOBAL,          ONLY:IOUT,NCOL,NROW,NLAY,IFREFM
C
C      **** Add DH onto the end of the USE list below ****
      USE GWFGHBMODULE, ONLY:NBOUND,MXBND,NGBVBL,IPRGHB,NPGHB,
      1                  IGHBPB,NNPGHB,GHBAUX,BNDS,DH
C
C      -----
      CALL SGWF2GHB7PNT(IGRID)

C
C1-----READ ITMP (NUMBER OF GHB'S OR FLAG TO REUSE DATA) AND
C1-----NUMBER OF PARAMETERS.

      IF(NPGHB.GT.0) THEN
        IF(IFREFM.EQ.0) THEN
          READ(IN,'(2I10)') ITMP,NP
        ELSE
          READ(IN,*) ITMP,NP
        END IF
      ELSE
        NP=0
        IF(IFREFM.EQ.0) THEN
          READ(IN,'(I10)') ITMP
        ELSE
          READ(IN,*) ITMP
        END IF
      END IF

```

```

      END IF

C
C-----CALCULATE SOME CONSTANTS
NAUX=NGHBVL-6
IOUTU = IOUT
IF (IPRGHB.EQ.0) IOUTU=-IOUT

C
C2-----DETERMINE THE NUMBER OF NON-PARAMETER GHB'S.
IF (ITMP.LT.0) THEN
  WRITE(IOUT,7)
  7  FORMAT(1X,/1X,
  1  'REUSING NON-PARAMETER GHB CELLS FROM LAST STRESS PERIOD')
ELSE
  NNPGHB=ITMP
END IF

C
C3-----IF THERE ARE NEW NON-PARAMETER GHB'S, READ THEM.
MXACTB=IGHBPB-1
IF (ITMP.GT.0) THEN
  IF (NNPGHB.GT.MXACTB) THEN
    WRITE(IOUT,99) NNPGHB, MXACTB
    99 FORMAT(1X,/1X,'THE NUMBER OF ACTIVE GHB CELLS (',I6,
    1           ') IS GREATER THAN MXACTB('',I6,''))'
    CALL USTOP(' ')
  END IF
  CALL ULSTRD(NNPGHB,BNDS,1,NGHBVL,MXBND,1,IN,IOUT,
  1           'BOUND. NO. LAYER   ROW   COL     STAGE     CONDUCTANCE',
  2           GHBAUX,20,NAUX,IFREFM,NCOL,NROW,NLAY,5,5,IPRGHB)
END IF
NBOUND=NNPGHB

C
C1C-----IF THERE ARE ACTIVE GHB PARAMETERS, READ THEM AND SUBSTITUTE
CALL PRESET('GHB')
IF (NP.GT.0) THEN
  NREAD=NGHBVL-1
  DO 30 N=1,NP
    CALL UPARLSTSUB(IN,'GHB',IOUTU,'GHB',BNDS,NGHBVL,MXBND,NREAD,
    1           MXACTB,NBOUND,5,5,
    2           'BOUND. NO. LAYER   ROW   COL     STAGE     CONDUCTANCE',
    3           GHBAUX,20,NAUX)
  30  CONTINUE
END IF

```

```
C
C-----PRINT NUMBER OF GHB'S IN CURRENT STRESS PERIOD.
      WRITE (IOUT,101) NBOUND
      101 FORMAT(1X,/1X,I6,' GHB CELLS')

C
C-----RETURN.

C
C(SPB)**** DH is assigned ****
      DH = BNDS(4,1)

C
      260 RETURN

      END

      SUBROUTINE GWF2GHB7FM(IGRID)

C      ****
C      ADD GHB TERMS TO RHS AND HCOF
C      ****
C
C      SPECIFICATIONS:
C      -----
C
C(SPB)***Add HNEW,NCOL,NROW,NLAY onto the end of the USE list below ***
      USE GLOBAL,           ONLY:IBOUND,RHS,HCOF,HNEW,NCOL,NROW,NLAY

C
C(SPB)**** Add DH onto the end of the USE list below ****
      USE GWFGHBMODULE, ONLY:NBOUND,BNDS,DH
C      -----
C
      CALL SGWF2GHB7PNT(IGRID)

C
C1-----IF NBOUND<=0 THEN THERE ARE NO GENERAL HEAD BOUNDS. RETURN.
      IF(NBOUND.LE.0) RETURN

C
C2-----PROCESS EACH ENTRY IN THE GENERAL HEAD BOUND LIST (BNDS).
      DO 100 L=1,NBOUND

C
C3-----GET COLUMN, ROW AND LAYER OF CELL CONTAINING BOUNDARY.
      IL=BNDS(1,L)
      IR=BNDS(2,L)
      IC=BNDS(3,L)

C
C(SPB)**** Gets linked cell column number ****
C      (assumes SPB's are in first and last columns)
```

```

C
  IF(IC.LT.NCOL)THEN
    ICLINK = NCOL
  ELSE
    ICLINK = 1
  END IF

C
C4-----IF THE CELL IS EXTERNAL THEN SKIP IT.
  IF(IBOUND(IC,IR,IL).LE.0) GO TO 100

C
C5-----SINCE THE CELL IS INTERNAL GET THE BOUNDARY DATA.

C(SPB)**** Assign head of the linked cell to the fictitious cell ****
  BNDS(4,L)=HNEW(ICLINK,IR,IL)

C
  HB=BNDS(4,L)
  C=BNDS(5,L)

C
C6-----ADD TERMS TO RHS AND HCOF.
  HCOF(IC,IR,IL)=HCOF(IC,IR,IL)-C

C
C(SPB)**** RHS manipulation varies depending on which side of ****
C      the model we are on
C
  IF(ICLINK.EQ.NCOL)THEN
    RHS(IC,IR,IL)=RHS(IC,IR,IL)-(C*(HB+DH))
  ELSE
    RHS(IC,IR,IL)=RHS(IC,IR,IL)-(C*(HB-DH))
  END IF

C
  100 CONTINUE

C
C7-----RETURN.
  RETURN
END
SUBROUTINE GWF2GHB7BD(KSTP,KPER,IGRID)
C ****
C      CALCULATE VOLUMETRIC BUDGET FOR GHB
C ****
C
C      SPECIFICATIONS:
C
-----
```

```

USE GLOBAL ,           ONLY:IOUT , NCOL , NROW , NLAY , IBOUND , HNEW , BUFF
USE GWFBASMODULE , ONLY:MSUM , ICBCFL , IAUXSV , DELT , PERTIM , TOTIM ,
1                         VBVL , VBNM
USE GWFGBMODULE , ONLY:NBOUND , IGHBCB , BNDS , NGHBVL , GHBAUX
C
DOUBLE PRECISION CCGHE , CHB , RATTIN , RATOUT , RRATE
CHARACTER*16 TEXT
DATA TEXT /' HEAD DEP BOUNDS'/
C-----+
CALL SGWF2GHB7PNT(IGRID)
C
C1-----INITIALIZE CELL-BY-CELL FLOW TERM FLAG (IBD) AND
C1-----ACCUMULATORS (RATTIN AND RATOUT).
ZERO=0.
RATOUT=ZERO
RATTIN=ZERO
IBD=0
IF (IGHBCB.LT.0 .AND. ICBCFL.NE.0) IBD=-1
IF (IGHBCB.GT.0) IBD=ICBCFL
IBDLBL=0
C
C2-----IF CELL-BY-CELL FLOWS WILL BE SAVED AS A LIST, WRITE HEADER.
IF (IBD.EQ.2) THEN
NAUX=NGHBVL-6
IF (IAUXSV.EQ.0) NAUX=0
CALL UBDSV4(KSTP , KPER , TEXT , NAUX , GHBAUX , IGHBCB , NCOL , NROW , NLAY ,
1           NBOUND , IOUT , DELT , PERTIM , TOTIM , IBOUND)
END IF
C
C3-----CLEAR THE BUFFER.
DO 50 IL=1,NLAY
DO 50 IR=1,NROW
DO 50 IC=1,NCOL
BUFF(IC,IR,IL)=ZERO
50 CONTINUE
C
C4-----IF NO BOUNDARIES, SKIP FLOW CALCULATIONS.
IF (NBOUND.EQ.0) GO TO 200
C
C5-----LOOP THROUGH EACH BOUNDARY CALCULATING FLOW.
DO 100 L=1,NBOUND
C

```

```

C5A----GET LAYER , ROW AND COLUMN OF EACH GENERAL HEAD BOUNDARY.

    IL=BNDS(1,L)
    IR=BNDS(2,L)
    IC=BNDS(3,L)
    RATE=ZERO

C

C5B----IF CELL IS NO-FLOW OR CONSTANT-HEAD , THEN IGNORE IT.

    IF(IBOUND(IC,IR,IL).LE.0) GO TO 99

C

C5C----GET PARAMETERS FROM BOUNDARY LIST.

    HB=BNDS(4,L)
    C=BNDS(5,L)
    CCGHB=C

C

C5D----CALCULATE THE FOW RATE INTO THE CELL.

    CHB=C*HB
    RRATE=CHB - CCGHB*HNEW(IC,IR,IL)
    RATE=RRATE

C

C5E----PRINT THE INDIVIDUAL RATES IF REQUESTED(IGHBCB<0).

    IF(IBD.LT.0) THEN
        IF(IBDLBL.EQ.0) WRITE(IOUT,61) TEXT,KPER,KSTP
        61   FORMAT(1X,/1X,A,' PERIOD ',I4,' STEP ',I3)
        WRITE(IOUT,62) L,IL,IR,IC,RATE
        62   FORMAT(1X,'BOUNDARY ',I6,' LAYER ',I3,' ROW ',I5,' COL ',
        1      I5,' RATE ',1PG15.6)
        IBDLBL=1
    END IF

C

C5F----ADD RATE TO BUFFER.

    BUFF(IC,IR,IL)=BUFF(IC,IR,IL)+RATE

C

C5G----SEE IF FLOW IS INTO AQUIFER OR OUT OF AQUIFER.

    IF(RATE.LT.ZERO) THEN

C

C5H----FLOW IS OUT OF AQUIFER SUBTRACT RATE FROM RATOUT.

    RATOUT=RATOUT-RRATE
    ELSE

C

C5I----FLOW IS INTO AQIFER; ADD RATE TO RATING.

    RATING=RATING+RRATE

END IF

```

```
C
C5J----IF SAVING CELL-BY-CELL FLOWS IN LIST, WRITE FLOW. ALSO
C5J----FLOW TO BNDS.

99 IF(IBD.EQ.2) CALL UBDSVB(IGHBCB,NCOL,NROW,IC,IR,IL,RATE,
1                      BNDS(:,L),NGHBVL,NAUX,6,IBOUND,NLAY)
BNDS(NGHBVL,L)=RATE

100 CONTINUE

C
C6-----IF CELL-BY-CELL TERMS WILL BE SAVED AS A 3-D ARRAY, THEN CALL
C6-----UTILITY MODULE UBUDSV TO SAVE THEM.

IF(IBD.EQ.1) CALL UBUDSV(KSTP,KPER,TEXT,IGHBCB,BUFF,NCOL,NROW,
1                         NLAY,IOUT)

C
C7-----MOVE RATES, VOLUMES AND LABELS INTO ARRAYS FOR PRINTING.

200 RIN=RATIN
ROUT=RATOUT
VBVL(3,MSUM)=RIN
VBVL(1,MSUM)=VBVL(1,MSUM)+RIN*DELT
VBVL(4,MSUM)=ROUT
VBVL(2,MSUM)=VBVL(2,MSUM)+ROUT*DELT
VBNM(MSUM)=TEXT

C
C8-----INCREMENT THE BUDGET TERM COUNTER.

MSUM=MSUM+1

C
C9-----RETURN.

RETURN
END
SUBROUTINE GWF2GHB7DA(IGRID)

C Deallocate GHB MEMORY
USE GWFGHBMODULE

C
CALL SGWF2GHB7PNT(IGRID)
DEALLOCATE(NBOUND)
DEALLOCATE(MXBND)
DEALLOCATE(NGHBVL)
DEALLOCATE(IGHBCB)
DEALLOCATE(IPRGHB)
DEALLOCATE(NPGHB)
DEALLOCATE(IGHBPB)
DEALLOCATE(NNPGHB)
DEALLOCATE(GHBAUX)
```

```
DEALLOCATE(BNDS)

C
C(SPB)**** Deallocate DH ****

DEALLOCATE(DH)

C
RETURN
END

SUBROUTINE SGWF2GHB7PNT(IGRID)

C Change GHB data to a different grid.

USE GWFGHBMODULE

C
NBOUND=>GWFGHBDAT(IGRID)%NBOUND
MXBND=>GWFGHBDAT(IGRID)%MXBND
NGHBVL=>GWFGHBDAT(IGRID)%NGHBVL
IGHBCB=>GWFGHBDAT(IGRID)%IGHBCB
IPRGHB=>GWFGHBDAT(IGRID)%IPRGHB
NPGHB=>GWFGHBDAT(IGRID)%NPGHB
IGHBPB=>GWFGHBDAT(IGRID)%IGHBPB
NNPGHB=>GWFGHBDAT(IGRID)%NNPGHB
GHBAUX=>GWFGHBDAT(IGRID)%GHBAUX
BNDS=>GWFGHBDAT(IGRID)%BNDS

C
C(SPB)**** Deallocate DH ****

DH=>GWFGHBDAT(IGRID)%DH

C
RETURN
END

SUBROUTINE SGWF2GHB7PSV(IGRID)

C Save GHB data for a grid.

USE GWFGHBMODULE

C
GWFGHBDAT(IGRID)%NBOUND=>NBOUND
GWFGHBDAT(IGRID)%MXBND=>MXBND
GWFGHBDAT(IGRID)%NGHBVL=>NGHBVL
GWFGHBDAT(IGRID)%IGHBCB=>IGHBCB
GWFGHBDAT(IGRID)%IPRGHB=>IPRGHB
GWFGHBDAT(IGRID)%NPGHB=>NPGHB
GWFGHBDAT(IGRID)%IGHBPB=>IGHBPB
GWFGHBDAT(IGRID)%NNPGHB=>NNPGHB
GWFGHBDAT(IGRID)%GHBAUX=>GHBAUX
GWFGHBDAT(IGRID)%BNDS=>BNDS

C
```

```
C(SPB)**** Deallocate DH ****
      GWFGHBDAT(IGRID)%DH=>DH
C
      RETURN
      END
```

Appendix B

The spatial periodic solute boundary source code

The modified FORTRAN source code of the Sink Source Mixing package in MT3DMS is presented below. The changes made to the code which provide spatial periodic function are highlighted via comments. In addition, the author is happy to provide the compiled MT3DMS or PHT3D executable with SPB function and/or any assistance with implementation.

```
C ****
C Supplement to 'Spatial Periodic boundary for MT3DMS' by Laatooe
C et al.
C This file demonstrates the implementation of the Spatial Periodic
C Boundary condition in MT3DMS by showing the required changes to
C the SSM module. The changes shown are for illustrative purposes
C and do not intended to guarantee universal, generic applicability
C of the code.
C Additions/changes to original SSM code are highlighted by comment
C lines C(SPB)**** preceding the required modification for SPB
C function.
C ****
C
SUBROUTINE SSM5AL(INSSM,IOUT,ISSGOUT,ISUM,ISUM2,NCOL,NROW,NLAY,
& NCOMP,LCIRCH,LCRECH,LCCRCH,LCIEVT,LCEVTR,LCCEVT,MXSS,LCSS,
& IVER,LCSSMC,LCSSG)
C ****
```

```

C THIS SUBROUTINE ALLOCATES SPACE FOR ARRAYS NEEDED IN THE SINK & SOURCE
C MIXING (SSM) PACKAGE.

C ****
C last modified: 02-20-2010
C

      IMPLICIT NONE

      INTEGER INSSM, IOUT, ISSGOUT, ISUM, ISUM2, NCOL, NROW, NLAY, NCOMP,
&          LCIRCH, LCRECH, LCCRCH, LCIEVT, LCEVTR, LCCEVT, MXSS, LCSS,
&          ISUMX, ISUMIX, NCR, ISOLD, ISOLD2, IVER, LCSSMC, LCSSG,
&          IERR, IOSTAT

      CHARACTER LINE*200

      LOGICAL FWEL, FDRN, FRCH, FEVT, FRIV, FGHB, FSTR, FRES, FFHB, FIBS,
&          FTLK, FLAK, FMNW, FDRT, FETS, FSWT, FSFR, FUZF

      COMMON /FC/FWEL, FDRN, FRCH, FEVT, FRIV, FGHB, FSTR, FRES, FFHB, FIBS,
&          FTLK, FLAK, FMNW, FDRT, FETS, FSWT, FSFR, FUZF

C

C--PRINT PACKAGE NAME AND VERSION NUMBER

      WRITE(IOUT,1000) INSSM
      1000 FORMAT(1X,'SSM5 -- SINK & SOURCE MIXING PACKAGE ,',
      & ' VERSION 5, FEBRUARY 2010, INPUT READ FROM UNIT',I3)

C

C--READ AND PRINT FLAGS INDICATING WHICH SINK/SOURCE OPTIONS
C--ARE USED IN FLOW MODEL

      IF(IVER.EQ.1) THEN
          READ(INSSM,'(6L2)') FWEL, FDRN, FRCH, FEVT, FRIV, FGHB
      ELSEIF(IVER.EQ.2) THEN
          READ(INSSM,'(A)') LINE
          WRITE(IOUT,1010) LINE
      ENDIF
      WRITE(IOUT,1020)
      IF(FWEL) WRITE(IOUT,1340)
      IF(FDRN) WRITE(IOUT,1342)
      IF(FRCH) WRITE(IOUT,1344)
      IF(FEVT) WRITE(IOUT,1346)
      IF(FRIV) WRITE(IOUT,1348)
      IF(FGHB) WRITE(IOUT,1350)
      IF(FSTR) WRITE(IOUT,1400)
      IF(FRES) WRITE(IOUT,1402)
      IF(FFHB) WRITE(IOUT,1404)
      IF(FIBS) WRITE(IOUT,1406)
      IF(FTLK) WRITE(IOUT,1408)
      IF(FLAK) WRITE(IOUT,1410)

```

```

    IF(FMNW) WRITE(IOUT,1412)
    IF(FDRT) WRITE(IOUT,1414)
    IF(FETS) WRITE(IOUT,1416)
    IF(FSWT) WRITE(IOUT,1418)
    IF(FSFR) WRITE(IOUT,1420)
    IF(FUZF) WRITE(IOUT,1422)

1010 FORMAT(1X,'HEADER LINE OF THE SSM PACKAGE INPUT FILE:',/1X,A)
1020 FORMAT(1X,'MAJOR STRESS COMPONENTS PRESENT IN THE FLOW MODEL:')
1340 FORMAT(1X,' o WELL [WEL]')
1342 FORMAT(1X,' o DRAIN [DRN]')
1344 FORMAT(1X,' o RECHARGE [RCH]')
1346 FORMAT(1X,' o EVAPOTRANSPIRATION [EVT]')
1348 FORMAT(1X,' o RIVER [RIV]')
1350 FORMAT(1X,' o GENERAL-HEAD-DEPENDENT BOUNDARY [GHB]')
1400 FORMAT(1X,' o STREAM [STR]')
1402 FORMAT(1X,' o RESERVOIR [RES]')
1404 FORMAT(1X,' o SPECIFIED-HEAD-FLOW BOUNDARY [FHB]')
1406 FORMAT(1X,' o INTERBED STORAGE [IBS]')
1408 FORMAT(1X,' o TRANSIENT LEAKAGE [TLK]')
1410 FORMAT(1X,' o LAKE [LAK]')
1412 FORMAT(1X,' o MULTI-NODE WELL [MNW]')
1414 FORMAT(1X,' o DRAIN WITH RETURN FLOW [DRT]')
1416 FORMAT(1X,' o SEGMENTED EVAPOTRANSPIRATION [ETS]')
1418 FORMAT(1X,' o SUBSIDENCE-WATER TABLE [SWT]')
1420 FORMAT(1X,' o STREAMFLOW-ROUTING [SFR]')
1422 FORMAT(1X,' o UNSATURATED-ZONE FLOW [UZF]')

C
--READ AND PRINT MAXIMUM NUMBER OF
--POINT SINKS/SOURCES PRESENT IN THE FLOW MODEL
ISSGOUT=0
READ(INSSM,'(2I10)',ERR=1,IOSTAT=IERR) MXSS,ISSGOUT
1 IF(IERR.NE.0) THEN
    BACKSPACE (INSSM)
    READ(INSSM,'(I10)') MXSS
ENDIF
WRITE(IOUT,1580) MXSS
1580 FORMAT(1X,'MAXIMUM NUMBER OF POINT SINKS/SOURCES =',I8)
IF(ISSGOUT.GT.0) THEN
    WRITE(IOUT,1582) ISSGOUT
1582 FORMAT(1X,'AVERAGE CONCENTRATIONS FOR LINKED GROUP',
&      ' SINKS/SOURCES SAVED In UNIT:',I3)
ENDIF

```

```

C
C--ALLOCATE SPACE FOR ARRAYS
  ISOLD=ISUM
  ISOLD2=ISUM2
  NCR=NCOL*NROW

C
C--INTEGER ARRAYS
  LCIRCH=ISUM2
  IF(FRCH) ISUM2=ISUM2+NCR
  LCIEVT=ISUM2
  IF(FEVT.OR.FETS) ISUM2=ISUM2+NCR

C
C--REAL ARRAYS
  LCRECH=ISUM
  IF(FRCH) ISUM=ISUM+NCR
  LCCRCH=ISUM
  IF(FRCH) ISUM=ISUM+NCR * NCOMP
  LCEVTR=ISUM
  IF(FEVT.OR.FETS) ISUM=ISUM+NCR
  LCCEVT=ISUM
  IF(FEVT.OR.FETS) ISUM=ISUM+NCR * NCOMP
  LCSS=ISUM
  ISUM=ISUM + 7*MXSS
  LCSSMC=ISUM
  ISUM=ISUM+NCOMP*MXSS
  LCSSG=ISUM
  ISUM=ISUM + 5*MXSS

C
C--CHECK HOW MANY ELEMENTS OF ARRAYS X AND IX ARE USED
  ISUMX=ISUM-ISOLD
  ISUMIX=ISUM2-ISOLD2
  WRITE(IOUT,1090) ISUMX,ISUMIX
1090 FORMAT(1X,I10,' ELEMENTS OF THE X ARRAY USED BY THE SSM PACKAGE'
& /1X,I10,' ELEMENTS OF THE IX ARRAY BY THE SSM PACKAGE')

C
C--NORMAL RETURN
  RETURN
  END

C
C
  SUBROUTINE SSM5RP(IN,IOUT,KPER,NCOL,NROW,NLAY,NCOMP,ICBUND,CNEW,
& CRCH,CEVT,MXSS,NSS,SS,SSMC)

```

```

C ****
C THIS SUBROUTINE READS CONCENTRATIONS OF SOURCES OR SINKS NEEDED BY
C THE SINK AND SOURCE MIXING (SSM) PACKAGE.
C ****
C last modified: 02-20-2010
C

IMPLICIT NONE

INTEGER IN, IOUT, KPER, NCOL, NROW, NLAY, NCOMP, ICBUND,
& MXSS, NSS, JJ, II, KK, NUM, IQ, INCRCH, INCEVT, NTMP, INDEX
REAL CRCH, CEVT, SS, SSMC, CSS, CNEW
LOGICAL FWEL, FDRN, FRIV, FGHB, FRCH, FEVT, FSTR, FRES, FFHB, FIBS,
& FTLK, FLAK, FMNW, FDRT, FETS, FSWT, FSFR, FUZF
CHARACTER ANAME*24, TYPESS(-1:100)*15
DIMENSION SS(7,MXSS), SSMC(NCOMP, MXSS), CRCH(NCOL, NROW, NCOMP),
& CEVT(NCOL, NROW, NCOMP),
& ICBUND(NCOL, NROW, NLAY, NCOMP), CNEW(NCOL, NROW, NLAY, NCOMP)
COMMON /FC/FWEL, FDRN, FRCH, FEVT, FRIV, FGHB, FSTR, FRES, FFHB, FIBS,
& FTLK, FLAK, FMNW, FDRT, FETS, FSWT, FSFR, FUZF

C
C--INITIALIZE.

TYPESS(-1)= 'CONSTANT CONC. '
TYPESS(1) = 'CONSTANT HEAD   '
TYPESS(2) = 'WELL          '
TYPESS(3) = 'DRAIN         '
TYPESS(4) = 'RIVER         '
TYPESS(5) = 'HEAD DEP BOUND '
TYPESS(15)= 'MASS LOADING  '
TYPESS(21)= 'STREAM        '
TYPESS(22)= 'RESERVOIR    '
TYPESS(23)= 'SP FLW HD BOUND'
TYPESS(24)= 'INTERBED STRG  '
TYPESS(25)= 'TRANSIENT LEAK '
TYPESS(26)= 'LAKE          '
TYPESS(27)= 'MULTI-NODE WELL'
TYPESS(28)= 'DRN W RET FLOW '
TYPESS(29)= 'SEGMENTED ET   '
TYPESS(50)= 'HSS MAS LOADING'
TYPESS(51)= 'SUBSIDENCE-WT  '
TYPESS(52)= 'STREAM FL ROUT.'
TYPESS(53)= 'UNSAT ZONE FLOW'

C
C--READ CONCENTRATION OF DIFFUSIVE SOURCES/SINKS (RECHARGE/E.T.)

```

```

C--FOR CURRENT STRESS PERIOD IF THEY ARE SIMULATED IN FLOW MODEL
  IF(.NOT.FRCH) GOTO 10

C
C--READ FLAG INCRCH INDICATING HOW TO READ RECHARGE CONCENTRATION
  READ(IN,'(I10)') INCRCH

C
C--IF INCRCH < 0, CONCENTRATIN REUSED FROM LAST STRESS PERIOD
  IF(INCRCH.LT.0) THEN
    WRITE(IOUT,1)
    GOTO 10
  ENDIF

  1 FORMAT(/1X,'CONCENTRATION OF RECHARGE FLUXES',
  & ' REUSED FROM LAST STRESS PERIOD')

C
C--IF INCRCH >= 0, READ AN ARRAY
C--CONTAINING CONCENTRATION OF RECHARGE FLUX [CRCH]
  WRITE(IOUT,2) KPER
  ANAME='RECH. CONC. COMP. NO.'
  DO INDEX=1,NCOMP
    WRITE(ANAME(19:21),'(I3.2)') INDEX
    CALL RARRAY(CRCH(1,1,INDEX),ANAME,NROW,NCOL,0,IN,IOUT)
  ENDDO

  2 FORMAT(/1X,'CONCENTRATION OF RECHARGE FLUXES',
  & ' WILL BE READ IN STRESS PERIOD',I3)

C
C--READ CONCENTRAION OF EVAPOTRANSPIRATION FLUX
  10 IF(.NOT.FEVT .AND. .NOT.FETS) GOTO 20

C
  IF(KPER.EQ.1) THEN
    DO INDEX=1,NCOMP
      DO II=1,NROW
        DO JJ=1,NCOL
          CEVT(JJ,II,INDEX)=-1.E-30
        ENDDO
      ENDDO
    ENDDO
  ENDIF

  READ(IN,'(I10)') INCEVT
  IF(INCEVT.LT.0) THEN
    WRITE(IOUT,11)
    GOTO 20
  ENDIF

```

```

11 FORMAT(/1X,'CONCENTRATION OF E. T. FLUXES',
& ' REUSED FROM LAST STRESS PERIOD')

C
  WRITE(IOUT,12) KPER
  ANAME='E. T. CONC. COMP. NO.'
  DO INDEX=1,NCOMP
    WRITE(ANAME(19:21),'(I3.2)') INDEX
    CALL RARRAY(CEVT(1,1,INDEX),ANAME,NROW,NCOL,0,IN,IOUT)
  ENDDO

12 FORMAT(/1X,'CONCENTRATION OF E. T. FLUXES',
& ' WILL BE READ IN STRESS PERIOD',I3)

C
20 CONTINUE

C
--READ AND ECHO POINT SINKS/SOURCES OF SPECIFIED CONCENTRATIONS
  READ(IN,'(I10)') NTMP

C
--RESET OLD CONCENTRATIONS IF REUSE OPTION NOT IN EFFECT
  IF(KPER.GT.1.AND.NTMP.GE.0) THEN
    DO NUM=1,NSS
      SS(4,NUM)=0.
    DO INDEX=1,NCOMP
      SSMC(INDEX,NUM)=0.
    ENDDO
    ENDDO
  ENDIF

C
  IF(NTMP.GT.MXSS) THEN
    WRITE(*,30)
    CALL USTOP(' ')
  ELSEIF(NTMP.LT.0) THEN
    WRITE(IOUT,40)
    RETURN
  ELSEIF(NTMP.EQ.0) THEN
    WRITE(IOUT,50) NTMP,KPER
    NSS=0
    RETURN
  ELSE
    NSS=NTMP
  ENDIF

C
  WRITE(IOUT,60)

```

```

DO NUM=1,NSS

C
  IF(NCOMP.EQ.1) THEN
    READ(IN,'(3I10,F10.0,I10)') KK,II,JJ,CSS,IQ
    SSMC(1,NUM)=CSS
  ELSE
    READ(IN,'(3I10,F10.0,I10)',ADVANCE='NO') KK,II,JJ,CSS,IQ
    READ(IN,*) (SSMC(INDEX,NUM),INDEX=1,NCOMP)
  ENDIF

C
  IF(IQ.EQ.-1) THEN
    DO INDEX=1,NCOMP
      IF(SSMC(INDEX,NUM).GE.0) THEN
        CNEW(JJ,II,KK,INDEX)=SSMC(INDEX,NUM)
        ICBUND(JJ,II,KK,INDEX)=-ABS(ICBUND(JJ,II,KK,INDEX))
      ENDIF
    ENDDO
    ELSEIF(IQ.EQ.15) THEN
      SS(5,NUM)=0.
    ELSEIF(IQ.EQ.2.AND.CSS.LT.0) THEN
      NTMP=-INT(CSS)
      IF(NTMP.LT.1.OR.NTMP.GT.NCOL*NROW*NLAY) THEN
        WRITE(*,79)
        CALL USTOP(' ')
      ENDIF
    ELSEIF(IQ.LT.1.OR.IQ.GT.100) THEN
      WRITE(*,80)
      CALL USTOP(' ')
    ENDIF
    SS(1,NUM)=KK
    SS(2,NUM)=II
    SS(3,NUM)=JJ
    SS(4,NUM)=CSS
    SS(6,NUM)=IQ
  C
    DO INDEX=1,NCOMP
      CSS=SSMC(INDEX,NUM)
      IF(CSS.NE.0 .OR. ICBUND(JJ,II,KK,INDEX).LT.0)
      &   WRITE(IOUT,70) NUM,KK,II,JJ,CSS,TYPESS(IQ),INDEX
      IF(CSS.LT.0 .AND. IQ.EQ.2)
      &   WRITE(IOUT,71) -INT(CSS)
    ENDDO
  
```

```

C
      ENDDO

30  FORMAT (/1X,'ERROR: MAXIMUM NUMBER OF POINT SINKS/SOURCES',
& ' EXCEEDED'/1X,'INCREASE [MXSS] IN SSM INPUT FILE')

40  FORMAT (/1X,'POINT SINKS/SOURCES OF SPECIFIED CONCENTRATION',
& ' REUSED FROM LAST STRESS PERIOD')

50  FORMAT (/1X,'NO. OF POINT SINKS/SOURCES OF SPECIFIED',
& ' CONCENTRATIONS =',I5,' IN STRESS PERIOD',I3)

60  FORMAT (/5X,' NO      LAYER      ROW      COLUMN      CONCENTRATION',
& '          TYPE          COMPONENT')

70  FORMAT (3X,4(I5,3X),1X,G15.7,5X,A15,I6)

71  FORMAT (8X,'>>RECIRCULATION WELL; INPUT CONCENTRATION',
& ' FROM NODE #',I10.8)

79  FORMAT (/1X,'ERROR: INVALID CELL LOCATION FOR RECIRCULATION',
& ' /1X,'          WELL CONCENTRATION IN THE SSM INPUT FILE')

80  FORMAT (/1X,'ERROR: INVALID CODE FOR POINT SINK/SOURCE TYPE',
& ' /1X,'          IN THE SSM INPUT FILE')

C
C--RETURN
      RETURN
      END

C
C
      SUBROUTINE SSM5FM(NCOL ,NROW ,NLAY ,NCOMP ,ICOMP ,ICBUND ,DELR ,DELC ,
& DH ,IRCH ,RECH ,CRCH ,IEVT ,EVTR ,CEVT ,MXSS ,NTSS ,SS ,SSMC ,SSG ,
& QSTO ,CNEW ,ISS ,A ,RHS ,NODES ,UPDLHS ,MIXELM)

C ****
C THIS SUBROUTINE FORMULATES MATRIX COEFFICIENTS FOR THE SINK/
C SOURCE TERMS UNDER THE IMPLICIT FINITE-DIFFERENCE SCHEME.
C ****
C last modified: 02-20-2010
C

      IMPLICIT NONE
      INTEGER   NCOL ,NROW ,NLAY ,NCOMP ,ICOMP ,ICBUND ,IRCH ,IEVT ,MXSS ,
&          NTSS ,NUM ,IQ ,K ,I ,J ,ISS ,N ,NODES ,MIXELM ,IGROUP ,
&          MHOST ,KHOST ,IHOST ,JHOST ,INDEX
      REAL     CNEW ,RECH ,CRCH ,EVTR ,CEVT ,SS ,SSMC ,SSG ,
&          CTMP ,QSS ,QCTMP ,DELR ,DELC ,DH ,QSTO ,A ,RHS
      LOGICAL  UPDLHS ,FWEL ,FDRN ,FRCH ,FEVT ,FRIV ,FGHB ,FSTR ,FRES ,
&          FFHB ,FIBS ,FTLK ,FLAK ,FMNW ,FDRT ,FETS ,FSWT ,FSFR ,FUZF
      DIMENSION ICBUND(NCOL ,NROW ,NLAY ,NCOMP ),SS(7,MXSS) ,SSG(5,MXSS) ,
&          SSMC(NCOMP ,MXSS) ,RECH(NCOL ,NROW) ,IRCH(NCOL ,NROW) ,

```

```

&          CRCH(NCOL,NROW,NCOMP),EVTR(NCOL,NROW),
&          IEVT(NCOL,NROW),CEVT(NCOL,NROW,NCOMP),
&          DELR(NCOL),DELC(NROW),CNEW(NCOL,NROW,NLAY,NCOMP),
&          DH(NCOL,NROW,NLAY),QSTO(NCOL,NROW,NLAY),
&          A(NODES),RHS(NODES)

COMMON /FC/FWEL,FDRN,FRCH,FEVT,FREV,FGHB,FSTR,FRES,FFHB,FIBS,
&        FTLK,FLAK,FMNW,FDRT,FETS,FSWT,FSFR,FUZF

C
--DETERMINE AVERAGE CONCENTRATION FOR LINKED SINK/SOURCE GROUPS
CALL CGROUP(NCOL,NROW,NLAY,NCOMP,ICOMP,MXSS,NTSS,
& SS,SSMC,SSG,ICBUND,CNEW,DELR,DELC,DH)

C
--FORMULATE [A] AND [RHS] MATRICES FOR EULERIAN SCHEMES
IF(MIXELM.GT.0) GOTO 1000

C
--TRANSIENT FLUID STORAGE TERM
IF(ISS.EQ.0 .AND. UPDLHS) THEN
DO K=1,NLAY
DO I=1,NROW
DO J=1,NCOL
IF(ICBUND(J,I,K,ICOMP).GT.0) THEN
N=(K-1)*NCOL*NROW+(I-1)*NCOL+J
A(N)=A(N)+QSTO(J,I,K)*DELR(J)*DELC(I)*DH(J,I,K)
ENDIF
ENDDO
ENDDO
ENDIF

C
--AREAL SINK/SOURCE TERMS
--(RECHARGE)
IF(.NOT.FRCH) GOTO 10
DO I=1,NROW
DO J=1,NCOL
K=IRCH(J,I)
IF(K.GT.0 .AND. ICBUND(J,I,K,ICOMP).GT.0) THEN
N=(K-1)*NCOL*NROW+(I-1)*NCOL+J
IF(RECH(J,I).LT.0) THEN
IF(UPDLHS) A(N)=A(N)+RECH(J,I)*DELR(J)*DELC(I)*DH(J,I,K)
ELSE
RHS(N)=RHS(N)
& -RECH(J,I)*CRCH(J,I,ICOMP)*DELR(J)*DELC(I)*DH(J,I,K)
ENDIF
ENDIF
ENDDO
ENDDO
ENDIF

```

```

        ENDIF
    ENDIF
ENDDO
ENDDO

C
C--(EVAPOTRANSPIRATION)

10 IF(.NOT.FEVT .AND. .NOT.FETS) GOTO 20
DO I=1,NROW
DO J=1,NCOL
K=IEVT(J,I)
IF(K.GT.0 .AND. ICBUND(J,I,K,ICOMP).GT.0) THEN
N=(K-1)*NCOL*NROW+(I-1)*NCOL+J
IF(EVTR(J,I).LT.0.AND.(CEVT(J,I,ICOMP).LT.0 .OR.
& CEVT(J,I,ICOMP).GE.CNEW(J,I,K,ICOMP))) THEN
IF(UPDLHS) A(N)=A(N)+EVTR(J,I)*DELR(J)*DELC(I)*DH(J,I,K)
ELSEIF(CEVT(J,I,ICOMP).GT.0) THEN
RHS(N)=RHS(N)
& -EVTR(J,I)*CEVT(J,I,ICOMP)*DELR(J)*DELC(I)*DH(J,I,K)
ENDIF
ENDIF
ENDDO
ENDDO

C
C--POINT SINK/SOURCE TERMS

20 DO NUM=1,NTSS
K=SS(1,NUM)
I=SS(2,NUM)
J=SS(3,NUM)
CTMP=SS(4,NUM)
IF(NCOMP.GT.1) CTMP=SSMC(ICOMP,NUM)
QSS=SS(5,NUM)
IQ=SS(6,NUM)
IF(ICBUND(J,I,K,ICOMP).LE.0.OR.IQ.LE.0) CYCLE
C
C(SPB)****

C--Reset CTMP for spatially periodic bounds between columns
IF(IQ.EQ.5.AND.J.EQ.1)THEN
IF(NCOMP.EQ.1) THEN
SS(4,NUM)=CNEW(NCOL,I,K,NCOMP)
CTMP=SS(4,NUM)
SSMC(1,NUM)=CTMP
ELSE

```

```

        DO INDEX=1 , NCOMP
        SSMC(INDEX , NUM)=CNEW(NCOL , I , K , INDEX)
    ENDDO
        CTMP=SSMC(ICOMP , NUM)
    ENDIF
    ELSEIF(IQ .EQ. 5 .AND. J .EQ. NCOL) THEN
        IF(NCOMP .EQ. 1) THEN
            SS(4 , NUM)=CNEW(1 , I , K , NCOMP)
            CTMP=SS(4 , NUM)
            SSMC(1 , NUM)=CTMP
        ELSE
            DO INDEX=1 , NCOMP
            SSMC(INDEX , NUM)=CNEW(1 , I , K , INDEX)
        ENDDO
            CTMP=SSMC(ICOMP , NUM)
        ENDIF
    ENDIF
--Ending spatially periodic update for columns
C(SPB)****

C--RESET QSS FOR MASS-LOADING SOURCES (IQ=15)
    IF(IQ .EQ. 15) THEN
        QSS=1./(DELR(J)*DELC(I)*DH(J , I , K))

C
C--GET AVERAGE CONC FOR LINKED SINK/SOURCE GROUPS (IQ=27)
    ELSEIF(IQ .EQ. 27) THEN
        IGROUP=SS(7 , NUM)
        CTMP=SSG(4 , IGROUP)

C
C--GET RETURN FLOW CONC FOR DRAINS WITH RETURN FLOW (IQ=28)
    ELSEIF(IQ .EQ. 28 .AND. QSS .GT. 0) THEN
        MHOST=SS(7 , NUM)
        KHOST=(MHOST -1)/(NCOL*NROW) + 1
        IHOST=MOD((MHOST -1) , NCOL*NROW)/NCOL + 1
        JHOST=MOD((MHOST -1) , NCOL) + 1
        CTMP=CNEW(JHOST , IHOST , KHOST , ICOMP)

C
C--GET CONCENTRATION FOR RECIRCULATED INJECTION WELL
C--(IF INPUT CONCENTRATION WAS SET TO A NEGATIVE INTEGER)
    ELSEIF(IQ .EQ. 2 .AND. CTMP .LT. 0 .AND. QSS .GT. 0) THEN
        MHOST=-INT(CTMP)
        KHOST=(MHOST -1)/(NCOL*NROW) + 1
        IHOST=MOD((MHOST -1) , NCOL*NROW)/NCOL + 1

```

```

JHOST=MOD((MHOST-1),NCOL) + 1
CTMP=CNEW(JHOST,IHOST,KHOST,ICOMP)

ENDIF

C
--ADD CONTRIBUTIONS TO MATRICES [A] AND [RHS]
N=(K-1)*NCOL*NROW+(I-1)*NCOL+J
IF(QSS.LT.0) THEN
  IF(UPDLHS) A(N)=A(N)+QSS*DELR(J)*DELC(I)*DH(J,I,K)
ELSE
  RHS(N)=RHS(N)-QSS*CTMP*DELR(J)*DELC(I)*DH(J,I,K)
ENDIF
ENDDO

C
--DONE WITH EULERIAN SCHEMES
GOTO 2000

C
--FORMULATE [A] AND [RHS] MATRICES FOR EULERIAN-LAGRANGIAN SCHEMES
1000 CONTINUE

C
--AREAL SINK/SOURCE TERMS
--(RECHARGE)
IF(.NOT.FRCH) GOTO 30
DO I=1,NROW
  DO J=1,NCOL
    K=IRCH(J,I)
    IF(K.GT.0 .AND. ICBUND(J,I,K,ICOMP).GT.0
    & .AND. RECH(J,I).GT.0) THEN
      N=(K-1)*NCOL*NROW+(I-1)*NCOL+J
      IF(UPDLHS) A(N)=A(N)-RECH(J,I)*DELR(J)*DELC(I)*DH(J,I,K)
      RHS(N)=RHS(N)
      & -RECH(J,I)*CRCH(J,I,ICOMP)*DELR(J)*DELC(I)*DH(J,I,K)
    ENDIF
  ENDDO
ENDDO

C
--(EVAPOTRANSPIRATION)
30 IF(.NOT.FEVT .AND. .NOT.FETS) GOTO 40
DO I=1,NROW
  DO J=1,NCOL
    K=IEVT(J,I)
    IF(K.GT.0 .AND. ICBUND(J,I,K,ICOMP).GT.0) THEN
      N=(K-1)*NCOL*NROW+(I-1)*NCOL+J
    ENDIF
  ENDDO
ENDDO

```

```

      IF(EVTR(J,I).LT.0.AND.(CEVT(J,I,ICOMP).LT.0 .OR .
&       CEVT(J,I,ICOMP).GE.CNEW(J,I,K,ICOMP))) THEN
         CYCLE
      ELSEIF(CEVT(J,I,ICOMP).GE.0) THEN
         IF(UPDLHS) A(N)=A(N)-EVTR(J,I)*DELR(J)*DELC(I)*DH(J,I,K)
         RHS(N)=RHS(N)
&       -EVTR(J,I)*CEVT(J,I,ICOMP)*DELR(J)*DELC(I)*DH(J,I,K)
      ENDIF
      ENDIF
      ENDDO
      ENDDO

C
--POINT SINK/SOURCE TERMS
40 DO NUM=1,NTSS
      K=SS(1,NUM)
      I=SS(2,NUM)
      J=SS(3,NUM)
      CTMP=SS(4,NUM)
      IF(NCOMP.GT.1) CTMP=SSMC(ICOMP,NUM)
      QSS=SS(5,NUM)
      IQ=SS(6,NUM)

C(SPB)****
--Reset CTMP for spatially periodic bounds between columns
      IF(IQ.EQ.5.AND.J.EQ.1)THEN
         IF(NCOMP.EQ.1) THEN
            SS(4,NUM)=CNEW(NCOL,I,K,NCOMP)
            CTMP=SS(4,NUM)
            SSMC(1,NUM)=CTMP
         ELSE
            DO INDEX=1,NCOMP
               SSMC(INDEX,NUM)=CNEW(NCOL,I,K,INDEX)
            ENDDO
            CTMP=SSMC(ICOMP,NUM)
         ENDIF
         ELSEIF(IQ.EQ.5.AND.J.EQ.NCOL)THEN
            IF(NCOMP.EQ.1) THEN
               SS(4,NUM)=CNEW(1,I,K,NCOMP)
               CTMP=SS(4,NUM)
               SSMC(1,NUM)=CTMP
            ELSE
               DO INDEX=1,NCOMP
                  SSMC(INDEX,NUM)=CNEW(1,I,K,INDEX)
               ENDDO
            ENDIF
         ENDIF
      ENDIF

```

```

        ENDDO
        CTMP=SSMC(ICOMP,NUM)
    ENDIF
ENDIF

C--Ending spatially periodic update for columns
C(SPB)****

C--SKIP IF NOT ACTIVE CELL
IF(ICBUND(J,I,K,ICOMP).LE.0.OR.IQ.LE.0) CYCLE
C
C--SKIP IF SINK CELL
IF(QSS.LE.0.AND.IQ.NE.15) CYCLE
C
C--COMPUTE PRODUCT OF Q*C
QCTMP=QSS*CTMP
C
C--RESET Q*C FOR MASS-LOADING SOURCES (IQ=15)
IF(IQ.EQ.15) THEN
    QSS=1./(DELR(J)*DELC(I)*DH(J,I,K))
    QCTMP=QSS*CTMP
    QSS=0.
C
C--RESET Q*C FOR LINKED SINK/SOURCE GROUPS (IQ=27)
ELSEIF(IQ.EQ.27) THEN
    IGROUP=SS(7,NUM)
    CTMP=SSG(4,IGROUP)
    QCTMP=QSS*CTMP
C
C--RESET Q*C FOR DRAINS WITH RETURN FLOW (IQ=28)
ELSEIF(IQ.EQ.28.AND.QSS.GT.0) THEN
    MHOST=SS(7,NUM)
    KHOST=(MHOST-1)/(NCOL*NROW) + 1
    IHOST=MOD((MHOST-1),NCOL*NROW)/NCOL + 1
    JHOST=MOD((MHOST-1),NCOL) + 1
    CTMP=CNEW(JHOST,IHOST,KHOST,ICOMP)
    QCTMP=QSS*CTMP
C
C--GET CONCENTRATION FOR RECIRCULATED INJECTION WELL
C--(IF INPUT CONCENTRATION WAS SET TO A NEGATIVE INTEGER)
ELSEIF(IQ.EQ.2 .AND. CTMP.LT.0 .AND. QSS.GT.0) THEN
    MHOST=-INT(CTMP)
    KHOST=(MHOST-1)/(NCOL*NROW) + 1
    IHOST=MOD((MHOST-1),NCOL*NROW)/NCOL + 1

```

```

JHOST=MOD((MHOST-1),NCOL) + 1
CTMP=CNEW(JHOST,IHOST,KHOST,ICOMP)
QCTMP=QSS*CTMP
ENDIF
C
C--ADD CONTRIBUTIONS TO MATRICES [A] AND [RHS]
N=(K-1)*NCOL*NROW+(I-1)*NCOL+J
IF(UPDLHS) A(N)=A(N)-QSS*DELR(J)*DELC(I)*DH(J,I,K)
RHS(N)=RHS(N)-QCTMP*DELR(J)*DELC(I)*DH(J,I,K)
ENDDO
C
C--DONE WITH EULERIAN-LAGRANGIAN SCHEMES
2000 CONTINUE
C
C--RETURN
RETURN
END
C
C
SUBROUTINE SSM5BD(NCOL,NROW,NLAY,NCOMP,ICOMP,ICBUND,DELR,DELC,
& DH,IRCH,RECH,CRCH,IEVT,EVTR,Cevt,MXSS,NTSS,SS,SSMC,SSG,
& QSTO,CNEW,RETA,DTRANS,ISS,RMASIO)
C ****
C THIS SUBROUTINE CALCULATES MASS BUDGETS ASSOCIATED WITH ALL SINK/
C SOURCE TERMS.
C ****
C last modified: 02-20-2010
C
IMPLICIT NONE
INTEGER NCOL,NROW,NLAY,NCOMP,ICOMP,ICBUND,IRCH,IEVT,MXSS,
& NTSS,NUM,IQ,K,I,J,ISS,IGROUP,MHOST,KHOST,IHOST,JHOST
REAL DTRANS,RECH,CRCH,EVTR,Cevt,SS,SSMC,SSG,CNEW,
& CTMP,QSS,RMASIO,DELR,DELC,DH,QSTO,RETA
LOGICAL FWEL,FDRN,FRCH,Fevt,Friv,FGHB,FSTR,FRES,FFHB,FIBS,
& FTLK,FLAK,FMNW,FDRT,FETS,FSWT,FSFR,FUZF
DIMENSION ICBUND(NCOL,NROW,NLAY,NCOMP),SS(7,MXSS),SSG(5,MXSS),
& SSMC(NCOMP,MXSS),RECH(NCOL,NROW),IRCH(NCOL,NROW),
& CRCH(NCOL,NROW,NCOMP),EVTR(NCOL,NROW),
& IEVT(NCOL,NROW),Cevt(NCOL,NROW,NCOMP),
& CNEW(NCOL,NROW,NLAY,NCOMP),DELR(NCOL),DELC(NROW),
& DH(NCOL,NROW,NLAY),QSTO(NCOL,NROW,NLAY),
& RETA(NCOL,NROW,NLAY,NCOMP),RMASIO(122,2,NCOMP)

```

```

COMMON /FC/FWEL,FDRN,FRCH,FEVT,FREV,FGHB,FSTR,FRES,FFHB,FIBS,
& FTLK,FLAK,FMNW,FDRT,FETS,FSWT,FSFR,FUZF
C
C--DETERMINE AVERAGE CONCENTRATION FOR LINKED SINK/SOURCE GROUPS
CALL CGROUP(NCOL,NROW,NLAY,NCOMP,ICOMP,MXSS,NTSS,
& SS,SSMC,SSG,ICBUND,CNEW,DELR,DELC,DH)
C
C--TRANSIENT GROUNDWATER STORAGE TERM
IF(ISS.NE.0) GOTO 50
C
C--RECORD MASS STORAGE CHANGES FOR DISSOLVED AND SORBED PHASES
DO K=1,NLAY
  DO I=1,NROW
    DO J=1,NCOL
      IF(ICBUND(J,I,K,ICOMP).LE.0) CYCLE
      CTMP=CNEW(J,I,K,ICOMP)
      IF(QSTO(J,I,K).GT.0) THEN
        RMASIO(118,1,ICOMP)=RMASIO(118,1,ICOMP)
        & +QSTO(J,I,K)*CTMP*DTRANS*DELR(J)*DELC(I)*DH(J,I,K)
      ELSE
        RMASIO(118,2,ICOMP)=RMASIO(118,2,ICOMP)
        & +QSTO(J,I,K)*CTMP*DTRANS*DELR(J)*DELC(I)*DH(J,I,K)
      ENDIF
    ENDDO
  ENDDO
ENDDO
C
C--AREAL SINK/SOURCE TERMS
C--(RECHARGE)
50 IF(.NOT.FRCH) GOTO 100
C
DO I=1,NROW
  DO J=1,NCOL
    K=IRCH(J,I)
    IF(K.EQ.0 .OR. ICBUND(J,I,K,ICOMP).LE.0) CYCLE
    CTMP=CRCH(J,I,ICOMP)
    IF(RECH(J,I).LT.0) CTMP=CNEW(J,I,K,ICOMP)
    IF(RECH(J,I).GT.0) THEN
      RMASIO(7,1,ICOMP)=RMASIO(7,1,ICOMP)+RECH(J,I)*CTMP*DTRANS*
      & DELR(J)*DELC(I)*DH(J,I,K)
    ELSE
      RMASIO(7,2,ICOMP)=RMASIO(7,2,ICOMP)+RECH(J,I)*CTMP*DTRANS*

```

```

&           DELR(J)*DELC(I)*DH(J,I,K)

      ENDIF

      ENDDO

      ENDDO

C
C--(EVAPOTRANSPIRATION)

100 IF(.NOT.FEVT .AND. .NOT.FETS) GOTO 200

C
DO I=1,NROW

DO J=1,NCOL

K=IEVT(J,I)

IF(K.EQ.0 .OR. ICBUND(J,I,K,ICOMP).LE.0) CYCLE

CTMP=CEVT(J,I,ICOMP)

IF(EVTR(J,I).LT.0.AND.(CTMP.LT.0 .or.

&                               CTMP.GE.CNEW(J,I,K,ICOMP))) THEN

CTMP=CNEW(J,I,K,ICOMP)

ELSEIF(CTMP.LT.0) THEN

CTMP=0.

ENDIF

IF(EVTR(J,I).GT.0) THEN

RMASIO(8,1,ICOMP)=RMASIO(8,1,ICOMP)+EVTR(J,I)*CTMP*DTRANS*

&           DELR(J)*DELC(I)*DH(J,I,K)

ELSE

RMASIO(8,2,ICOMP)=RMASIO(8,2,ICOMP)+EVTR(J,I)*CTMP*DTRANS*

&           DELR(J)*DELC(I)*DH(J,I,K)

ENDIF

ENDDO

ENDDO

C
C--POINT SINK/SOURCE TERMS

200 DO NUM=1,NTSS

K=SS(1,NUM)

I=SS(2,NUM)

J=SS(3,NUM)

QSS=SS(5,NUM)

IQ=SS(6,NUM)

CTMP=SS(4,NUM)

IF(NCOMP.GT.1) CTMP=SSMC(ICOMP,NUM)

C
C--SKIP IF NOT ACTIVE CELL

IF(ICBUND(J,I,K,ICOMP).LE.0.OR.IQ.LE.0) CYCLE

C

```

```

C--RESET QSS FOR MASS-LOADING SOURCES (IQ=15)
  IF(IQ.EQ.15) THEN
    QSS=1./(DELR(J)*DELC(I)*DH(J,I,K))

  C
C--GET AVERAGE CONC FOR LINKED SINK/SOURCE GROUPS (IQ=27)
  ELSEIF(IQ.EQ.27) THEN
    IGROUP=SS(7,NUM)
    CTMP=SSG(4,IGROUP)

  C
C--GET RETURN FLOW CONC FOR DRAINS WITH RETURN FLOW (IQ=28)
  ELSEIF(IQ.EQ.28 .AND. QSS.GT.0) THEN
    MHOST=SS(7,NUM)
    KHOST=(MHOST-1)/(NCOL*NROW) + 1
    IHOST=MOD((MHOST-1),NCOL*NROW)/NCOL + 1
    JHOST=MOD((MHOST-1),NCOL) + 1
    CTMP=CNEW(JHOST,IHOST,KHOST,ICOMP)

  C
C--GET CONCENTRATION FOR RECIRCULATED INJECTION WELL
C--(IF INPUT CONCENTRATION WAS SET TO A NEGATIVE INTEGER)
  ELSEIF(IQ.EQ.2 .AND. CTMP.LT.0 .AND. QSS.GT.0) THEN
    MHOST=-INT(CTMP)
    KHOST=(MHOST-1)/(NCOL*NROW) + 1
    IHOST=MOD((MHOST-1),NCOL*NROW)/NCOL + 1
    JHOST=MOD((MHOST-1),NCOL) + 1
    CTMP=CNEW(JHOST,IHOST,KHOST,ICOMP)

  ENDIF

  C
  IF(QSS.LT.0) CTMP=CNEW(J,I,K,ICOMP)

  C
  IF(ICBUND(J,I,K,ICOMP).GT.0.AND.IQ.GT.0) THEN
    IF(QSS.GT.0) THEN
      RMASIO(IQ,1,ICOMP)=RMASIO(IQ,1,ICOMP)+QSS*CTMP*DTRANS*
      & DELR(J)*DELC(I)*DH(J,I,K)
    ELSE
      RMASIO(IQ,2,ICOMP)=RMASIO(IQ,2,ICOMP)+QSS*CTMP*DTRANS*
      & DELR(J)*DELC(I)*DH(J,I,K)
    ENDIF
  ENDIF

  C
  ENDDO

  C
C--RETURN

```

```

400 RETURN
END

C
C
SUBROUTINE SSM50T(NCOL ,NROW ,NLAY ,KPER ,KSTP ,NTRANS ,NCOMP ,ICOMP ,
& ICBUND ,MXSS ,NTSS ,NSS ,SS ,SSG ,PRTOUT ,TIME2 ,IOUT ,ISSGOUT)
C ****
C THIS SUBROUTINE SAVES INFORMATION FOR MULTI-NODE WELLS .
C ****
C last modified: 02-15-2005
C
IMPLICIT NONE
INTEGER NCOL ,NROW ,NLAY ,kper ,kstp ,ntrans ,NCOMP ,ICOMP ,ICBUND ,
& MXSS ,NTSS ,NSS ,NUM ,IQ ,K ,I ,J ,iGroup ,IOUT ,iFlag ,
& ISSGOUT ,IU
REAL SS ,CTMP ,TIME2 ,SSG
LOGICAL PRTOUT
DIMENSION ICBUND(NCOL ,NROW ,NLAY ,NCOMP) ,SS(7 ,MXSS) ,SSG(5 ,MXSS)

C--IF ISSGOUT = 0, SAVE AVERAGE CONC. OF MULTI-NODE WELLS TO
C--STANDARD OUTPUT FILE WHENEVER PRTOUT IS TRUE
C--OTHERWISE SAVE TO UNIT DEFINED BY ISSGOUT

IF(ISSGOUT.LE.0) THEN
  IF(.NOT.PRTOUT) GOTO 1200
  IU=IOUT
  WRITE(IU,1000)
  WRITE(IU,1002)
ELSE
  IU=ISSGOUT
  IF(KPER*KSTP*NTRANS.EQ.1) WRITE(IU,1002)
ENDIF

DO NUM=1 ,NTSS
  K =ss(1 ,num)
  I =ss(2 ,num)
  J =ss(3 ,num)
  IQ=ss(6 ,num)
  iGroup=ss(7 ,num)
  if(iGroup.le.0) cycle
  ctmp=ssg(4 ,iGroup)
  iFlag=int(ssg(1 ,iGroup))

```

```

        if(iFlag.ne.-999) then
          ssg(1,iGroup)=-999
          write(IU,1004) kper,kstp,ntrans,time2,iGroup,k,i,j,ctmp
        endif
      ENDDO

      IF(ISSGOUT.LE.0) WRITE(IU,1010)

1000 format(/1x,80(''))
1002 format(1x,'Stress   Time   Transport       Total           MNW   Layer',
     & ' Row Column Average',
     & ' /1x,'Period   Step     Step     Elapsed Time   Group   [K]  ',
     & '[I]   [J]   Conc.   ')
1004 format(1x, i4, 2x, i5, 3x, i5, 3x, g15.7, 2x, 4i6, 1x, g15.7)
1010 format(1x,80(''))/)

C
1200 RETURN
END

C
C
      subroutine cgroup(ncol,nrow,nlay,ncomp,icomp,mxss,ntss,
     & ss,ssmc,ssg,icbund,cnew,delr,delc,dh)
C ****
C this subroutine calculates the average concentration for a linked
C group sink/source such as a multi-node well
C ****
C last modification: 02-15-2005
C
      implicit none
      integer k,i,j,iGroup,num,IQ,icbund,icomp,ncomp,mxss,ntss,
     & ncol,nrow,nlay
      real ss,ssmc,ssg,cold,cnew,delr,delc,dh,ctmp,qss,csink,
     & QC_group,Q_group,Qnet_group,cavg
      dimension ss(7,mxss),ssmc(ncomp,mxss),ssg(5,mxss),
     & cnew(ncol,nrow,nlay,ncomp),delr(ncol),delc(nrow),
     & dh(ncol,nrow,nlay),icbund(ncol,nrow,nlay,ncomp)

C
C--clear storage array
C
      do iGroup=1,ntss
        do i=1,5
          ssg(i,iGroup)=0.

```

```

        enddo
    enddo

c
c--get cumulative QC and Q (sinks only), and net Q (sinks/sources)
c

    do num=1,ntss
        k=ss(1,num)
        i=ss(2,num)
        j=ss(3,num)
        ctmp=ss(4,num)
        if(icomp.gt.1) ctmp=ssmc(icomp,num)
        qss=ss(5,num)
        IQ=ss(6,num)
        iGroup=ss(7,num)

c
c--skip if at an inactive cell
        if(icbund(j,i,k,icomp).le.0) cycle
c
c--skip if not a linked group sink/source
        if(iGroup.eq.0 .or. IQ.ne.27) cycle
c
c--get cell concentration
        csink=cnew(j,i,k,icomp)
c
c--get volumetric |Q|*C, |Q|, and Q
        if(qss.lt.0) then
            QC_group=abs(qss)*delr(j)*delc(i)*dh(j,i,k)*csink
            Q_group =abs(qss)*delr(j)*delc(i)*dh(j,i,k)
        else
            QC_group=0.
            Q_group =0.
        endif
        Qnet_group = qss*delr(j)*delc(i)*dh(j,i,k)

c
c--cumulate and store in ssg
        ssg(1,iGroup) = ssg(1,iGroup) + QC_group
        ssg(2,iGroup) = ssg(2,iGroup) + Q_group
        ssg(5,iGroup) = ssg(5,iGroup) + Qnet_group

c
c--get user-specified conc for any cell in the group
        ssg(3,iGroup) = max( ctmp,ssg(3,iGroup) )

c

```

```
c--done
      enddo

c
c--get composite concentrations
c

do iGroup=1,ntss
  cavg = 0.

  QC_group = ssg(1,iGroup)
  Q_group = ssg(2,iGroup)
  Qnet_group = ssg(5,iGroup)
  ctmp = ssg(3,iGroup)

  if(Qnet_group.gt.0) then
    cavg=(QC_group+Qnet_group*ctmp)/(Q_group+Qnet_group)
  elseif(Q_group.gt.0) then
    cavg =QC_group/Q_group
  endif

  ssg(4,iGroup) = cavg
enddo

c
c--normal return
c

return
end
```

Bibliography

Banta, E.

2000. MODFLOW-2000, the U.S. geological survey modular ground-water model documentation of packages for simulating evapotranspiration with a segmented function (ETS1) and drains with return flow (DRT1). Technical report, Denver, Colorado: USGS.

Bardini, L., F. Boano, M. Cardenas, R. Revelli, and L. Ridolfi

2012. Nutrient cycling in bedform induced hyporheic zones. *Geochimica et Cosmochimica Acta*, 84:47–61.

Bardini, L., F. Boano, M. B. Cardenas, a. H. Sawyer, R. Revelli, and L. Ridolfi

2013. Small-scale permeability heterogeneity has negligible effects on nutrient cycling in streambeds. *Geophysical Research Letters*, 40(6):1118–1122.

Bencala, K. E., V. C. Kennedy, G. W. Zellweger, A. P. Jackman, and R. J. Avanzino

1984. Interactions of solutes and streambed sediment 1. An experimental-analysis of cation and anion transport in a mountain stream. *Water Resources Research*, 20(12):1797–1803.

Boano, F., J. W. Harvey, A. Marion, A. Packman, R. Revelli, L. Ridolfi, and A. Worman

2014. Hyporheic flow and transport processes: Mechanisms, models, and biogeochemical implications,. *Reviews of Geophysics*, 52:603–679.

Bottacin-Busolin, a. and a. Marion

2010. Combined role of advective pumping and mechanical dispersion on time scales of bed form-induced hyporheic exchange. *Water Resources Research*, 46(8):W08518.

- Boulton, A. J., S. Findlay, P. Marmonier, E. H. Stanley, and H. M. Valett
1998. The functional significance of the hyporheic zone in streams and rivers. *Annual Review of Ecology and Systematics*, 29:59–81.
- Briggs, M. A., F. D. Day-Lewis, J. B. T. Ong, J. W. Harvey, and J. W. Lane
2014. Dual-domain mass transfer parameters from electrical hysteresis: Theory and analytical approach applied to laboratory, synthetic streambed, and groundwater experiments. *Water Resources Research*, 50:8281–8299.
- Briggs, M. A., F. D. Day-lewis, J. P. Zarnetske, and J. W. Harvey
2015. A physical explanation for the development of redox microzones in hyporheic flow. *Geophysical Research Letters*, 42:4402–4410.
- Brunke, M. and T. Gosner
1997. The ecological signaificance of exchange processes between rivers and groundwater. *Freshwater Biology*, 37:1–33.
- Cardenas, M. B., P. L. M. Cook, H. Jiang, and P. Traykovski
2008. Constraining denitrification in permeable wave-influenced marine sediment using linked hydrodynamic and biogeochemical modeling. *Earth and Planetary Science Letters*, 275:127–137.
- Cardenas, M. B. and M. N. Gooseff
2008a. Comparison of hyporheic exchange under covered and uncovered channels based on linked surface and groundwater flow simulations. *Water Resources Research*, 44(3):n/a–n/a.
- Cardenas, M. B. and M. N. Gooseff
2008b. Comparison of hyporheic exchange under covered and uncovered channels based on linked surface and groundwater flow simulations. *Water Resources Research*, 44(3):W03418.
- Cardenas, M. B. and J. L. Wilson
2006. The influence of ambient groundwater discharge on exchange zones induced by current-bedform interactions. *Journal of Hydrology*, 331(1-2):103–109.

- Cardenas, M. B. and J. L. Wilson
2007a. Dunes, turbulent eddies, and interfacial exchange with permeable sediments. *Water Resources Research*, 43(8).
- Cardenas, M. B. and J. L. Wilson
2007b. Effects of current-bed form induced fluid flow on the thermal regime of sediments. *Water Resources Research*, 43(8).
- Cardenas, M. B. and J. L. Wilson
2007c. Exchange across a sediment-water interface with ambient groundwater discharge. *Journal of Hydrology*, 346(3-4):69–80.
- Cardenas, M. B. and J. L. Wilson
2007d. Hydrodynamics of coupled flow above and below a sediment-water interface with triangular bedforms. *Advances in Water Resources*, 30(3):301–313.
- Cardenas, M. B. and J. L. Wilson
2007e. Thermal regime of dune-covered sediments under gaining and losing water bodies. *Journal of Geophysical Research*, 112(G4):G04013.
- Conant, B. J., J. A. Cherry, and R. W. Gillham
2004. A PCE groundwater plume discharging to a river: Influence of the streambed and near-river zone on contaminant distributions. *Journal of Contaminant Hydrology*, 73(1-4):249–279.
- Cook, P. G., S. Lamontagne, D. Berhane, and J. F. Clark
2006. Quantifying groundwater discharge to Cockburn River, southeastern Australia, using dissolved gas tracers ^{222}Rn and SF 6. *Water Resources Research*, 42(10):n/a–n/a.
- Dahm, C. N., N. B. Grimm, P. Marmonier, H. M. Valett, and P. Vervier
1998. Nutrient dynamics at the interface between surface and groundwaters. *Freshwater Biology*, 40:427–451.

- Durlofsky, L.
1991. Numerical Calculation of equivalent grid block permeability tensors for heterogeneous porous media. *Water Resources Research*, 27(5):699–708.
- Durlofsky, L. and J. F. Brady
1987. Analysis of the Brinkman equation as a model for flow in porous media. *Phys. Fluids*, 30:3329–3341.
- Elliott, H. and N. H. Brooks
- 1997a. Transfer of nonsorbing solutes to a streambed with bed forms : Theory. *Water Resources Research*, 33(1):123–136.
- Elliott, H. and N. H. Brooks
- 1997b. Transfer of nonsorbing solutes to a streambed with bedforms: Laboratory experiments. *Water Resources Research*, 33(1):137–151.
- Fanelli, R. M. and L. K. Lautz
2008. Patterns of water, heat, and solute flux through streambeds around small dams. *Ground Water*, 46(5):671–687.
- Fehlman, H. M.
1985. *Resistance components and velocity distributions of open channel flows over bedforms*. PhD thesis, Colorado State University, Fort Collins.
- Findlay, S. and B. Ab
1995. Importance of surface-subsurface The hyporheic zone exchange in stream ecosystems : The hyporheic zone. *Limnology and Oceanography*, 40(1):159–164.
- Fleckenstein, J. H., S. Krause, D. M. Hannah, and F. Boano
2010. Groundwater-surface water interactions: New methods and models to improve understanding of processes and dynamics. *Advances in Water Resources*, 33(11):1291–1295.

- Fleckenstein, J. H., R. G. Niswonger, and G. E. Fogg
2006. River-aquifer interactions, geologic heterogeneity, and low-flow management.
Ground Water, 44(6):837–852.
- Fox, A., F. Boano, and S. Arnon
2014. Impact of losing and gaining stream flow conditions on hyporheic exchange fluxes induced by dune-shaped bedforms. *Water Resources Research*, 50:1895–1907.
- Gandy, C. J., J. W. N. Smith, and A. P. Jarvis
2007. Attenuation of mining-derived pollutants in the hyporheic zone: A review.
Science of the Total Environment, 373(2-3):435–446.
- Gomez, J. D., J. L. Wilson, and M. B. Cardenas
2012. Residence time distributions in sinuosity-driven hyporheic zones and their biogeochemical effects. *Water Resources Research*, 48(9):n/a–n/a.
- Goode, D. J.
1996. Direct Simulation of Groundwater Age. *Water Resources Research*, 32(2):289–296.
- Gooseff, M. N., D. M. McKnight, W. B. Lyons, and A. E. Blum
2002. Weathering reactions and hyporheic exchange controls on stream water chemistry in a glacial meltwater stream in the McMurdo Dry Valleys. *Water Resources Research*, 38(12):1279.
- Greig, S. M., D. A. Sear, and P. A. Carling
2007. A review of factors influencing the availability of dissolved oxygen to incubating salmonid embryos. *Hydrological Processes*, 21(3):323–334.
- Grimm, N. B. and S. G. Fisher
1984. Exchange between interstitial and surface water : Implications for stream metabolism and nutrient cycling. *Hydrobiologia*, 111:219–228.
- Harbaugh, A. W.
2005. MODFLOW-2005, the U.S. Geological Survey modular groundwater model: The

- ground-water flow process. U.S. Geological Survey techniques and Methods. Technical report, USGS, Reston, Virginia.
- Harvey, J. W., J. K. Böhlke, M. a. Voytek, D. Scott, and C. R. Tobias
2013. Hyporheic zone denitrification: Controls on effective reaction depth and contribution to whole-stream mass balance. *Water Resources Research*, 49(10):6298–6316.
- Harvey, J. W. and B. J. Wagner
2000. Quantifying hydrologic interactions between streams and their subsurface hyporheic zones. In *Streams and Ground Waters*, J. Jones and P. Mulholland, eds., Pp. 3–43. San Diego, California: Academic Press.
- Harvey, J. W., B. J. Wagner, and K. E. Bencala
1996. Evaluating the reliability of the stream tracer approach to characterize stream-subsurface water exchange. *Water Resources Research*, 32(8):2441–2451.
- Hayashi, M. and D. Rosenberry
2002. Effects of ground water exchange on the hydrology and ecology of surface water. *Ground Water*, 40(3):309–316.
- Hester, E. T., K. I. Young, and M. a. Widdowson
2013. Mixing of surface and groundwater induced by riverbed dunes: Implications for hyporheic zone definitions and pollutant reactions. *Water Resources Research*, 49(9):5221–5237.
- Hunter, K. S., Y. F. Wang, and P. Van Cappellen
1998. Kinetic modeling of microbially-driven redox chemistry of subsurface environments: coupling transport, microbial metabolism and geochemistry. *Journal of Hydrology*, 209(1-4):53–80.
- Janssen, F., M. B. Cardenas, A. H. Sawyer, T. Dammrich, J. Krietsch, and D. de Beer
2012. A comparative experimental and multiphysics computational fluid dynamics study of coupled surface-subsurface flow in bed forms. *Water Resources Research*, 48(8):n/a–n/a.

- Jin, G., H. Tang, B. Gibbes, L. Li, and D. Barry
2010. Transport of nonsorbing solutes in a streambed with periodic bedforms. *Advances in Water Resources*, 33(11):1402–1416.
- Jin, G. Q., H. W. Tang, L. Li, and D. A. Barry
2011. Hyporheic flow under periodic bed forms influenced by low-density gradients. *Geophysical Research Letters*, 38.
- Jones, J. B. and P. J. Mulholland
2000. *Streams and Groundwaters*. San Diego, California: Academic Press.
- Karwan, D. L. and J. E. Saiers
2012. Hyporheic exchange and streambed filtration of suspended particles. *Water Resources Research*, 48(1):W01519.
- Krause, S., D. M. Hannah, J. H. Fleckenstein, C. M. Heppell, D. Kaeser, R. Pickup, G. Pinay, a. L. Robertson, and P. J. Wood
2011. Inter-disciplinary perspectives on processes in the hyporheic zone. *Ecohydrology*, 4(4):481–499.
- Krause, S., L. Heathwaite, A. Binley, and P. Keenan
2009. Nitrate concentration changes at the groundwater-surface water interface of a small Cumbrian river. *Hydrological Processes*, 23(15):2195–2211.
- Laatloe, T., V. E. A. Post, and A. D. Werner
2013. Spatial periodic boundary condition for MODFLOW, Groundwater. *Groundwater*, 52:606–612.
- Laatloe, T., A. D. Werner, and V. E. A. Post
2014. Spatial periodicity in bedform scale solute and thermal transport models of the hyporheic zone. *Water Resources Research*, 50.
- Laatloe, T., A. D. Werner, and V. E. A. Post
submitted. A spatially periodic boundary condition for MT3DMS and PHT3D. *Ground Water*.

Ma, R. and C. M. Zheng

2010. Effects of density and viscosity in modeling heat as a groundwater tracer. *Ground Water*, 48(3):380–389.

Marzadri, A., D. Tonina, and A. Bellin

2011. A semi-analytical three dimensional process-based model for hyporheic nitrogen dynamics in gravel bed rivers. *Water Resources Research*, 47:W11518.

McClain, M. E., E. W. Boyer, C. L. Dent, S. E. Gergel, N. B. Grimm, P. M. Groffman, S. C. Hart, J. W. Harvey, C. A. Johnston, E. Mayorga, W. H. McDowell, and G. Pinay 2003. Biogeochemical hot spots and hot moments at the interface of terrestrial and aquatic ecosystems. *Ecosystems*, 6(4):301–312.

Orghidan, T.

1959. Ein neuer Lebensraum des unterirdischen Wassers: Der hyporheische Biotop. *Archiv für Hydrobiologie*, 55:392–414.

Panday, S. and C. Langevin

2012. Improving sub-grid scale accuracy of boundary features in regional finite-difference models. *Advances in Water Resources*, 41:65–75.

Parkhurst, D. L. and C. A. J. Appelo

1999. User's guide to PHREEQC—A computer program for speciation, reaction-path, 1D-transport, and inverse geochemical calculations. Technical report, Technical report, U.S. Geological Survey Water Resources Investigations.

Prommer, H., D. A. Barry, and C. Zheng

2003. MODFLOW/ MT3DMS-based reactive multicomponent transport modeling. *Ground Water*, 41(2):247–257.

Qian, Q., V. R. Voller, and H. G. Stefan

2008. A vertical dispersion model for solute exchange induced by underflow and periodic hyporheic flow in a stream gravel bed. *Water Resources Research*, 44(7):n/a–n/a.

- Renard, P. and G. de Marsily
1997. Calculating equivalent permeability: a review. *Advances in Water Resources*, 20(5-6):253–278.
- Robertson, A. and P. J. Wood
2010. Ecology of the hyporheic zone: origins, current knowledge and future directions. *Fundamental and Applied Limnology*, 176(4):279–289.
- Rutherford, J. C., J. D. Boyle, A. H. Elliott, T. V. J. Hatherell, and T. W. Chiu
1995. Modeling benthic oxygen uptake by pumping. *Journal of Environmental Engineering-Asce*, 121(1):84–95.
- Salehin, M., A. I. Packman, and M. Paradis
2004. Hyporheic exchange with heterogeneous streambeds: Laboratory experiments and modeling. *Water Resources Research*, 40:W11504.
- Savant, S., D. D. Reible, and L. J. Thibodeaux
1987. Convective-transport within stable river sediments. *Water Resources Research*, 23(9):1763–1768.
- Sawyer, A. H. and M. B. Cardenas
2009. Hyporheic flow and residence time distributions in heterogeneous cross-bedded sediment. *Water Resources Research*, 45(8):n/a–n/a.
- Sawyer, A. H. and M. B. Cardenas
2012. Effect of experimental wood addition on hyporheic exchange and thermal dynamics in a losing meadow stream. *Water Resources Research*, 48(10):n/a–n/a.
- Shum, K. T.
1992. Wave-induced advective transport below a rippled water-sediment interface,. *Journal of Geophysical Research*, 97(C1):789–808.
- Stonedahl, S. H., J. W. Harvey, A. Worman, M. Salehin, and A. I. Packman
2010. A multiscale model for integrating hyporheic exchange from ripples to meanders. *Water Resources Research*, 46:14.

- Storey, R. G., W. F. Howard, and D. D. Williams
2003. Factors controlling riffle-scale hyporheic exchange flows and their seasonal changes in a gaining stream: A three-dimensional groundwater flow model. *Water Resources Research*, 39(2):1034.
- Thibodeaux, L. and J. Boyle
1987. Bedform-generated convective-transport in bottom sediment. *Nature*.
- Tonina, D. and J. M. Buffington
2011. Effects of stream discharge, alluvial depth and bar amplitude on hyporheic flow in pool-riffle channels. *Water Resources Research*, 47(8):n/a–n/a.
- Van Cappellen, P. and Y. F. Wang
1996. Cycling of iron and manganese in surface sediments: a general theory for the coupled transport and reaction of carbon, oxygen, nitrogen, sulfur, iron, and manganese. *American Journal of Science*, 296(March):197–243.
- White, D. S.
1993. Perspectives on defining and delineating hyporheic zones. *Journal of the North American Benthological Society*, 12(1):61–69.
- Winter, T. C.
1999. Relation of streams, lakes, and wetlands to groundwater flow systems. *Hydrogeology Journal*, 7(1):28–45.
- Woessner, W. W.
2000. Stream and Fluvial Plain Ground Water Interactions: Rescaling Hydrogeologic Thought. *Ground Water*.
- Wörman, A., A. I. Packman, H. Johansson, and K. Jonsson
2002. Effect of flow-induced exchange in hyporheic zones on longitudinal transport of solutes in streams and rivers Ha. *Water Resources Research*, 38(1).

- Zarnetske, J. P., R. Haggerty, S. M. Wondzell, V. a. Bokil, and R. González-Pinzón
2012. Coupled transport and reaction kinetics control the nitrate source-sink function
of hyporheic zones. *Water Resources Research*, 48(11):n/a–n/a.
- Zheng, C. and G. D. Bennett
1995. *Applied Contaminant Transport Modeling: Theory and Practice*. New York:
Van Nostrand Rheinhold.
- Zheng, C. and P. P. Wang
1999. MT3DMS: A modular three-dimensional multispecies model for simulation of
advection, dispersion and chemical reactions of contaminants in groundwater systems:
Documentation and user's guide. Technical report, U.S. Army Eng. Res. and Dev.
Cent., Vicksburg, Miss.